

**HEAT AND FLUID FLOW ANALYSIS IN A  
CHANNEL PARTIALLY FILLED WITH  
PERMEABLE ISOTROPIC POROUS LAYER**

**A Thesis Submitted to  
the Graduate School of Engineering and Sciences of  
İzmir Institute of Technology  
in Partial Fulfillment of the Requirements for the Degree of**

**MASTER OF SCIENCE**

**in Mechanical Engineering**

**by  
Eren UÇAR**

**December 2012  
İZMİR**

We approve the thesis of **Eren UÇAR**

**Examining Committee Members:**

---

**Assoc. Prof. Dr. Moghtada MOBEDİ**  
Department of Mechanical Engineering  
İzmir Institute of Technology

---

**Prof. Dr. M. Barış ÖZERDEM**  
Department of Energy Systems Engineering  
Bahçeşehir University

---

**Assist. Prof. Dr. Ünver ÖZKOL**  
Department of Mechanical Engineering  
İzmir Institute of Technology

**14 December 2012**

---

**Assoc. Prof. Dr. Moghtada MOBEDİ**  
Supervisor, Department of Mechanical Engineering  
İzmir Institute of Technology

---

**Prof. Dr. Metin TANOĞLU**  
Head of the Department of  
Mechanical Engineering

---

**Prof. Dr. R. Tuğrul SENGER**  
Dean of the Graduate School of  
Engineering and Sciences

## **ACKNOWLEDGEMENTS**

It is a pleasure to thank the many people who made this thesis possible.

I would like to thank my supervisor, Assoc. Prof. Moghtada Mobedi. This thesis would not be possible without his guidance and support and also his great efforts to explain things clearly and simply.

I wish to thank my entire extended family for providing a loving environment, their encouragement, great patience and unconditional help.

I would like to express my special thanks to Ufuk Şirin who have taught me writing codes, helping me get through the difficult times, and for all the emotional support. I am thankful to Tuhfe Göçmen and Erman Barış Aytar for their support and eternal friendship. Also I am grateful to thank my office friends for their camaraderie and entertainment.

Above all, my brother, Ahmet Rasim Uçar, deserves special mention for his encouragement throughout my life. With my deepest gratitude, I dedicate this study to him.

## ABSTRACT

### HEAT AND FLUID FLOW ANALYSIS IN A CHANNEL PARTIALLY FILLED WITH PERMEABLE ISOTROPIC POROUS LAYER

A theoretical study is performed on heat and fluid flow in a parallel plate channel completely and partially filled with porous medium. An asymmetric heat flux is imposed onto the boundary conditions of the channel fully filled with porous media. However, a symmetrical heat flux is applied to the channel partially filled with porous medium. Dimensional analysis is performed on three parallel plates having different permeability and effective thermal conductivity values. The dimensionless analysis is performed for parallel plates with different values of  $Da$  and thermal conductivity ratio. Darcy-Brinkman model is used to investigate the velocity distribution in porous media. The dimensional and dimensionless energy equation and appropriate boundary conditions are written for the analyzed channels. The dimensional equations of motion and heat are solved by numerical methods, while the dimensionless form of those equations are analytically solved to obtain analytical expressions for the velocity and temperature fields in the channel. The dimensional temperature and velocity profiles, obtained by numerical methods, are compared with the analytical expressions of dimensionless temperature and velocity profiles and good agreement between the results were observed. For both fully filled asymmetric heated channel and partially filled symmetrical heated channel, it is observed that the traditional temperature difference (difference between surface and mean temperatures) is not proper to be used in the individual heat transfer coefficient since heat transfer coefficient approaches to infinity and changes sign without changing of heat transfer direction. Hence, a proper temperature difference is required to be defined.

## ÖZET

### GEÇİRGEN İZOTROPİK GÖZENEKLİ KATMAN İLE KISMİ OLARAK DOLDURULMUŞ KANALDA ISI VE AKIŞ ANALİZİ

Bu çalışma, tamamen ve kısmen gözenekli ortamla doldurulmuş paralel kanallar içerisindeki ısı ve akışkan akışının teorik olarak incelenmesidir. Tamamen gözenekli ortamla doldurulmuş kanalların üst ve alt duvarlarına sabit fakat farklı miktarda ısı akısı verilirken, kısmen doldurulmuş kanalın duvarlarına sabit ve eşit miktarda ısı verilmiştir. Boyutsal analiz; farklı geçirgenliklere ve farklı etkin ısı iletim katsayılarına sahip üç paralel kanala yapılmıştır. Boyutsuz analiz de farklı Darcy numarasına ve farklı ısı iletim oranına sahip paralel kanallar üzerine yapılmıştır. Gözenekli ortam içerisindeki hız dağılımları Darcy- Brinkman modeli kullanılarak elde edilmiştir. İncelenen kanallar için boyutlu ve boyutsuz enerji denklemleriyle sınır koşulları yazılmıştır. Boyutlu hız ve enerji denklemleri nümerik olarak çözülürken, boyutsuz hız ve enerji denklemleri analitik olarak çözülmüştür. Boyutlu nümerik analizlerin sonuçlarıyla boyutsuz analitik analizlerin sonuçları karşılaştırılmış ve birbirleri arasında uyum olduğu gözlemlenmiştir. Zorlanmış taşınımında genel olarak kullanılan ısı farkı ifadesinin, asimetrik bir biçimde ısıtılan tam doldurulmuş kanallarda ve simetrik ısıtılan kısmen doldurulmuş kanallarda kullanılmasının, ısı taşınım katsayısının sonsuza gitmesi ve ısı transferinin yönü değişmezken ısı taşınım katsayısının işaretinin değişmesi gerekçesiyle bu tip çalışmalar için uygun olmadığı gözlemlenmiştir. Dolayısıyla yeni bir ısı farkı ifadesinin tanımlanması gerekmektedir.

# TABLE OF CONTENTS

LIST OF FIGURES .....	ix
LIST OF TABLES.....	xiii
LIST OF SYMBOLS .....	xiv
CHAPTER 1. INTRODUCTION .....	1
CHAPTER 2. A REVIEW ON HEAT AND FLUID FLOW IN CHANNEL/ DUCT PARTIALLY FILLED WITH POROUS MEDIUM.....	5
CHAPTER 3. BASIC CONCEPTS .....	20
3.1. Porosity, Permeability and Fluid Flow in Porous Media.....	21
3.2. Heat Transfer Analysis in Porous Media.....	24
3.3. Theoretical Background of the Forced Convection in the Clear Fluid Channel.....	25
CHAPTER 4. DIMENSIONAL STUDY ON CHANNEL COMPLETELY FILLED WITH POROUS MEDIUM, ASYMMETRIC HEAT FLUX BUNDARY CONDITION .....	28
4.1. The considered problem.....	28
4.2. Mathematical formulation and governing equations .....	29
4.2.1. Fluid Flow Analysis.....	29
4.2.2. Heat Flow Analysis.....	31
4.2.3. Pressure drop calculation.....	31
CHAPTER 5. DIMENSIONLESS STUDY ON CHANNEL COMPLETELY FILLED WITH POROUS MEDIUM: ASYMMETRIC HEAT FLUX BUNDARY CONDITION .....	33
5.1. The considered problem.....	33
5.2. Mathematical formulation and governing equations .....	34

5.2.1. Fluid Flow Analysis.....	34
5.2.2. Heat Flow Analysis.....	37
5.2.3. Pressure Drop Calculations.....	43
CHAPTER 6. DIMENSIONAL STUDY ON CHANNEL PARTIALLY FILLED WITH POROUS MEDIUM; SYMMETRIC HEAT FLUX BOUNDARY CONDITION.....	45
6.1. The considered problem.....	45
6.2. Mathematical formulation and governing equations .....	46
6.2.1. Fluid Flow Analysis.....	46
6.2.2. Heat Flow Analysis.....	48
6.2.3. Pressure Drop Calculation .....	49
CHAPTER 7. DIMENSIONLESS STUDY ON CHANNEL PARTIALLY FILLED WITH POROUS MEDIUM; SYMMETRIC HEAT FLUX BOUNDARY CONDITION.....	50
7.1. The considered problem.....	50
7.2. Mathematical formulation and governing equations .....	51
7.2.1. Fluid Flow Analysis.....	51
7.2.2. Heat Flow Analysis.....	55
7.2.3. Pressure Drop Calculations.....	63
CHAPTER 8. NUMERICAL APPROACH FOR THE SOLUTION OF GOVERNING EQUATIONS.....	65
8.1. Numerical Solution Procedure for Completely Filled Problem discussed in Chapter 4.....	65
8.1.1. Solution of the Momentum Equation .....	66
8.1.2. Solution of the Energy Equation.....	68
8.2. Numerical Solution Procedure for Completely Filled Problem discussed in Chapter 6.....	70
8.2.1. Solution of the Momentum Equation .....	71
8.2.2. Solution of the Energy Equation.....	72

CHAPTER 9. RESULTS AND DISCUSSION.....	74
9.1. Results for a Channel with Symmetrical Heated Walls.....	74
9.1.1. Dimensional Analysis.....	74
9.1.1.1. The Analyzed Channels.....	74
9.1.1.2. Results.....	78
9.1.2. Dimensionless Analysis.....	84
9.1.2.1. Comparison of the Numerical with Analytical Results .....	85
9.1.2.2. Effect of Da.....	89
9.2. Results for a Channel with Asymmetrical Heated Walls .....	96
9.2.1. Dimensional Analysis for Completely Filled Channels .....	96
9.2.1.1. The Analyzed Channels.....	96
9.2.1.2. Results.....	97
9.2.2. Dimensionless Analysis for Completely Filled Channels .....	105
9.2.2.1. Comparison of the Numerical with Analytical Results .....	105
9.2.2.2. Effect of Da.....	108
9.3.1. Dimensional Analysis for Partially Filled Channels .....	114
9.3.1.1. The Analysed Channels .....	114
9.3.1.2. Results.....	116
9.3.2. Dimensionless Analysis for Partially Filled Channels .....	124
9.3.2.1. Comparison of the Numerical with Analytical Results .....	124
9.3.2.2. Effect of Da.....	128
 CHAPTER 10. CONCLUSION .....	 137
 REFERENCES .....	 140
 APPENDIX A. CONSTANTS.....	 142



# LIST OF FIGURES

<u>Figure</u>	<u>Page</u>
Figure 1.1. The examples of porous medium; Granular porous materials used in the construction industry.....	3
Figure 3.1. Schematic demonstration of a porous medium .....	20
Figure 3.2. Microscopic and macroscopic view a) Microscopic approach, b) Macroscopic approach.....	21
Figure 4.1. Schematic view of the considered channel.....	29
Figure 5.2. Differential volume from the considered duct .....	39
Figure 6.1. Schematic view of the considered channel.....	46
Figure 7.1. Schematic view of the considered channel.....	51
Figure 7.2. Differential volume from the considered duct .....	57
Figure 8.1. The flowchart for the solution of the momentum equation.....	67
Figure 8.2. The node direction used in momentum equation .....	68
Figure 8.3. The flowchart for the solution of the energy equation .....	69
Figure 8.4. The node directions used in energy equation .....	69
Figure 9.1. Three channels filled with square bars analyzed in this section: (a) High Permeable channel (b) Medium Permeable channel (c) Low Permeable channel .....	75
Figure 9.2. A micro-view of a square bar .....	77
Figure 9.3. Dimensional velocity distributions for the flows with different permeabilities.....	79
Figure 9.4. Isotherm lines through the low conductive solid used channel: (a) High Permeable channel (b) Medium Permeable channel (c) Low Permeable channel .....	80
Figure 9.5. Isotherm lines through the high conductive solid used channel: (a) High Permeable channel (b) Medium Permeable channel (c) Low Permeable channel .....	82
Figure 9.6. Mean Temperature and wall temperature values through the channels. ....	83
Figure 9.7. Nu values through the channels: Blue lines indicate glass used channel while black lines indicate aluminum alloy used channel.....	84

Figure 9.8. Comparison of the converted normalized velocity profiles, which are obtained by numerical results, with the analytical results: (a) High Permeable channel (b) Medium Permeable channel (c) Low Permeable channel .....	86
Figure 9.9. Comparison of the converted dimensional temperature profiles which are obtained by numerical results with the analytical results: (a) The medium permeable channel when the material of the solid is glass (b) The low permeable channel when the material of solid is aluminum alloy .....	88
Figure 9.10. Normalized velocity distributions for the flows with different Da. ....	90
Figure 9.11. Dimensionless temperature distributions for the flows with different Da.....	91
Figure 9.12. Logarithmic plot of Da vs. Nu.....	91
Figure 9.13. Logarithmic plot of Heat transfer increment ratio vs. the Da .....	92
Figure 9.14. Logarithmic plot of friction coefficient vs. Da.....	93
Figure 9.15. Logarithmic plot of pressure drop increment ratio vs. Da .....	94
Figure 9.16. Logarithmic plot of overall performance vs. the Da .....	95
Figure 9.17. The considered channel with exposed heat fluxes on to the walls.....	97
Figure 9.18. Isotherm lines through the low conductive solid used channel with asymmetrical heating:(a) High Permeable channel (b) Medium Permeable channel (c) Low Permeable channel.....	99
Figure 9.19. Isotherm lines through the high conductive solid used channel with asymmetrical heating: (a) High Permeable channel (b) Medium Permeable channel (c) Low Permeable channel.....	101
Figure 9.20. $Nu_1$ (upper wall) and $Nu_2$ (lower wall) variations vs. $q''_{w1}/q''_{w2}$ for high permeable channel when the material of solid is glass. ....	102
Figure 9.21. The outlet temperatures of the considered channel while $Nu_2$ changes its direction.....	104
Figure 9.22. The variation of mean, upper and lower walls temperatures at the outlet of the channel with heat flux ratio .....	105
Figure 9.23. Comparison of the dimensionless temperature profiles which are obtained by numerical results with the analytical results: (a) The medium permeable channel when the material of the solid is aluminum alloy (b) The low permeable channel when the	

material of solid is glass.....	107
Figure 9.24. Dimensionless temperature distributions for the flows with different Da when (a) $q_r=0.5$ , (b) $q_r=5$ , (c) $q_r=50$ . .....	109
Figure 9.25. Logarithmic plot of Da vs. Nu for upper wall ( $Nu_1$ ) and Nu for lower wall ( $Nu_2$ ) for $q_r=0.5$ .....	110
Figure 9.26. Logarithmic plot of heat transfer increment ratio vs. the Da (a) The upper wall heat transfer increment (b) The lower wall heat transfer increment .....	112
Figure 9.27. Logarithmic plot of overall performance for upper and lower wall vs. the Da .....	113
Figure 9.28. Three channels filled with square bars analysed in this section: (a) High Permeable channel (b) Medium Permeable channel (c) Low Permeable channel .....	115
Figure 9.29. The dimensional velocity distributions for the flows with different permeability values for partially filled channel. ....	117
Figure 9.30. Isotherm lines through the low conductive solid (glass) used channel: (a) Partially filled with high permeable material (b) Partially filled with medium permeable material (c) Partially filled with low permeable material.....	118
Figure 9.31. Isotherm lines through the high conductive solid (aluminium) used channel: (a) Partially filled with high permeable material (b) Partially filled with medium permeable material (c) Partially filled with low permeable material .....	120
Figure 9.32. Wall temperature values through the channels (a) The channel partially filled with glass particles (b) The channel partially filled with aluminium particles. ....	121
Figure 9.33. Outlet temperature values through the channels (a) the channel partially filled with glass particles (b) the channel partially filled with aluminium particles. ....	123
Figure 9.34. Comparison of the normalized velocity profiles which are obtained by converted form of numerical results and the analytical results: (a) The channel partially filled with high permeable material (b) The channel partially filled with medium permeable material (c) The channel partially filled with low permeable material.....	125

Figure 9.35. Comparison of the dimensionless temperature profiles which are obtained by converted form of numerical results and the analytical results: (a) The high permeable channel partially filled with aluminum alloy particles (b) The low permeable channel partially filled with glass particles .....	127
Figure 9.36. Dimensionless velocity distributions for the flows with different Da.....	129
Figure 9.37. Dimensionless temperature distributions for the flows with different Da when (a) $K^*=0.01$ , (b) $K^*=1$ , (c) $K^*=100$ . .....	130
Figure 9.38. Logarithmic plot of Da vs. Nu for upper wall ( $Nu_1$ ) and Nu for lower wall ( $Nu_2$ ). .....	132
Figure 9.39. Logarithmic plot of Da vs. overall Nu .....	133
Figure 9.40. Logarithmic plot of heat transfer increment ratio vs. the Da for partially filled channel.....	134
Figure 9.41. Friction coefficient vs. logarithmic plot of Da for partially filled channel.....	134
Figure 9.42. Friction coefficient vs. logarithmic plot of Da for partially filled channel.....	135
Figure 9.43. Logarithmic plot of overall performance vs. Da for partially filled channel .....	136

# LIST OF TABLES

<b><u>Table</u></b>	<b><u>Page</u></b>
Table 1.1. A list of various methods .....	1
Table 2.1. The summary of the literature survey .....	10
Table 9.1. Thermophysical properties of fluid and solids .....	76
Table 9.2. The flow parameters for the considered channels. ....	78
Table 9.3. Comparison of the analytical and numerical results for Nu .....	89
Table 9.4. Thermal Conductivities of several solids and fluids.....	95
Table 9.5. The values of upper wall Nu ( $Nu_1$ ), lower wall Nusselt number ( $Nu_2$ ) and overall Nu (Nu) .....	103
Table 9.6. Comparison of the analytical and numerical results for the Nu .....	108
Table 9.7. The fully developed Nu for upper and lower wall according to the particle types used in the lower part of the channel.....	124
Table 9.8. Comparison of the analytical and numerical results for the individual Nu .....	128

## LIST OF SYMBOLS

$A$	Area, $m^2$
$C_p$	Specific heat at constant pressure, J/kg K
$Da$	Darcy number
$f$	Friction coefficient
$F$	Forchheimer constant
$G$	Pressure gradient in x- direction
$h$	Convective heat transfer coefficient, $W/m^2 K$
$H$	Half height of channel
$i, j$	Direction of x,y in the numerical solution
$k$	Thermal conductivity, W/m K
$\bar{k}$	Carmen- Kozeny constant
$K$	Permeability, $m^2$
$K^*$	The ratio of effective conductivity over fluid conductivity
$L$	Length of the channel, m
$M$	Dimensionless viscosity ratio parameter
$Nu$	Nusselt number
$n, m$	Node number
$P$	Pressure, Pa
$Q$	Volume flow rate, $m^3/s$
$Re$	Reynolds number
$q''$	Heat flux, $W/m^2$
$S$	Porous media shape parameter
$T$	Temperature, K
$T_i$	Initial temperature, K
$u$	Velocity component along x- direction, m/s
$U$	Dimensionless velocity component along dimensionless X- direction, m/s
$\hat{u}$	Dimensionless normalized velocity
$U_0$	Superficial velocity, m/s
$U^f$	Pore velocity, m/s
$x$	Coordinate along the axis of the channel, m

$y$	Coordinate normal to the surfaces of the channel, m
$X, Y$	Dimensionless coordinates

### Greek letters

$\beta$	Coefficient for the walls
$\varepsilon$	porosity
$\theta$	Dimensionless temperature
$\mu$	Dynamic viscosity, kg/m s
$\nu$	Kinematic viscosity of fluid, m <sup>2</sup> /s
$\xi$	Porous thickness
$\xi_l$	Location of porous thickness
$\rho$	Density, kg/m <sup>3</sup>
$\tau$	Shear stress, Pa

### Subscripts

$c$	Clear fluid region
$eff$	effective
$f$	fluid
$m$	mean
$p$	porous
$r$	ratio
$s$	solid
$t$	total
$w$	wall
$w1$	Upper wall
$w2$	Lower wall
$\mu$	average
$1$	Belongs to the upper wall
$2$	Belongs to the lower wall

# CHAPTER 1

## INTRODUCTION

A heat transfer phenomenon is widely faced in the most engineering applications. The enhancement of heat transfer is one of the topic gains attentions of researchers in recent years. By enhancing of heat transfer not only the size of the equipment can be reduced but also the equipment thermal efficiency can be significantly improved. That's why the heat transfer enhancement techniques are being developed over 140 years. A.E.Bergles [1] identified fifteen different heat transfer enhancement techniques. These techniques are classified as passive methods and active methods. The list of active and passive techniques is given in Table 1.1.

Table 1.1. A list of various methods [1]

Passive Techniques	Active Techniques
Treated surfaces	Mechanical aids
Rough surfaces	Surface vibration
Extended surfaces	Fluid vibration
Displaced enhancement devices	Electrostatic fields
Swirl flow devices	Injection
Coiled tubes	Suction
Surface tension devices	Jet impingement
Additives for liquids	

The difference between passive and active methods is the passive techniques do not require direct input of external power. The active techniques need addition of external power, this external power facilitates desired flow modification and provides improvement in the rate of heat transfer. In the case of passive techniques, modifications of surface or geometry of channels is required. Sometimes, incorporation of an insert or material can also be used to enhance the heat transfer.



As Vafai stated in his book [2], the enhancement of heat transfer basically can be made by reducing the thermal resistance of the heat transfer process. The definition of the thermal resistance should be made according to the mode of heat transfer; convection, conduction or radiation. This thesis is concerning about forced convection that's why the following equation is used to define heat transfer process:

$$q = h A (T_w - T_{ref}) \quad (1.1)$$

In Equation 1.1,  $q$  is the heat transfer rate (W),  $(T_w - T_{ref})$  is the temperature difference,  $h$  is the convective heat transfer coefficient (W/m<sup>2</sup>k), and  $A$  is the heat transfer area (m<sup>2</sup>). There are two ways to provide a low the thermal resistance as a) increasing the heat transfer coefficient  $h$  and/or b) increasing the heat transfer area  $A$ . This thesis focuses on enhancing the convection heat transfer with both increasing of heat transfer area  $A$  and increasing of the heat transfer coefficient,  $h$ , by using porous media. The causes of the improvement of the heat transfer coefficient due to the usage of porous media are: a) the porous substrate provides mixing effect between the fluid and the wall, b) increasing the fluid effective thermal conductivity, c) making a thinner hydrodynamic boundary layer.

Porous medium is defined as a material consisting of finite volume solids with an interconnected void [3]. The solids can be either rigid or under a small deformation. The flow can be passed in the voids between the solids. The distribution of voids is irregular as well as their shape in a natural porous medium. Beach sand, sandstone, wood, and the human lung can be the examples of natural porous media. Rather than natural porous medium, there are artificial porous medium as regular shaped. Figure 1.1 shows an example of the natural porous medium as limestone used in constructive industry [3]:

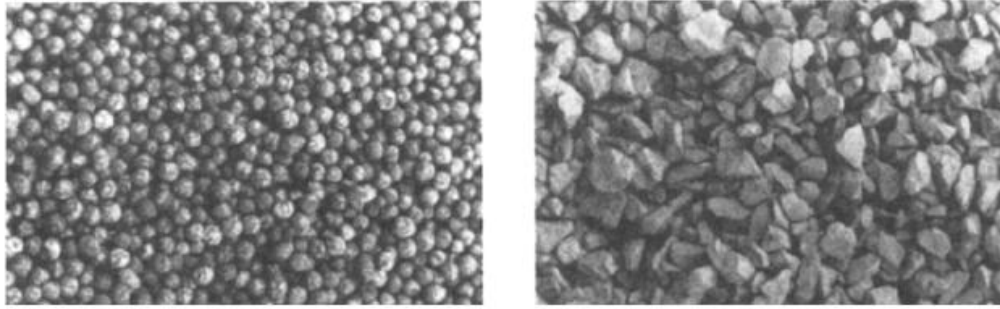


Figure 1.1. The examples of porous medium; Granular porous materials used in the construction industry [3]

Convective heat transfer in porous media has received increasing interest over 30 years, because it has numerous applications in many engineering areas. The applications for the use of porous media as an improving factor of convection heat transfer are electronic cooling applications, heat exchangers, heat pipes etc. Porous media provides the augmentation of the heat transfer as well as a decrease the size of these devices due to the increment of the amount of heat dissipation per unit area.

However, completely filling the system with the porous media may be penalized by increasing pressure drop too much which in turns increases the cost of the pumping work of the system. In fact, the major challenge in designing a system is to achieve a high heat transfer rate using minimum pumping power. Therefore engineers prefer partially filling of the channels or duct in which heat transfer occurs, rather than complete fill of the channel to reduce the pressure drop. That's why a considerable attention is paid to study heat transfer in channels partially filled with porous materials.

In the present study, forced convection heat transfer enhancement in parallel plate channels by using porous media is theoretically investigated. The steady state analysis is performed for all cases in the study. Pressure drop and heat transfer effects are investigated both numerically and analytically. The comparison between analytical solutions results and numerical solutions are shown for the studied cases.

The present study starts with the comprehensive review of the literature on forced convection heat transfer in channels or ducts partially filled with porous medium in Chapter 2. In Chapter 3, information about basic concepts is given to provide a background for the next chapters of the study. It provides knowledge about the definition of porous media with all relevant terms, definition of dimensional and dimensionless parameters, analyzing energy and momentum equation used in porous media and theoretical background of the forced convection in the clear fluid channel.

In this thesis, four different analyses are made. In all cases, steady laminar flow is considered. Efforts are focused on identifying the influence of dimensional and dimensionless parameters on velocity field, heat transfer and pressure drop properties in completely and partially filled channels. The analysis starts with a dimensional study on a parallel plate channel completely filled with porous medium in Chapter 4.

The dimensional momentum and energy equations with asymmetrical heat flux boundary conditions are presented. A dimensionless study on channel completely filled with porous medium with asymmetrical heat flux boundary conditions is performed in Chapter 5. In this case, all the governing equations are made dimensionless and solved analytically. The pressure drop along the considered channel is calculated by analytically. In Chapter 6, a dimensional study is made about a channel which partially filled by porous medium with symmetric heat flux boundary conditions. For the last case, dimensionless form of equations of momentum, energy and pressure drop are solved analytically for the channel partially filled by porous medium which has symmetrical heat flux boundary conditions. In Chapter 8, numerical approach for the solutions of dimensional form of the governing equations is given. Results and discussions are presented for the all aforementioned cases in Chapter 9. In this chapter, numerical results which are velocity, temperature and pressure drop for the dimensional problems are given. Furthermore the results of dimensionless velocity and temperature expressions are given. The results are presented via graphics and tables. The conformity between numerical result and analytical results are also examined for three different type porous media and it is given in Chapter 9. The studies issues in this thesis are concluded in Chapter 10.

## CHAPTER 2

# A REVIEW ON HEAT AND FLUID FLOW IN CHANNEL/DUCT PARTIALLY FILLED WITH POROUS MEDIUM

The use of porous media to improve forced convection heat transfer in channels has wide range of applications. That is why; several numerical and experimental studies on internal flows in a channel or duct have been examined in order to provide a deeper understanding of the transport mechanism of momentum and heat transfer in porous media. In some application area of porous media, the channel is not completely filled with porous medium. That is why; several studies on the heat and fluid flow in partially porous medium filled channels can be found in literature. In this section, an extended review has been performed on the reported studies about heat and fluid flow in the partially porous medium filled channels.

A considerable number of investigations on forced convection in partially filled porous channel and ducts have been performed for steady state assumption. Poulikakos and Kazmierczak [4] investigated the problem of forced convection in a duct partially filled with a porous medium, analytically and numerically. They used two channel geometries and two types of boundary conditions; parallel plates and circular ducts with constant heat flux and constant wall temperature. The Brinkman extended Darcy model was used to describe the flow within the porous material. The impact of the presence of a porous region near an impermeable wall on the heat and fluid flow characteristics of the considered channels was investigated. They concluded that thickness of the porous region, Darcy number ( $Da$ ) and the ratio of effective thermal conductivity of the porous medium to the fluid thermal conductivity have similar effects on the heat and fluid flow for both channel geometries and boundary conditions. The study also states that, the dependence of the Nusselt number ( $Nu$ ) on the thickness of the porous region is not uniform so they found a thickness at which the  $Nu$  value reaches minimum.

Al-Nimr et al. [5] employed a porous substrates in a tubeless solar collector to improve the convective heat transfer between the absorber plate and the fluid. The collector efficiency has been improved by 3-32 % under favor of porous substance and

also the study concluded with that there is an optimum porous substrate thickness beyond which the collector efficiency does not considerably change due to the increasing cost of the compensation the pressure drop with pump. Pulsating flow and heat transfer in a channel whose walls are layered by a porous medium was considered by Guo et al. [6] for constant heat flux thermal condition on the outer surface. The Birnkman-Forcheimer extended Darcy model was used to obtain velocity profile in the channel. The study focuses the effects of pulsation in partially filled channel on heat transfer and an optimum porous layer thickness for the maximum effective thermal diffusivity. Kuznetsov investigated the problem of forced convection partially porous medium filled channel with Couette flow [7 - 8]. Kuznetsov used the Birnkman-Forcheimer extended Darcy model and obtain analytical expressions for velocity and temperature distributions. Different thermal boundary conditions for Couette flow were studied and the long expressions for velocity and temperature profile were obtained. The influence of Da number on the velocity profile and Nu were discussed. The optimum porous thickness ratio for partially filled ducts or channels with concerning about pressure drop were obtained by Mohamad [9]. He stated that the inertia term has significant effect on Nu, but not for highly porous domains. The author also studied on the relation between the length of developing region of the channel and Da number. It was concluded that the flow developing length is not strong function of Da number.

Developing flow characteristics of fluid flow and enhanced heat transfer in a partially filled channel was examined by Jen and Yan [10]. They developed a three dimensional computational model and they solved all Navier-Stokes equations for considered domain. The authors presented the variation of friction factor and Nu as a function of axial position. Moreover, the authors analyzed the effects of the size of porous layer inside the channel partially filled with porous medium on heat and fluid flow. The effects of porous layer thickness and permeability of layer on the rate of entropy generation in the developing and fully developed region of a partially filled duct was investigated by Morosuk [11]. Morosuk performed analytical and numerical study on entropy generation in a channel and duct whose center is filled with a porous layer. They concluded that the mechanism of entropy generation is mainly dominated by friction and drag force in the porous medium. The author also stated that the maximum entropy generation occurs at the interface and the entropy generation has the highest value at the entrance region. A detailed numerical study was performed by Sayehvand and Shokouhmand [12] on a channel with porous layers on its wall. The studied the

effects of thickness of porous layer,  $Da$ , and the conductivity ratio. They mainly showed that for highly conducting porous media, heat transfer is systematically augmented independent of Darcy value. Yang et al. [13] studied about optimum porous fractions for forced convection in a partially filled tube. An expression for the optimal porous core diameter ratio was presented in this study. Steady and pulsatile flow for the local thermal non equilibrium condition was numerically investigated by Forooghi et al. [14] for the partially filled duct with center located porous layer. They show that, solid to fluid thermal conductivity ratio is very important. As the solid to fluid thermal conductivity ratio increases  $Nu$  increases. It is also stated that when the thickness of porous media is very low,  $Nu$  is negatively affected by the porous media. An analytical investigation for the channel which is partially filled by bidisperse porous medium was presented by Kuznetsov and Nield [15]. One side of the channel is filled with porous layer while fluid flow in the other side. The effects of conductivity ratio, velocity ratio, volume fraction, internal heat exchange parameter, and the position of the porous-fluid interface on to the  $Nu$  were investigated for both symmetrical and asymmetrical heat flux boundary condition. A singular behavior of the  $Nu$  was found for the asymmetric case. Satyamurty and Bhargavi [16] studied the forced convection in a thermally developing region of a parallel plate channel with one side located porous layer. The walls of the channel are maintained at a constant temperature. It was found that the maximum enhancement in heat transfer occurs at a porous fraction of 0.8 at a  $Da$  of 0.001 and the maximum enhancement per unit pressure drop occurs at a porous fraction of 0.7. An analysis for fully developed steady state of forced convection in a parallel plate channel partly occupied by porous medium was made by Nield and Kuznetsov [17]. The porous layer is located at the center of channel and lateral boundaries. The authors investigated the change of  $Nu$  according to the predetermined criteria such as thermal conductivity ratio, thickness of porous medium, the interface position etc. They showed that,  $Nu$  is strongly affected from the thickness of porous layer and thermal conductivity ratio rather than the other parameters. Shokouhmand et al. [18] studied the effect of porous insert position on enhance heat transfer in a parallel plate channel partially filled with a fluid saturated porous medium. Two type of porous insert position are studied as porous layer was attached to the walls and porous layer oriented the center of the channel. In this paper, it was found that the pressure loss was higher when the location of the porous media is in the channel core. However, the inserting porous layer in the channel core results in higher  $Nu$ , so the location should be determined

according to the type of the system. Recently, Teamah et al. [19] have presented a numerical study on the effect of the shape of the porous layer on heat and fluid flow in a cylindrical duct. The shapes of the porous layer have been taken as; cylindrical shape placed at the centerline of the pipe, annular shape, and finally a cylindrical shape porous layer is located at the center of pipe but far from the channel inlet. In the study, a critical radius was determined and it was obtained that the pressure drop and Nu have the highest value when the porous has a cylindrical shape placed at the centerline of the pipe. The conclusion of the study consistent with the conclusion of the study of Shokouhmand et al. [18].

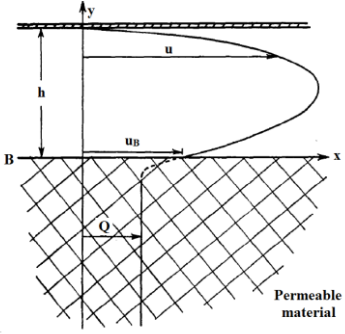
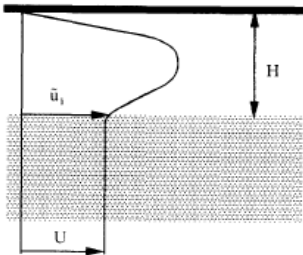
The interfacial conditions between a porous medium and a fluid layer was examined in several studies. One of the study about the interfacial condition of partial filled channel was examined by Beavers and Joseph [20]. In their work, the authors presented an empirical correlation for the boundary conditions at the porous-fluid interface. An extensive analytical investigation on the momentum transportation in partially porous channel was conducted by Kuznetsov [21]. Kuznetsov showed that accounting for a jump in the stress and for the difference between the fluid and effective viscosity can essentially influence velocity profiles in the fluid layer. This influence decreases with an increase in the inertial parameter and a decrease in the Da. Kuznetsov [22] also investigated the heat and fluid transfer in a parallel plate channel with a porous layer core analytically. The stress jump factor at the interface region was studied and the effects of this factor were explained in detail. It is stated that, Nu has a different value for different thickness ratios and it has a maximum value for a specified thickness whose magnitude and position depend on the Da. Alazmi and Vafai [23] investigated the different interfacial conditions between a porous medium. The studied configuration consists of a fluid layer sandwiched between a porous medium from above and the solid boundary from below. In the study, it was presented that the variances have a more pronounced effect on the velocity field and a substantially small effect on the temperature field and yet even smaller effect on the Nu distribution. Goyeau et al. [24] concerned with the momentum balance at the interface between a liquid and a porous substrate. The study presents a new interfacial model which has a good agreement between their numerical modeling and some existing models in the literature. The validity of one type of the interfacial boundary condition (BJ boundary condition) was examined by Auriault [25]. The study stated that an intrinsic boundary condition should be used when BJ condition is not appropriate because of the separation of scales.

The transient heat transfer characteristics of the partially filled channels are the main subject of the several studies. A numerical study was presented by Alkam and Al-Nimr [26] for a transient non-Darcian forced convection flow in two dimensional cylindrical coordinate system by using Brinkman-Forcheimer extended Darcy model. The porous layer is placed at the wall of the cylinder. The study concluded that porous substrates could give rise to considerably augmentation of Nu. In their study, it was also mentioned that the porous medium thickness has effects on the steady state time of the problem. The unsteadiness of the partially filled channel problem was also investigated by Al-Nimr and Alkam [27]. They solved transient fluid flow in a parallel plate channels partially filled with porous layer by using Green's function method. The effects of the geometry, solid matrix and the fluid on the hydrodynamic behavior were investigated. The Brinkman extended Darcy model is used to simulate the flow inside the porous medium. Later, the same previous group gave a mathematical model that uses Green's function to simulate the transient hydrodynamics of a non-Darcian fluid flow in circular channels partially filled with its core [28]. Alkam et al. [29] performed a numerical study about the transient region of the partially filled channels. The porous layer is located on a wall of the parallel plate channel. In this paper, they used the Darcy-Brinkman-Forcheimer model to simulate the flow inside the porous domain. The study reports heat transfer can be enhanced using higher thermal conduction ratio, decreasing Da and increasing microscopic inertial coefficient. Another study about developing region in parallel plate channel partially filled with two porous substance of equal thickness mounted at inner walls was done by Alkam et al. [30]. They found that splitting of the same amount of porous substrate on the inner channel walls is more efficient than using the same amount as a single porous substrate mounted on one side of the inner channel. Moreover, if the porous layer is used on one wall, the pressure gradient has been found to be higher for all porous layer thickness.

The summarized studies are shown in the Table 2.1. to simplify comprehension of the problems according to the dimensions, governing equations, outer surface thermal conditions and solution methods. The figures of the studies also are given in the table.

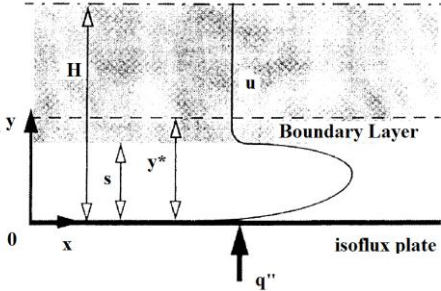
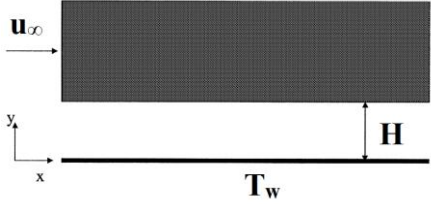
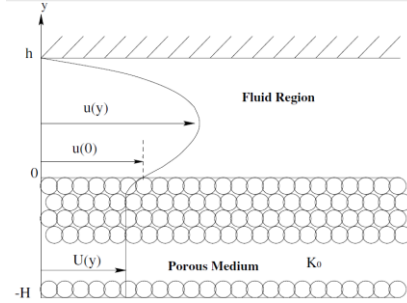


Table 2.1. The summary of the literature survey

Authors	Dimension	Governing equations	Outer surfaces thermal condition	Interface condition (Velocity and thermal)	Solution method	Figure of studied channel/duct
Beavers and Joseph [20]	2D Cartesian coordinate system	Darcy Equation	-	B-J model	Experimental and Analytical	
Kuznetsov [21]	2D Cartesian coordinate system	Brinkman Forchhimer extended Darcy	-	B-J model	Analytical	

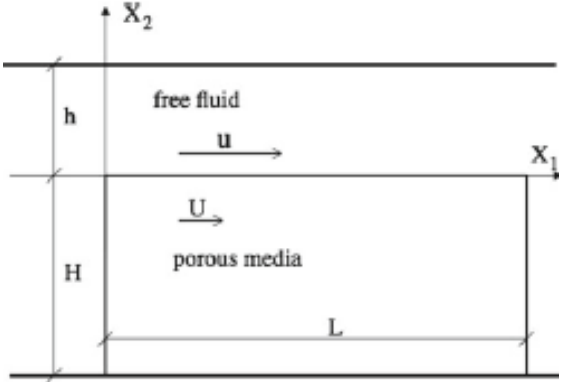
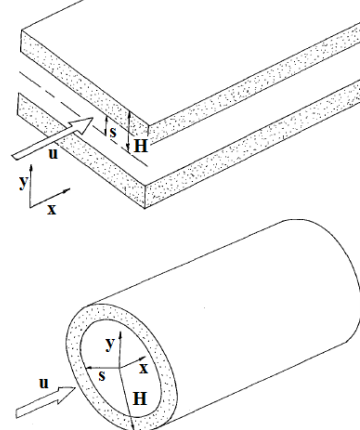
(cont. on next page)

Table 2.1 (cont.)

<p>Kuznetsov [22]</p>	<p>2D Cartesian coordinate system</p>	<p>Brinkman Forchhimer extended Darcy</p>	<p>Constant heat flux. Axisymmetric B.C.</p>	<p>B-J model Continuity of heat flux</p>	<p>Analytical</p>	
<p>Alazmi and Vafai [23]</p>	<p>2D Cartesian coordinate system</p>	<p>Brinkman Forchhimer extended Darcy</p>	<p>Constant wall temperature</p>	<p>All different models</p>	<p>Analytical</p>	
<p>Goyeau et al. [24]</p>	<p>2D Cartesian coordinate system</p>	<p>Brinkman extended Darcy</p>	<p>-</p>	<p>Continuity of shear stress and B-J Model</p>	<p>Analytical and Numerical</p>	

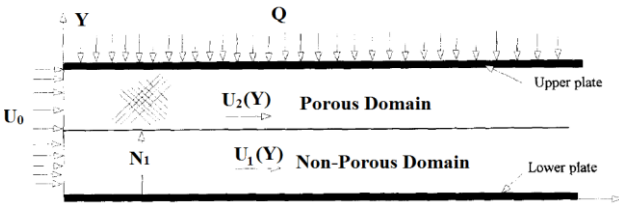
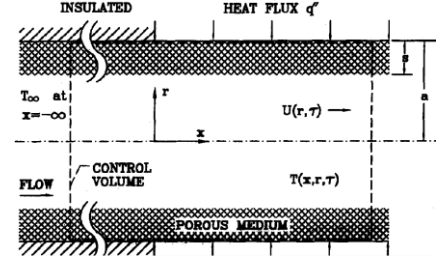
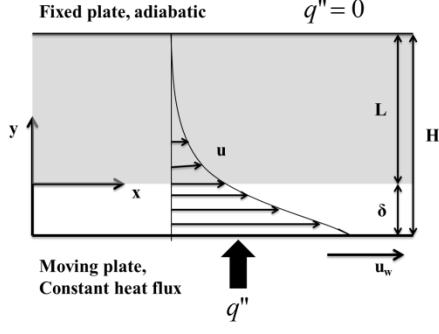
(cont. on next page)

Table 2.1 (cont.)

<p>Auriault [25]</p>	<p>2D Cartesian coordinate system</p>	<p>Darcy Equation</p>	<p>-</p>	<p>B-J Model</p>	<p>Analytical and Experimental</p>	
<p>Poulikakos and Kazmierczak [4]</p>	<p>2D Cartesian coordinate system and Cylindrical coordinate system</p>	<p>Brinkman extended Darcy</p>	<p>Constant heat flux and Constant wall temperature</p>	<p>Continuity of shear stress and Continuity of heat flux</p>	<p>Analytical and Numerical</p>	

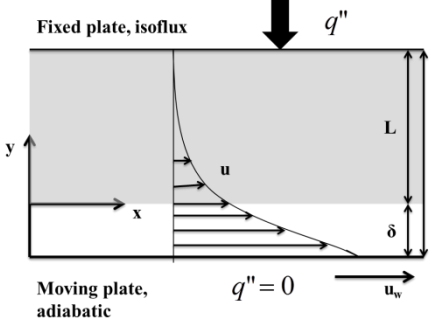

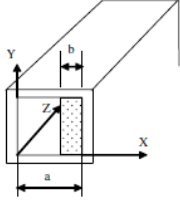
(cont. on next page)

Table 2.1 (cont.)

<p>Al-Nimr and Alkam [5]</p>	<p>2D Cartesian coordinate system</p>	<p>Brinkman Forchhimer extended Darcy</p>	<p>Upper plate subjected to a constant heat flux</p>	<p>Continuity of shear stress and Continuity of heat flux</p>	<p>Numerical</p>	
<p>Guo et al. [6]</p>	<p>2D Cylindrical coordinate system</p>	<p>Brinkman Forchhimer extended Darcy</p>	<p>Constant heat flux</p>	<p>-</p>	<p>Numerical</p>	
<p>Kuznetsov [7]</p>	<p>2D Cartesian coordinate system</p>	<p>Brinkman Forchhimer extended Darcy</p>	<p>Moving plate is subject to a uniform heat flux The fixed plate is adiabatic.</p>	<p>B-J Model Continuity of heat flux</p>	<p>Analytical</p>	


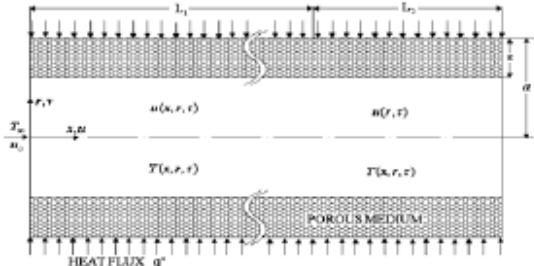
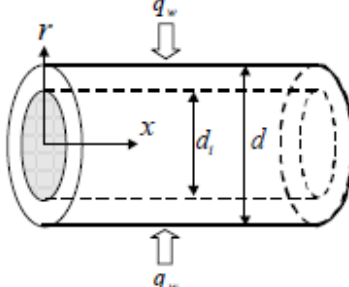
(cont. on next page)

Table 2.1 (cont.)

<p>Kuznetsov [8]</p>	<p>2D Cartesian coordinate system</p>	<p>Brinkman Forchhimer extended Darcy</p>	<p>Moving plate is adiabatic.  The fixed plate is subject to a uniform heat flux</p>	<p>B-J Model  Continuity of heat flux</p>	<p>Analytical</p>	
<p>Mohamad [9]</p>	<p>2D Cartesian coordinate system and Cylindrical coordinate system</p>	<p>Complete momentum equations</p>	<p>Constant wall temperature</p>	<p>-</p>	<p>Numerical  Analytical Eq. given  (No solutions)</p>	
<p>Jen and Yan [10]</p>	<p>3D Cartesian coordinate system</p>	<p>Complete momentum equations</p>	<p>Constant wall temperature</p>	<p>-</p>	<p>Numerical</p>	

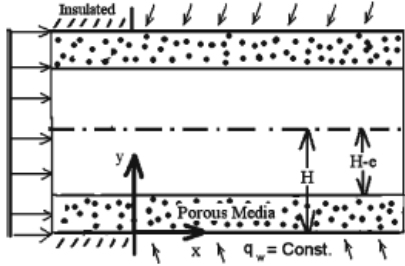
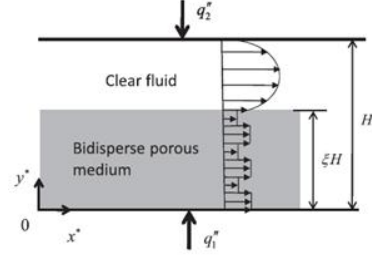
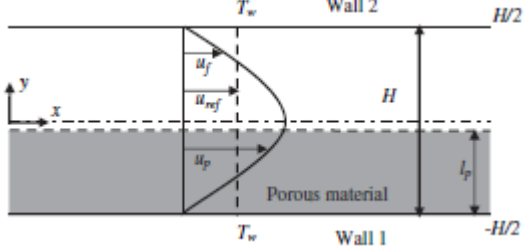
(cont. on next page)

Table 2.1 (cont.)

<p>Morosuk [11]</p>	<p>2D Cylindrical coordinate system</p>	<p>Brinkman Forchhimer extended Darcy</p>	<p>Constant wall temperature</p>	<p>Continuity of shear stress and Continuity of heat flux</p>	<p>Analytical and Numerical</p>	
<p>Sayehvand and Shokouhmand [12]</p>	<p>2D Cylindrical coordinate system</p>	<p>Complete momentum equations</p>	<p>Constant heat flux</p>	<p>-</p>	<p>Numerical</p>	
<p>Yang et al. [13]</p>	<p>2D Cylindrical coordinate system</p>	<p>Brinkman extended Darcy</p>	<p>Constant heat flux</p>	<p>Continuity of shear stress and Continuity of heat flux</p>	<p>Analytical and Numerical</p>	

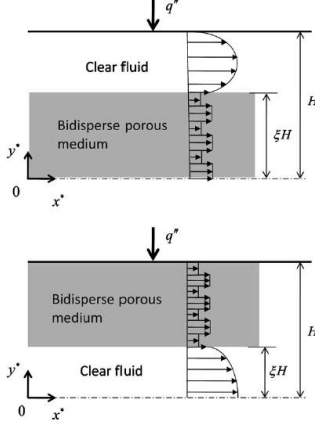
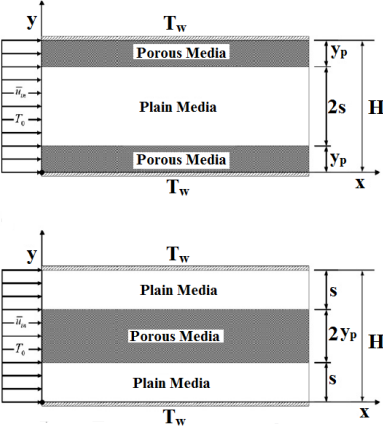
(cont. on next page)

Table 2.1 (cont.)

<p>Forooghi et al. [14]</p>	<p>2D Cartesian coordinate system</p>	<p>Brinkman Forchhimer extended Darcy</p>	<p>Constant Heat Flux.</p>	<p>Continuity of shear stress and a new B.C. is derived</p>	<p>Numerical</p>	
<p>Nield and Kuznetsov [15]</p>	<p>2D Cartesian coordinate system</p>	<p>Darcy's Law</p>	<p>Constant Heat Flux.</p>	<p>B-J Model and Variable Porosity model</p>	<p>Analytical</p>	
<p>Satyamurty and Bhargavi [16]</p>	<p>2D Cartesian coordinate system</p>	<p>Brinkman extended non-Darcy model</p>	<p>Constant wall temperature</p>	<p>B-J Model and Continuity of heat flux</p>	<p>Analytical; Velocity Numerical; Temperature</p>	

(cont. on next page)

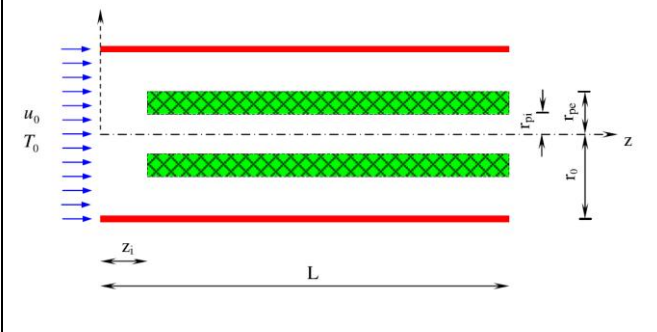
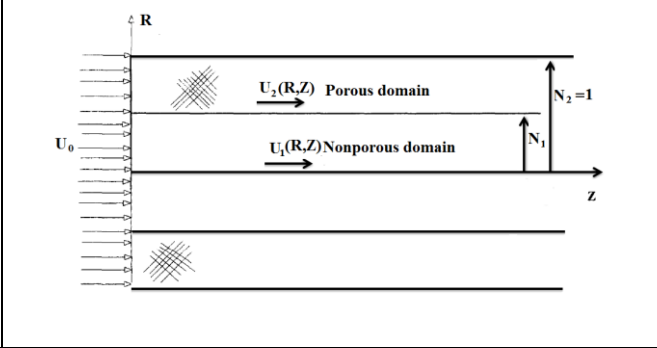
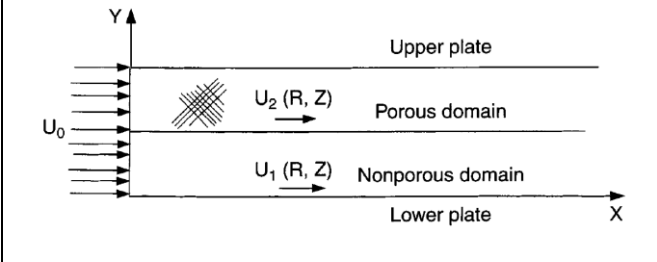
Table 2.1 (cont.)

<p>Kuznetsov and Nield [17]</p>	<p>2D Cartesian coordinate system</p>	<p>Darcy's Law</p>	<p>Constant Heat Flux.</p>	<p>B-J Model and Variable Porosity model</p>	<p>Analytical</p>	
<p>Shokouhmand et al. [18]</p>	<p>2D Cartesian coordinate system</p>	<p>Brinkman extended Darcy model</p>	<p>Constant wall temperature</p>	<p>Analytical Equations taken from [4] and [11]</p>	<p>Numerical</p>	

(cont. on next page)

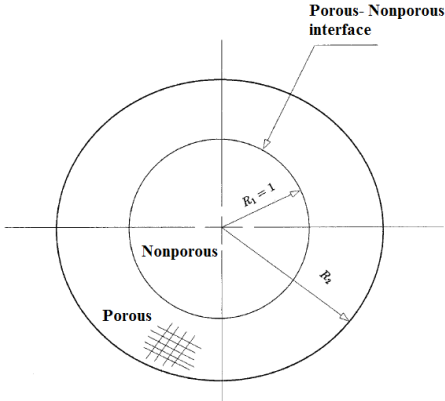
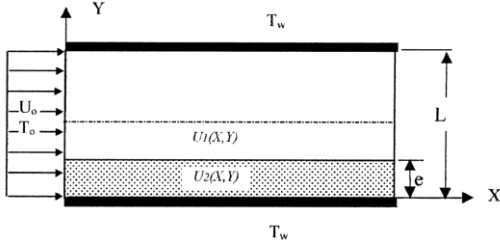
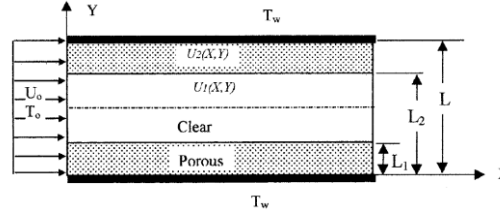


Table 2.1 (cont.)

<p>Teamah et al. [19]</p>	<p>2D Cylindrical coordinate system</p>	<p>Brinkman Forchhimer extended Darcy</p>	<p>Constant wall temperature</p>	<p>-</p>	<p>Numerical</p>	
<p>Alkam and Al-Nimr [26]</p>	<p>2D Cylindrical coordinate system</p>	<p>Brinkman Forchhimer extended Darcy</p>	<p>Constant wall temperature</p>	<p>Continuity of shear stress and Continuity of heat flux</p>	<p>Numerical</p>	
<p>Al-Nimr and Alkam [27]</p>	<p>2D Cartesian coordinate system</p>	<p>Brinkman extended Darcy</p>	<p>Constant heat flux and Constant wall temperature</p>	<p>Continuity of shear stress and Continuity of heat flux</p>	<p>Analytical and Numerical</p>	

(cont. on next page)

Table 2.1 (cont.)

<p>Alkam and Al-Nimr [28]</p>	<p>2D Cylindrical coordinate system</p>	<p>Complete momentum equations</p>	<p>Constant wall temperature</p>	<p>Continuity of shear stress and Continuity of heat flux</p>	<p>Analytical</p>	
<p>Alkam et al. [29]</p>	<p>2D Cartesian coordinate system</p>	<p>Brinkman Forchhimer extended Darcy</p>	<p>Constant wall temperature</p>	<p>Continuity of shear stress and Continuity of heat flux</p>	<p>Numerical</p>	
<p>Alkam et al. [30]</p>	<p>2D Cartesian coordinate system</p>	<p>Brinkman Forchhimer extended Darcy</p>	<p>Constant wall temperature</p>	<p>Continuity of shear stress and Continuity of heat flux</p>	<p>Numerical</p>	

## CHAPTER 3

### BASIC CONCEPTS

Porous medium is basically material containing voids between some particulate phases. Groundwater flows, or blood flowing into the lungs are examples of the fluid flow through a porous medium. Before discussing the appropriate modeling equations, it might be useful to review the commonly used terms in porous media.

Figure 3.1 shows a sample of the porous media studied in some chapter of this thesis. It consists of two phase as solid phase (impermeable rigid material) and fluid phase. The studied fluid in this study is assumed Newtonian fluid.

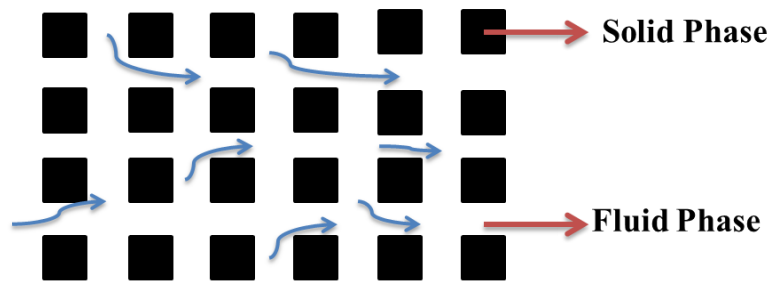


Figure 3.1. Schematic demonstration of a porous medium

The microscopic analysis which has to be done for each voids or particulate substance may not be appropriate due to the difficulty of determination of velocity and heat transfer mechanisms in each void or solid in the porous media. That's why; fluid flow through porous medium is analyzed in terms of the method of volume averaging which is called as "macroscopic approach". Figure 3.2 shows the fluid flow from microscopic and macroscopic view of point. As is seen, for microscopic analysis of fluid flow in a porous media, flow in each direction should be considered. Unlike the microscopic approach, macroscopic approach of the fluid flow in porous medium provides taking unidirectional flow through the porous channels as seen in Figure 3.2 (b). In this study, all presented governing equations have been derived based on

macroscopic assumption. So the reader should be aware of that the flow parameters such as  $u$ ,  $v$ ,  $T$ ,  $P$  are averaging quantities.

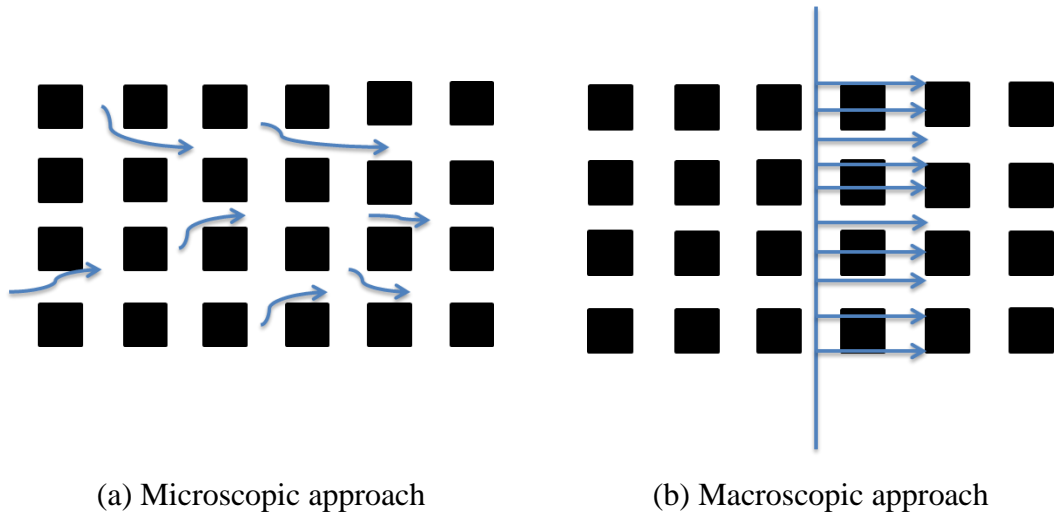


Figure 3.2. Microscopic and macroscopic view

### 3.1. Porosity, Permeability and Fluid Flow in Porous Media

Darcy's law is the basic law to define in the macroscopic view of the fluid flow in the porous medium. By considering a control volume of porous medium, let the fluid flow through the control volume is  $Q$ , and the cross section area of the control volume is  $A$ , thus the superficial velocity  $U_0$ , is the total flow rate divided by cross section area.

$$\vec{U}_0 = \frac{Q}{A} \quad (3.1)$$

The presence of the solid particles within the control volume reduces the area available for fluid flow. The fluid has to squeeze through smaller area to preserve fluid continuity with the entering superficial flow. Hence the velocity within the control volume named "pore velocity,  $U^f$ " will be greater than the superficial velocity and defined with volume fraction of solids. Void fraction of a porous media is volume of voids between solids divided by total porous media volume. The void fraction is called as the *porosity* of the porous medium. Porosity is shown with  $\epsilon$ .

$$\varepsilon = \frac{V_f}{V_t} \quad (3.2)$$

As it can be seen in Equation 3.2, porosity can be calculated as the ratio of the volume occupied by the fluid  $V_f$ , to the total volume  $V_t$ . The pore velocity can be found from the following relation:

$$\vec{U}^f = \frac{\vec{U}_0}{\varepsilon} \quad (3.3)$$

Porosity can be related to resistance to fluid flow through the porous medium. Considering Equation 3.3, it is obvious that when no solid are present, the porosity equals unity and that brings the pore velocity will be the same as the superficial velocity. On the other hand, when the control volume is full of solids, porosity becomes zero and the resistance in the channel becomes infinity. For a porous medium with uniform porosity distribution, the resistance to fluid flow due to the porosity increases pressure drop along the channel. So, it can be said that the porosity in a channel with uniform porosity causes a pressure gradient with respect to distance. Henry Darcy (1803-1858) observed this pressure gradient over sand filters at France during [3] and concluded that macroscopic velocity of the porous medium is directly proportional to the pressure gradient established along the channel and the permeability of the space and inversely proportional to the viscosity of the fluid. So Darcy stated the following equation to define macroscopic velocity in the porous channels:

$$\frac{\mu}{K} \vec{U}_0 = - \frac{d\vec{P}}{dx} \quad (3.4)$$

where  $\mu$  stands for the dynamic viscosity of fluid flows in the void between solids and  $K$  is the permeability in Equation 3.4. The permeability is a feature of porous media permits for flowing of the fluid. There are many numerical and numerical studies for determination of permeability for different types of porous media. Many relations have been suggested by researchers. However, the most common relation is the equation

called as Carmen-Kozeny relation. The equation depends on the shape of the porous medium in channel [31] as:

$$K = \frac{\varepsilon^3 H^2}{\bar{k}(1-\varepsilon)^2} \quad (3.5)$$

where  $\bar{k}$  is the Kozeny constant and H is characteristic length. Darcy equation (Equation 3.4) is not sufficient for all systems. A modification should be done for boundary effects particularly for internal flow. The modified Darcy equation called as Brinkman-extended Darcy law:

$$\mu_{eff} \frac{d^2 \bar{U}_0}{dy^2} - \frac{\mu}{K} \bar{U}_0 = \frac{d\bar{P}}{dx} \quad (3.6)$$

The constant of  $\mu_{eff}$  seen in Equation 3.6 is “effective dynamic viscosity”, which depends on fluid and structure of the porous medium. The ratio between effective dynamic viscosity,  $\mu_{eff}$  and fluid dynamic viscosity can be found with the help of porosity [3]:

$$\frac{\mu_{eff}}{\mu} = \frac{1}{\varepsilon} \quad (3.7)$$

Darcy equation is also insufficient for high velocity problems in porous media. The inertial effects should be considered when the analysis is made for high velocity flows. Another modification should be done to observe the inertial effects of the porous medium. Therefore the final form of the Darcy equation is:

$$\mu_{eff} \frac{d^2 \bar{U}_0}{dy^2} - \frac{\mu}{K} \bar{U}_0 - \frac{d\bar{P}}{dx} - \frac{\rho F}{K^{1/2}} \bar{U}_0^2 = 0 \quad (3.8)$$

The first term in the above equation is Brinkman term, the second and third terms are Darcy law and finally the fourth term includes the effect of inertial forces. The new parameter,  $F$ , is the Forchheimer constant and stands for the inertial

contribution of the porous medium. For most of the studies, the Brinkman-Forchheimer extension of the Darcy law is used to describe fluid flow through a porous medium. It is possible to account for non-Darcian effects, which are of importance in many engineering applications by using this form of motion equation. The Brinkman term describes viscous effects and adds possibility to apply a nonslip boundary condition at the walls of a considered channel. The Forchheimer term describes forming drag of the channels, and counting for this term is important for high flow velocity. In this thesis, the Brinkman extended Darcy Law is considered to determine the fluid flow field in the porous medium due to the small velocities are assumed during the analysis.

### 3.2. Heat Transfer Analysis in Porous Media

The flow is steady, two dimensional and the assumption of neglecting viscosity is considered throughout the study. The working fluid is Newtonian and flow is thermally developed. As the first law of thermodynamics states, the total energy of the system should be conserved. So there is a thermal equilibrium between fluid and solid material. The energy balance of the system:

$$\rho C_p \left( u \frac{\partial T}{\partial x} + v \frac{\partial T}{\partial y} \right) = k_{eff} \left( \frac{\partial^2 T}{\partial x^2} + \frac{\partial^2 T}{\partial y^2} \right) \quad (3.9)$$

The new term  $k_{eff}$  is the effective thermal conductivity and can be found with the help of porosity and conductivities of solid and fluid in the flow as:

$$k_{eff} = \varepsilon k_f + (1 - \varepsilon)k_s \quad (3.10)$$

In Equation 3.9, the gradient of temperature in x direction is much greater than temperature gradient in y-direction. Hence, under the fully developed assumption, the final form of the energy equation for porous media is:

$$\rho C_p \left( u \frac{\partial T}{\partial x} \right) = k_{eff} \left( \frac{\partial^2 T}{\partial y^2} \right) \quad (3.11)$$

### 3.3. Theoretical Background of the Forced Convection in the Clear Fluid Channel

Brief information about forced convection in clear fluid flow should be given to simplify the comprehension of the study. The given equations are to define an incompressible, hydrodynamically and thermally fully developed clear fluid channel. The  $v$  velocity component of the flow is zero. The laminar flow is considered and the fluid is considered as Newtonian. The fluid flow equation which is driven from Navier-Stokes equations for channel with height of  $2H$ , and its boundary conditions can be written as [32]:

$$\mu \frac{\partial^2 u}{\partial y^2} - \frac{\partial P}{\partial x} = 0 \quad u(\pm H) = 0 \quad (3.12)$$

The heat flow analysis equation for clear fluid channel which have height of  $2H$  can be written as Equation 3.13. The viscous dissipation terms are neglected and it is assumed that the temperature gradient term in  $y$ -direction is much greater than temperature gradient term in  $x$ -direction. The final form of the energy equation for clear fluid flow is [32]:

$$(\rho C_p)_f u \frac{\partial T}{\partial x} = k_f \frac{\partial^2 T}{\partial y^2} \quad (3.13)$$

The subscript of  $f$  stands for to show the parameters belong to the fluid. The energy equation for clear flow channel and porous channel is almost the same except the effective thermal conductivity term in Equation 3.11.

As the Newton's law of cooling stated, the heat flux per unit area  $q''$  is proportional to the temperature difference:



$$q'' = h(T_w - T) \quad (3.14)$$

The dimensionless form of the heat transfer coefficient  $h$  is called as  $Nu$ . It is defined as the ratio of convection heat transfer to fluid conduction heat transfer. If a layer with length of  $L$  is considered as a moving plate than the problem is convection so the Equation 3.14 is valid. However, if the problem is about a layer with length of  $L$  which is static then the problem becomes conduction problem so:

$$q'' = k(T_w - T) / L \quad (3.15)$$

So the  $Nu$  is the ratio of Equation 3.14 and 3.15:

$$Nu = \frac{hL}{k} \quad (3.16)$$

Our considered problem is the layer of problem  $L$  taken as  $2H$ :

$$Nu = \frac{h 2H}{k} \quad (3.17)$$

The  $Nu$  for forced convection in parallel plate clear fluid channel with symmetrical constant heat flux boundary condition is known as [32]:

$$Nu = 4.1176 \quad (3.18)$$

The pressure drop along the clear fluid channel can be calculated with the help of friction factor " $f$ ". If we consider a channel which has the mean velocity of  $u_{mean}$ , the friction factor for this channel can be written as:

$$f = \frac{\left(-\frac{dP}{dx}\right)2H}{\frac{1}{2}\rho u_m^2} \quad (3.19)$$

By finding dimensionless mean velocity and making some mathematical manipulations the multiplication of Reynolds number and friction factor is found as 24 [32] for the clear fluid channel. This result will be used to compare the pressure drop between the fulfilled and partially filled porous channels.

## CHAPTER 4

### **DIMENSIONAL STUDY ON CHANNEL COMPLETELY FILLED WITH POROUS MEDIUM, ASYMMETRIC HEAT FLUX BOUNDARY CONDITION**

In this chapter, the dimensional heat and fluid flow equations for a channel completely filled with porous medium are presented. The boundary conditions are also written. These equations with the presented boundary conditions are solved numerically. The numerical solution method is described in Chapter 8. The obtained results from numerical dimensional solution are presented in Chapter 9.

#### **4.1. The Considered Problem**

The considered channel is shown in Figure 4.1. The distance between the plates is  $2H$ . An incompressible, hydrodynamically and thermally fully developed and steady flow in a channel bounded by two parallel plates is considered. The flow is laminar and the fluid is assumed to be Newtonian. The viscous dissipation terms are neglected and it is also assumed that the temperature gradient in  $y$ -direction is much greater than it is in  $x$ -direction. The Brinkman-Darcy equation and energy equation for a channel completely filled with porous medium are given. The porous medium is considered as isotropic with permeability of constant  $K$ . The upper and lower channel walls are subjected to asymmetric heat flux boundary condition. The uniform heat fluxes are denoted as  $q''_{w1}$  and  $q''_{w2}$ , they have opposite sides (-) and (+) respectively.

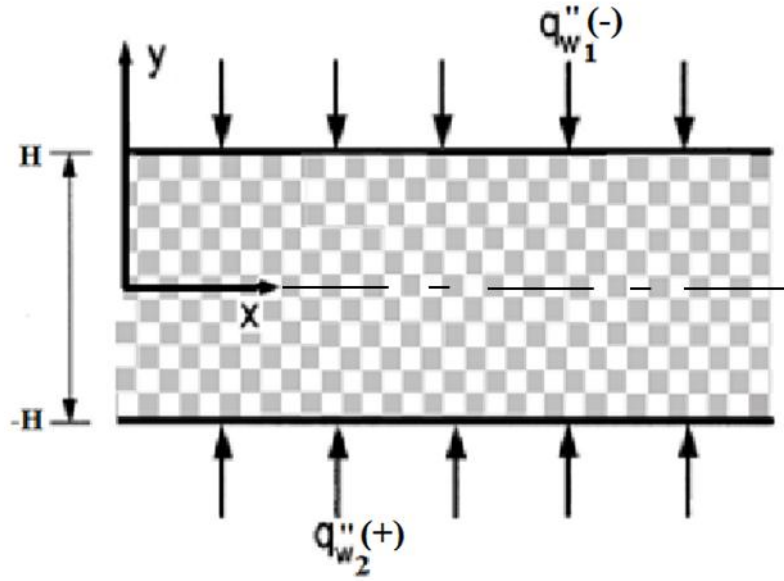


Figure 4.1. Schematic view of the considered channel

## 4.2. Mathematical Formulation and Governing Equations

### 4.2.1. Fluid Flow Analysis

The flow in the channel considered as hydrodynamically and thermally fully developed, laminar and unidirectional which is parallel to the x-axis. The y- component of velocity is zero so it can be written that:

$$v = 0, \quad \frac{\partial u}{\partial x} = 0, \quad \frac{\partial P}{\partial y} = 0 \quad (4.1)$$

According to assumptions mentioned, the appropriate Brinkman –extended Darcy Equation as written below.

$$\mu_{eff} \frac{d^2 u}{dy^2} - \frac{\mu}{K} u - \frac{dP}{dx} = 0 \quad (4.2)$$

In Equation (4.2)  $\mu_{eff}$  represents the effective viscosity of fluid and the porous structures,  $\mu$  is dynamic viscosity of the fluid,  $K$  is the permeability of the porous medium. The ratio of effective dynamic viscosity and the dynamic viscosity of fluid can be written as follows:

$$\frac{\mu_{eff}}{\mu_f} = \frac{1}{\varepsilon} \quad (4.3)$$

In Equation (4.3), subscripts  $f$  and  $s$  refer to the fluid and solid substrate, respectively. The term “ $\varepsilon$ ” which is seen in Equation (4.3) is porosity. The porosity can be found as the ratio of the volume occupied by the fluid to the total volume.

$$\varepsilon = \frac{V_f}{V} \quad (4.4)$$

It can be assumed that the maximum velocity should be in the middle of channel and no-slip conditions at the channel walls. So we can write the boundary conditions to solve the Equation (4.5) as:

$$\begin{aligned} y = H &\Rightarrow u = 0 \\ y = -H &\Rightarrow u = 0 \\ \left. \frac{\partial u}{\partial y} \right|_{y=0} &= 0 \end{aligned} \quad (4.5)$$

The mean velocity of the fluid in the channel can be calculated by using following definition as Equation (4.6).

$$u_{mean} = \frac{\int_{-H}^H u dy}{\int_{-H}^H dy} \quad (4.6)$$

## 4.2.2. Heat Flow Analysis

Under the assumptions of neglecting viscous dissipation effect and heat generation, final form of the energy equation:

$$(\rho C_p)_f u \frac{\partial T}{\partial x} = k_{eff} \frac{\partial^2 T}{\partial y^2} \quad (4.7)$$

where  $\rho$  is density,  $C_p$  is specific heat at constant pressure and  $k_{eff}$  indicates the effective conductivity of the fluid and solid porous material. The effective conductivity can be written as Equation (4.8).

$$k_{eff} = \varepsilon k_f + (1 - \varepsilon)k_s \quad (4.8)$$

The boundary conditions for defined energy equation can be written by using the fluxes on the wall so they can be written as:

$$\begin{aligned} y = +H &\Rightarrow q''_{w1} = -k_{eff} \left. \frac{\partial T}{\partial y} \right|_{y=H} \\ y = -H &\Rightarrow q''_{w2} = -k_{eff} \left. \frac{\partial T}{\partial y} \right|_{y=-H} \\ x = 0 &\Rightarrow T = T_i \end{aligned} \quad (4.9)$$

The given equations for the considered problem are solved numerically and the results will be given in Chapter 9. The boundary condition at  $x = 0$  for the Equation (4.7) is considered as the entrance temperature of the fluid to the channel.

## 4.2.3. Pressure Drop Calculation

Pressure drop calculation for dimensional problem is done by numerically. Calculations start with a given specific flow rate and an assumed negative pressure

gradient value. Equation (4.2) and related boundary conditions, Equation (4.5), are solved numerically with using this assumed pressure gradient value. The mean velocity is calculated by numerically with using the solution of Equation (4.2).The calculation continues until the mean velocity which is found by the solution of Equation (4.2) converges to the given specific flow rate.

## CHAPTER 5

### **DIMENSIONLESS STUDY ON CHANNEL COMPLETELY FILLED WITH POROUS MEDIUM: ASYMMETRIC HEAT FLUX BOUNDARY CONDITION**

In this chapter, the dimensionless form of the heat and fluid flow equations for a channel filled with porous medium and an asymmetric heat flux boundary condition are presented. The dimensionless boundary conditions are also written. These equations with the presented boundary conditions are solved analytically and the obtained mathematical expressions for velocity, temperature, Nu and pressure gradient are also presented. The results of the solutions are shown in Chapter 9.

#### **5.1. The Considered Problem**

Figure 5.1 depicts the schematic diagram of the problem. The Brinkman-Darcy equation and energy equation are solved for a channel completely filled with porous medium. The upper and lower channel walls are subjected to asymmetric heat flux boundary condition. The uniform heat fluxes are denoted as  $q''_{w1}$  and  $q''_{w2}$ . They have opposite sides (-) and (+) respectively.



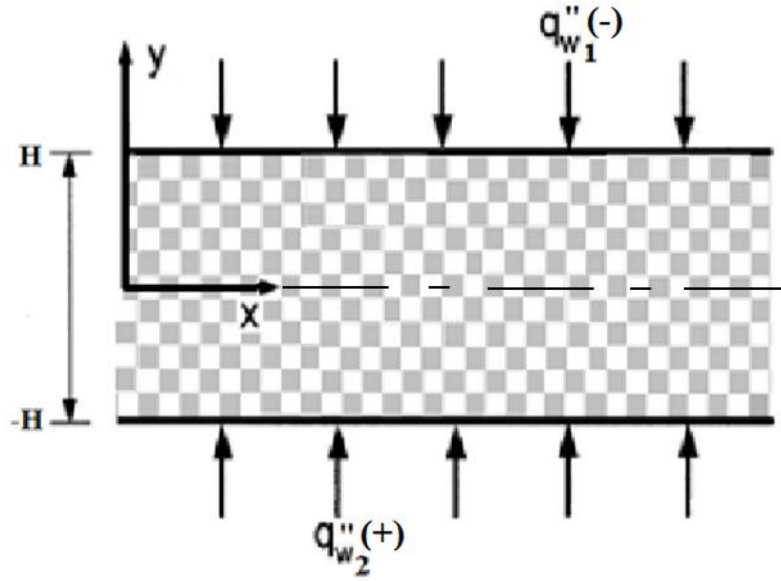


Figure 5.1. Schematic view of the considered channel

An incompressible, hydrodynamically and thermally fully developed and steady flow in a channel bounded by two parallel plates is considered. The distance between the plates is  $2H$ . The fluid is assumed to be Newtonian and its thermophysical properties are assumed to be constant. The porous medium is considered as isotropic with permeability of constant  $K$ . The viscous dissipation terms are neglected and also it is assumed that the temperature gradient in  $y$ -direction is much greater than it is in  $x$ -direction.

## 5.2. Mathematical Formulation and Governing Equations

### 5.2.1. Fluid Flow Analysis

Considering Figure 5.1, since flow in the channel is hydrodynamically fully developed, laminar and unidirectional  $u = u(y)$ , which is parallel to the  $x$ -axis, the following assumptions can be made:

$$v = 0, \quad \frac{\partial u}{\partial x} = 0, \quad \frac{\partial P}{\partial y} = 0 \quad (5.1)$$

The  $v$  parameter which is the velocity in  $y$ -direction it cancels out. So the considered problem can be analyzed by using Brinkman –extended Darcy Equation as written below:

$$\mu_{eff} \frac{d^2u}{dy^2} - \frac{\mu}{K}u - \frac{dP}{dx} = 0 \quad (5.2)$$

where  $\mu_{eff}$  represents the effective viscosity of fluid and the porous structures,  $\mu$  is dynamic viscosity of the fluid. At this point the boundary conditions for the Equation (5.2) should be defined. Equation (5.3) indicates the boundary conditions for the Equation (5.2).

$$\begin{aligned} y = H &\Rightarrow u = 0 \\ y = -H &\Rightarrow u = 0 \\ \left. \frac{\partial u}{\partial y} \right|_{y=0} &= 0 \end{aligned} \quad (5.3)$$

The following non-dimensional variables have been introduced to obtain dimensionless form of the Brinkman-extended Darcy equation, Equation (5.2).

$$Y = \frac{y}{H}, \quad M = \frac{\mu_{eff}}{\mu}, \quad G = -\frac{\partial P}{\partial x}, \quad Da = \frac{K}{H^2}, \quad U = \frac{\mu u}{GH^2} \quad (5.5)$$

The  $G$  term which is seen at dimensionless velocity parameter indicates the negative pressure gradient along the axis. By using defined dimensionless parameters, the governing equation, Equation (5.2), transforms into the following form.

$$M \frac{d^2U}{dY^2} - \frac{1}{Da}U + 1 = 0 \quad (5.6)$$

At this point another parameter which is porous media shape factor,  $S$ , can be defined by Equation (5.7). By combining this coefficient with the Equation (5.6), final

form of the dimensionless Brinkman-extended Darcy equation can be rewritten as Equation (5.8).

$$S = \frac{1}{\sqrt{M Da}} \quad (5.7)$$

$$\frac{d^2U}{dY^2} - S^2U + \frac{1}{M} = 0 \quad (5.8)$$

To find a dimensionless form of boundary conditions Equation (5.5) can be used again and the final form of boundary conditions can be obtained as;

$$\begin{aligned} Y = 1 &\Rightarrow U = 0 \\ Y = -1 &\Rightarrow U = 0 \\ \left. \frac{\partial U}{\partial Y} \right|_{Y=0} &= 0 \end{aligned} \quad (5.9)$$

Now, solving Equation (5.8) with using Equation (5.9) gives the dimensionless velocity distribution as;

$$U(Y) = \frac{1 - \text{Cosh}(S Y) \text{Sech}(S)}{MS^2} \quad (5.10)$$

The mean velocity of the fluid in the channel can be calculated by using following definition as Equation (5.11).

$$u_{mean} = \frac{\int_{-H}^H u dy}{\int_{-H}^H dy} \quad (5.11)$$

The dimensionless parameter can be used again to derive a dimensionless mean velocity definition which is:

$$U_m = \frac{1}{2} \int_{-1}^{+1} U(Y) dY \quad (5.12)$$

According to this definition, the expression for dimensionless mean velocity can be found:

$$U_m = \frac{S - \text{Tanh}(S)}{MS^3} \quad (5.13)$$

The normalized velocity can be calculated by dividing Equation (5.10) to the Equation (5.13) which gives Equation (5.14).

$$\hat{u} = \frac{S(-1 + \text{Cosh}(SY) \text{Sech}(S))}{-S + \text{Tanh}(S)} \quad (5.14)$$

### 5.2.2. Heat Flow Analysis

The energy equation, while neglecting viscous dissipation effect and heat generation, may be written under the assumptions such as hydrodynamically and thermally fully developed laminar flow channel as:

$$(\rho C_p)_f u \frac{\partial T}{\partial x} = k_{eff} \frac{\partial^2 T}{\partial y^2} \quad (5.15)$$

where  $\rho$  is density,  $C_p$  is specific heat at constant pressure and  $k_{eff}$  indicates the effective conductivity of the fluid and solid porous material. For obtaining dimensionless form of energy equation firstly we should define the average wall temperature  $T_{w\mu}$ , the average wall heat flux,  $q''_{\mu}$  and the dimensionless temperature such as:

$$T_{w\mu} = \frac{T_{w1} + T_{w2}}{2}, \quad q''_{\mu} = \frac{q''_{w1} + q''_{w2}}{2}, \quad \theta = \frac{T - T_{w\mu}}{T_m - T_{w\mu}} \quad (5.16)$$

The mean temperature  $T_m$  which is seen in Equation (5.16) can be defined as:

$$T_m = \frac{\int_{-1}^1 \rho C_p u T dy}{\int_{-1}^1 \rho C_p u dy} \quad (5.17)$$

Writing the dimensionless temperature definition, Equation (5.16), and the other dimensionless variables Equation (5.5) onto the Equation (5.15) gives the following form:

$$(\rho C_p)_f u \left[ \frac{\partial T_{w\mu}}{\partial x} + \theta \left( \frac{\partial T_m}{\partial x} - \frac{\partial T_{w\mu}}{\partial x} \right) + (T_m - T_{w\mu}) \frac{\partial \theta}{\partial x} \right] = k_{eff} (T_m - T_{w\mu}) \frac{\partial^2 \theta}{\partial Y^2} \quad (5.18)$$

If we consider the heat fluxes are constant and the gradient of the wall heat fluxes with respect to x-direction must be zero, the followings can be written:

$$\begin{aligned} \frac{dq''_1}{dx} = \frac{d[h(T_{w1} - T_m)]}{dx} = 0 &\Rightarrow \frac{dT_{w1}}{dx} = \frac{dT_m}{dx} \\ \frac{dq''_2}{dx} = \frac{d[h(T_{w2} - T_m)]}{dx} = 0 &\Rightarrow \frac{dT_{w2}}{dx} = \frac{dT_m}{dx} \\ \frac{dT_{w1}}{dx} + \frac{dT_{w2}}{dx} = \frac{d(T_{w1} + T_{w2})}{dx} = 2 \frac{dT_{w\mu}}{dx} = 2 \frac{dT_m}{dx} &\Rightarrow \frac{dT_{w\mu}}{dx} = \frac{dT_m}{dx} \end{aligned} \quad (5.19)$$

The thermally and hydrodynamically fully developed assumption brings the dimensionless temperature gradient in x-direction be zero. By using this assumption and Equation (5.19), the energy equation becomes:

$$(\rho C_p)_f u \frac{\partial T_m}{\partial x} = k_{eff} (T_m - T_{w\mu}) \frac{\partial^2 \theta}{\partial Y^2} \quad (5.20)$$

If we consider a differential volume such as Figure 5.2 the total energy of the fluid is conserved. It should be reminded that there is no heat generation.

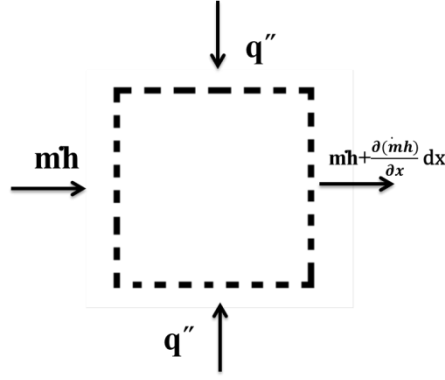


Figure 5.2. Differential volume from the considered duct

The energy entering must be equal to the energy leaving the boundaries so:

$$2H \rho u_m C_p T_m + q''_{w1} dx + q''_{w2} dx = 2H \rho u_m C_p T_m + \frac{\partial(2H \rho u_m C_p T_m)}{\partial x} dx \quad (5.21)$$

$$\frac{q''_{w1} + q''_{w2}}{2} = H \rho u_m C_p \frac{dT_m}{dx} \Rightarrow \frac{dT_m}{dx} = \frac{q''_{w\mu}}{H \rho u_m C_p}$$

The definition of overall Nu is considered as applied heat fluxes at the walls will be transferred to the fluid. The heat transfer rate to the fluid can be also expressed as equation (5.22):

$$Nu = \frac{h 2H}{k_{eff}} \quad (5.22)$$

$$q_{\mu}'' = h(T_{w\mu} - T_m)$$

The overall Nu for the considered problem can be defined as:

$$Nu = \frac{2Hq_{\mu}''}{k_{eff}(T_{w\mu} - T_m)} \quad (5.23)$$

At this point after some mathematical manipulation with Equation (5.18), Equation (5.21) and using the definition of overall Nu yields the following second order ordinary differential equations:

$$\frac{\partial^2 \theta}{\partial Y^2} + \frac{1}{2} \hat{u} Nu = 0 \quad (5.24)$$

Two boundary conditions are needed to solve second order ordinary differential equation shown above, so according to considered problem another parameter for specifying boundary temperature can be defined such as:

$$\beta = \frac{T_{w2} - T_{w1}}{2(T_m - T_{w\mu})} \quad (5.25)$$

By considering the definition of  $\beta$ , the related boundary conditions can be given as:

$$\begin{aligned} Y = 1 &\Rightarrow \theta = -\beta \\ Y = -1 &\Rightarrow \theta = \beta \end{aligned} \quad (5.26)$$

When the dimensionless heat transfer equation, Equation (5.24), solve with related boundary conditions, Equation (5.26), the equation for dimensionless temperature distribution can be found like:

$$\theta(Y) = \frac{-\beta Y + Nu (2\text{Cosh}(SY) + \text{Cosh}(S)(-2 + S^2 - S^2 Y^2))}{4S(S \text{Cosh}(S) - \text{Sinh}(S))} \quad (5.27)$$

If we want to investigate the distribution of dimensionless temperature according to Equation (5.27), we should find more clear definition for  $\beta$ , for that reason we can use the heat fluxes at the walls and making the fluxes dimensionless as:

$$\begin{aligned} q''_{w1} &= -k_{eff} \left. \frac{\partial T}{\partial y} \right|_{y=H} = -k_{eff} \frac{(T_m - T_{w\mu})}{H} \left. \frac{\partial \theta}{\partial Y} \right|_{Y=1} \\ q''_{w2} &= -k_{eff} \left. \frac{\partial T}{\partial y} \right|_{y=-H} = -k_{eff} \frac{(T_m - T_{w\mu})}{H} \left. \frac{\partial \theta}{\partial Y} \right|_{Y=-1} \end{aligned} \quad (5.28)$$

If another dimensionless parameter  $q_r$  is defines as the ratio between  $q''_{w1}$  and  $q''_{w2}$ , the relation between in Equation (5.28) gives another definition for  $\beta$  in terms of  $q_r$ :

$$\beta = \frac{Nu}{2} \left( \frac{q_r + 1}{q_r - 1} \right) \quad (5.29)$$

To obtain an expression for Nu we can use the compatibility condition[32]:

$$\int_{-1}^1 \theta \hat{u} dY = 2 \quad (5.30)$$

The dimensionless temperature and the normalized velocity were found in Equation (5.27) and Equation (5.14). So the overall Nu can be found as:

$$Nu = \frac{24S(S \text{Cosh}(S) - \text{Sinh}(S))^2}{15 \text{Sinh}(2S) + (4S^3 - 24S) \text{Cosh}^2(S) - 6S} \quad (5.31)$$

The definition of individual Nu for each wall can be expressed as by using overall Nu expression.

$$Nu_1 = -\frac{2Hq''_{w1}}{k_{eff}(T_{w1} - T_m)} \quad (5.32)$$

$$Nu_2 = -\frac{2Hq''_{w2}}{k_{eff}(T_{w2} - T_m)}$$

We can apply the conservation of energy onto each wall which gives:

$$h(T_m - T_{w1}) = k_{eff} \frac{(T_m - T_{w\mu})}{H} \frac{\partial \theta}{\partial Y} \Big|_{Y=1}$$

$$h(T_m - T_{w2}) = k_{eff} \frac{(T_m - T_{w\mu})}{H} \frac{\partial \theta}{\partial Y} \Big|_{Y=-1} \quad (5.33)$$



To determine the individual Nu the following mathematical manipulations are done with using Equation (5.33):

$$\begin{aligned}
\left. \frac{\partial \theta}{\partial Y} \right|_{Y=1} &= \frac{h H (T_m - T_{w1})}{k_{eff} (T_m - T_{w\mu})} = \frac{1}{2} Nu_1 \frac{(T_m - T_{w1})}{(T_m - T_{w\mu})} \\
&= \frac{1}{2} Nu_1 \frac{\left( T_m - \frac{T_{w1}}{2} - \frac{T_{w1}}{2} + \frac{T_{w2}}{2} - \frac{T_{w2}}{2} \right)}{(T_m - T_{w\mu})} = \frac{1}{2} Nu_1 \frac{\left( T_m - T_{w\mu} + \frac{T_{w2} - T_{w1}}{2} \right)}{(T_m - T_{w\mu})} \\
&= \frac{1}{2} Nu_1 (1 + \beta)
\end{aligned} \tag{5.34}$$

The same procedure can be applied to the lower wall so:

$$\begin{aligned}
\left. \frac{\partial \theta_p}{\partial Y} \right|_{Y=-1} &= \frac{h H (T_m - T_{w2})}{k_{eff} (T_m - T_{w\mu})} = \frac{1}{2} Nu_2 \frac{(T_m - T_{w2})}{(T_m - T_{w\mu})} \\
&= \frac{1}{2} Nu_2 \frac{\left( T_m - \frac{T_{w2}}{2} - \frac{T_{w2}}{2} + \frac{T_{w1}}{2} - \frac{T_{w1}}{2} \right)}{(T_m - T_{w\mu})} = \frac{1}{2} Nu_2 \frac{\left( T_m - T_{w\mu} + \frac{T_{w1} - T_{w2}}{2} \right)}{(T_m - T_{w\mu})} \\
&= \frac{1}{2} Nu_2 (1 - \beta)
\end{aligned} \tag{5.35}$$

By using Equation (5.34), Equation (5.35), and Equation (5.27) with Equation (5.29) gives following individual Nu equations:

$$\begin{aligned}
Nu_1 &= -\frac{4 Nu q_r}{-2 + Nu + q_r (Nu + 2)} \\
Nu_2 &= \frac{4 Nu}{2 + Nu + q_r (Nu - 2)}
\end{aligned} \tag{5.36}$$

### 5.2.3. Pressure Drop Calculations

It can be predictable that the porous media in the channel brings pressure drop increments. To calculate this pressure drop in the channel, friction factor  $f$  can be defined. If we consider a channel which has the mean velocity of  $u_{mean}$ , the friction factor for this channel can be written as:

$$f = \frac{\left(-\frac{dP}{dx}\right)2H}{\frac{1}{2}\rho u_m^2} \quad (5.37)$$

According to fully developed assumption, the flow has a constant pressure gradient along the x-axis and this negative gradient is denoted by  $G$ , as given in dimensionless parameters, Equation (5.5), so:

$$f = \frac{4GH}{\rho u_m^2} \quad (5.38)$$

The definition of dimensionless velocity, Equation (5.5), brings more clear equation for friction factor.

$$f = \frac{4}{U_m} \frac{\mu}{\rho u_m H} \quad (5.39)$$

With using the definition of Reynolds number for internal flow final form for the equation of friction factor can be written as the following form.

$$f \text{ Re} = \frac{8}{U_m} \quad (5.40)$$

The mean velocity term was found like Equation (5.13), so by using Equation (5.40) the friction factor for specified Reynolds number can be found as:

$$f \text{ Re} = \frac{8}{Da \left( 1 - \frac{\text{Tanh}(S)}{S} \right)} \quad (5.41)$$

## CHAPTER 6

### **DIMENSIONAL STUDY ON CHANNEL PARTIALLY FILLED WITH POROUS MEDIUM; SYMMETRIC HEAT FLUX BOUNDARY CONDITION**

In this chapter, a channel which is partially filled with porous medium is investigated numerically. The porous medium layer is mounted to a one wall while the other wall of the channel is in contact with clear fluid. The dimensional heat and fluid flow equations and appropriate boundary conditions are presented. The numerical solution method is described in Chapter 8. The obtained results are presented in Chapter 9.

#### **6.1. The Considered Problem**

The considered channel is partially filled with porous medium. As it can be seen in Figure 6.1., the distance between the plates is  $2H$ . A new variable,  $\zeta$ , represents the distance between core of the channel and layer of interface. The value of  $\zeta$  changes between  $-H$  and  $+H$ . The porous medium is considered as isotropic with permeability of constant  $K$ . An incompressible, hydrodynamically and thermally fully developed and steady flow in a channel bounded by two parallel plates is considered. The flow is laminar and the fluid is assumed to be Newtonian. The viscous dissipation terms are neglected and also it is assumed that the temperature gradient in  $y$ -direction is much greater than it is in  $x$ -direction. The Brinkman-Darcy equation and energy equation for a channel partially filled with porous medium are given. The upper and lower channel walls are subjected to symmetric heat flux boundary condition. The uniform heat flux is denoted as  $q''$  and it has opposite sides  $(-)$  and  $(+)$  for upper and lower wall respectively.

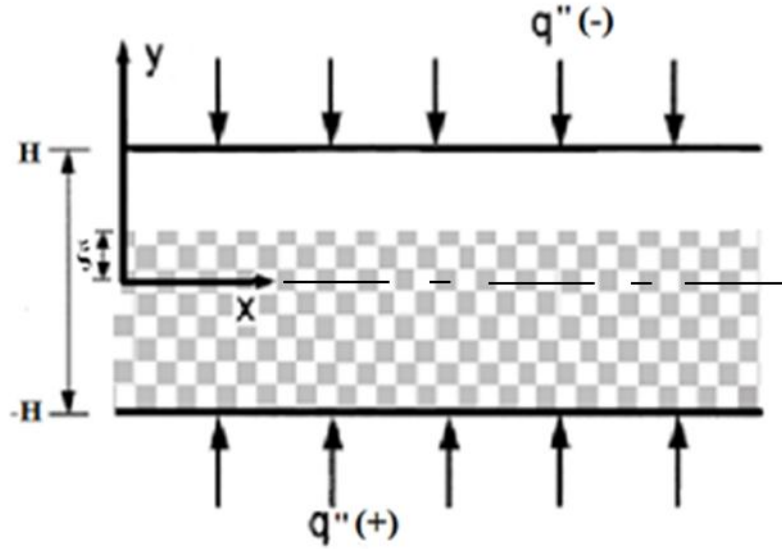


Figure 6.1. Schematic view of the considered channel

## 6.2. Mathematical Formulation and Governing Equations

### 6.2.1. Fluid Flow Analysis

Two different equations for fluid flow can be written; for clear region and porous region. The momentum equation for clear region can be written as:

$$u \frac{\partial u}{\partial x} + v \frac{\partial u}{\partial y} = -\frac{1}{\rho} \frac{\partial P}{\partial x} + \nu \left( \frac{\partial^2 u}{\partial x^2} + \frac{\partial^2 u}{\partial y^2} \right) \quad (6.1)$$

Considered channel flow is hydrodynamically and thermally fully developed, laminar and unidirectional which is parallel to the x-axis and the y- component of velocity is zero. In the channel, there are two regions as a) a region in which pure fluid flows and b) a region in which fluid flows through the porous media.

After mentioned assumptions, the equation of motion for clear fluid region can be written as:

$$v \frac{\partial^2 u_c}{\partial y^2} - \frac{1}{\rho} \frac{\partial P}{\partial x} = 0 \quad (6.2)$$

For more clear understanding the subscript,  $c$ , is used. It indicates that the term belongs to the clear fluid part of channel.

As previous chapters the porous part fluid flow of the channel can be analyzed by using Brinkman –extended Darcy equation. In this equation the subscript,  $p$ , is used to indicate that term belongs to the porous part.

$$\mu_{eff} \frac{d^2 u_p}{dy^2} - \frac{\mu}{K} u_p - \frac{dP}{dx} = 0 \quad (6.3)$$

In Equation (6.3)  $\mu_{eff}$  represents the effective viscosity of fluid and the porous structures,  $\mu$  is dynamic viscosity of the fluid,  $K$  is the permeability of the porous medium. The subscript of  $p$  stands for porous portion and  $u_p$  shows the fluid velocity in porous layer. Boundary conditions for the Equations (6.2) and (6.3) can be written as:

$$y = \pm H \Rightarrow u = 0$$

$$\tau_c(\xi H) = \tau_p(\xi H) \Rightarrow \mu \left. \frac{du_c}{dy} \right|_{y=\xi H} = \mu_{eff} \left. \frac{du_p}{dy} \right|_{y=\xi H} \quad (6.4)$$

The  $\tau$  in Equation (6.4) represents the shear stress. As seen from Equation (6.4), continuous shear stress model is used to define boundary condition at the interface boundary between porous layer and clear fluid region and there is no slip for velocity value at the boundary.

The mean velocity of the fluid in the channel can be calculated by using following definition.

$$u_{mean} = \frac{\int_{-H}^{\xi H} u_p dy + \int_{\xi H}^H u_c dy}{\int_{-H}^{+H} dy} \quad (6.5)$$

## 6.2.2. Heat Flow Analysis

Under the assumptions of thermally and hydrodynamically fully developed laminar flow in a parallel plate channel, neglecting viscous dissipation effect and heat generation, final form of the energy equation:

$$(\rho C_p)_f u \frac{\partial T}{\partial x} = k \frac{\partial^2 T}{\partial y^2} \quad (6.6)$$

where  $\rho$  is density,  $C_p$  is specific heat at constants pressure and  $k$  indicates the conductivity of the material considered. There are two different material (i.e. clear region and porous region) in the channel so two energy equation obtained. For simplicity, the compact form of the energy equation for both clear flow part and porous part can be written as:

$$(\rho C_p)_f u \frac{\partial T}{\partial x} = (\lambda(k_{eff} - k_f) + k_f) \frac{\partial^2 T}{\partial y^2} \quad (6.7)$$

where  $k_f$  and  $k_{eff}$  are the thermal conductivity of the fluid and the effective conductivity of the porous structures. The parameter of  $\lambda$  is defined as:

$$\begin{aligned} \xi H \leq y < H &\Rightarrow \lambda = 0 \\ -H \leq y \leq \xi H &\Rightarrow \lambda = 1 \end{aligned} \quad (6.8)$$

The boundary conditions for defined energy equation can be written by using the fluxes on the wall. It also can be assumed that conduction heat fluxes and the interface temperature are equal between the porous and clear media so:

$$\begin{aligned}
q'' &= -k_f \left. \frac{\partial T}{\partial y} \right|_{y=H} \\
q'' &= -k_{eff} \left. \frac{\partial T}{\partial y} \right|_{y=-H} \\
k_f \left. \frac{\partial T}{\partial y} \right|_{y=\xi H} &= k_{eff} \left. \frac{\partial T}{\partial y} \right|_{y=\xi H} \\
T_c(\xi H) &= T_p(\xi H) \\
x = 0 &\Rightarrow T = T_i
\end{aligned} \tag{6.9}$$

The given equations for the considered problem are solved numerically and the results will be given in Chapter 9. It can be seen from Equation (6.9), the boundary condition at  $x = 0$  for the Equation (6.7) is considered as the entrance temperature of the fluid to the channel.

### 6.2.3. Pressure Drop Calculation

Pressure drop calculation for dimensional problem is done, numerically. Calculations start with a specific flow rate and an assumed negative pressure gradient value. Equation of motion for clear fluid region and porous region, Equation (6.2) and Equation (6.3), are solved numerically with using this assumed pressure gradient value. The mean velocity is calculated by numerically with using the solution of Equation (6.2) and Equation (6.3). The calculation continues until the mean velocity which is found by the numerical solution converges to the given specific flow rate.



## CHAPTER 7

### **DIMENSIONLESS STUDY ON CHANNEL PARTIALLY FILLED WITH POROUS MEDIUM; SYMMETRIC HEAT FLUX BOUNDARY CONDITION**

In this chapter, a channel which is partially filled with porous medium is investigated analytically. A symmetrical heat flux is imposed to the channel walls. The heat and fluid flow equations and appropriate boundary conditions are presented into dimensionless form. The analytical solutions of the given equations are also presented.

#### **7.1. The Considered Problem**

As it can be shown in Figure 7.1, the considered channel is partially filled with porous medium. The distance between the plates is  $2H$  and  $\zeta$  represents the distance between core of the channel and layer of interface. The value of  $\zeta$  is between  $-1$  and  $+1$ . The porous medium is considered as an isotropic with permeability of constant  $K$ . An incompressible, hydrodynamically and thermally fully developed and steady flow in a channel bounded by two parallel plates is considered. The flow is laminar and the fluid is assumed to be Newtonian. The viscous dissipation terms are neglected and also it is assumed that the temperature gradient in  $y$ -direction is much greater than it is in  $x$ -direction. The dimensionless form of equation for motion for clear fluid region, Brinkman-Darcy equation for porous region and energy equation are given. The upper and lower channel walls are subjected to symmetric heat flux boundary condition. The uniform heat flux is denoted as  $q''$  and it have opposite sides  $(-)$  and  $(+)$  for upper wall and lower wall respectively.

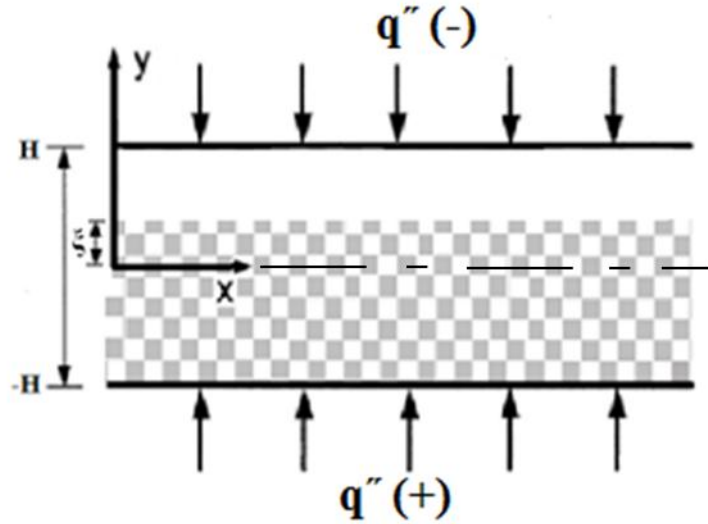


Figure 7.1. Schematic view of the considered channel

## 7.2. Mathematical Formulation and Governing Equations

### 7.2.1. Fluid Flow Analysis

Two different equations for fluid flow can be written; for clear region and porous region. The momentum equation for clear region can be written as:

$$u \frac{\partial u}{\partial x} + v \frac{\partial u}{\partial y} = -\frac{1}{\rho} \frac{\partial P}{\partial x} + \nu \left( \frac{\partial^2 u}{\partial x^2} + \frac{\partial^2 u}{\partial y^2} \right) \quad (7.1)$$

Considered channel flow is hydrodynamically and thermally fully developed, laminar and unidirectional which is parallel to the x-axis and the y- component of velocity is zero. In the channel, there are two regions as a) a region in which pure fluid flows and b) a region in which fluid flows through the porous media.

After mentioned assumptions, the equation of motion for clear fluid region can be written as:

$$v \frac{\partial^2 u_c}{\partial y^2} - \frac{1}{\rho} \frac{\partial P}{\partial x} = 0 \quad (7.2)$$

For more clear understanding the subscript,  $c$ , is used. It indicates that the term belongs to the clear fluid part of channel.

As previous chapters the porous part fluid flow of the channel can be analyzed by using Brinkman –extended Darcy equation. In this equation the subscript,  $p$ , is used to indicate that term belongs to the porous part.

$$\mu_{eff} \frac{d^2 u_p}{dy^2} - \frac{\mu}{K} u_p - \frac{dP}{dx} = 0 \quad (7.3)$$

In Equation (7.3)  $\mu_{eff}$  represents the effective viscosity of fluid and the porous structures,  $\mu$  is dynamic viscosity of the fluid,  $K$  is the permeability of the porous medium. The subscript of  $p$  stands for porous portion and  $u_p$  shows the fluid velocity in porous layer. Boundary conditions for the Equations (7.2) and (7.3) can be written as:

$$y = \pm H \Rightarrow u = 0$$

$$\tau_c(\xi H) = \tau_p(\xi H) \Rightarrow \mu \left. \frac{du_c}{dy} \right|_{y=\xi H} = \mu_{eff} \left. \frac{du_p}{dy} \right|_{y=\xi H} \quad (7.4)$$

The  $\tau$  in Equation (7.4) represents the shear stress. As seen from Equation (7.4), continuous shear stress model is used to define boundary condition at the interface boundary between porous layer and clear fluid region and there is no slip for velocity value at the boundary. To reduce the number of the parameters for the problem, the dimensionless form of Equation (7.2) and (7.3) and related boundary conditions, Equation (7.4), can be found by using the following dimensionless parameters:

$$\begin{aligned}
Y &= \frac{y}{H}, M = \frac{\mu_{eff}}{\mu}, Da = \frac{K}{H^2}, G = -\frac{\partial P}{\partial x}, S = \frac{1}{\sqrt{M Da}}, \\
U &= \frac{\mu u}{GH^2}, T_{w\mu} = \frac{T_{w1} + T_{w2}}{2}, \theta = \frac{T - T_{w\mu}}{T_m - T_{w\mu}}, K^* = \frac{k_{eff}}{k_f}
\end{aligned} \tag{7.5}$$

Da, M and S are Darcy number, viscosity ratio and porous media shape parameter, respectively. After applying the above dimensionless parameters into Equations (7.2) and (7.3), the dimensionless form of the momentum equation for fluid flow in clear region and Darcy-Brinkman equations for fluid flow in porous region is obtained:

$$\begin{aligned}
\frac{d^2 U_c}{dY^2} + 1 &= 0 \\
\frac{d^2 U_p}{dY^2} - S^2 U_p + \frac{1}{M} &= 0
\end{aligned} \tag{7.6}$$

$U_c$  and  $U_p$  are the dimensionless velocity of fluid at the clear and porous regions. The dimensionless forms of boundary conditions Equation (7.4) can also be obtained by using the dimensionless parameters of Equation (7.5).

$$\begin{aligned}
Y = 1 &\Rightarrow U_c = 0 \\
Y = -1 &\Rightarrow U_p = 0 \\
Y = \xi &\Rightarrow \tau_c = \tau_p \\
Y = \xi &\Rightarrow U_c = U_p = U_i
\end{aligned} \tag{7.7}$$

In the Equation (7.7) the  $\tau$  shows stress at the interface and  $U_i$  is the dimensionless velocity at the interface between porous and clear region.

The solutions of Equation (7.6) with boundary conditions given in Equation (7.7) yield velocity distribution equations for each region. The velocity distribution equation for clear region is found as:

$$U_c = C_0 + C_1 Y + C_2 Y^2 \quad (7.8)$$

where

$$C_0 = -\frac{2U_i - \xi + \xi^2}{2(-1 + \xi)}, C_1 = \frac{-1 + 2U_i + \xi + (-1 + \xi)\xi}{2(\xi - 1)}, C_2 = -\frac{1}{2} \quad (7.9)$$

According to the solution of Equation (7.6), the velocity distribution equation for porous region is found as:

$$U_p = P_0 + P_1 \text{Sinh}\left(\frac{\xi - Y}{S}\right) + P_2 \text{Sinh}\left(\frac{Y + 1}{S}\right) \quad (7.10)$$

where

$$P_0 = \frac{S^2}{M}, P_1 = -\frac{S^2}{M \text{Sinh}\left(\frac{\xi + 1}{S}\right)}, P_2 = \frac{M U_i - S^2}{M \text{Sinh}\left(\frac{\xi + 1}{S}\right)} \quad (7.11)$$

Since shear stress is continuous at the surface, the interface velocity can be found as:

$$U_i = \frac{S(-1 + \xi) \left( M(-1 + \xi) - 2S \text{Tanh}\left(\frac{1 + \xi}{2S}\right) \right)}{2M \left( S - (-1 + \xi) \text{Coth}\left(\frac{1 + \xi}{2S}\right) \right)} \quad (7.12)$$

The dimensionless form of mean velocity of the fluid in the channel can be calculated as:

$$u_{mean} = \frac{\int_{-H}^{\xi H} u_p dy + \int_{\xi H}^H u_c dy}{\int_{-H}^{+H} dy} \Rightarrow U_{mean} = \frac{\int_{-1}^{\xi} U_p dY + \int_{\xi}^1 U_c dY}{2} \quad (7.13)$$

The solution of the Equation (7.13) with Equation (7.8) and (7.10) gives:

$$U_{mean} = \frac{-M(6U_i + (-1 + \xi)^2)(-1 + \xi) + 12S^2(1 + \xi) + 24S(-2S^2 + MU_i) \sinh\left(\frac{1 + \xi}{2S}\right)}{24M} \quad (7.14)$$

Finally, the dimensionless normalized velocity for each region can be determined as:

$$\hat{u} = \frac{U}{U_{mean}} \quad (7.15)$$

The solution of Equation 7.15 is found by the help of Equation 7.8, Equation 7.10 and Equation 7.14.

### 7.2.2. Heat Flow Analysis

Under the assumptions of thermally and hydrodynamically fully developed laminar flow in a parallel plate channel, neglecting viscous dissipation effect and heat generation, final form of the energy equation:

$$(\rho C_p)_f u \frac{\partial T}{\partial x} = k \frac{\partial^2 T}{\partial y^2} \quad (7.16)$$

where  $\rho$  is density,  $C_p$  is specific heat at constants pressure and  $k$  indicates the conductivity of the material considered. There are two different material (i.e. clear

region and porous region) in the channel so two energy equation obtained. For simplicity, the compact form of the energy equation for both clear flow part and porous part can be written as:

$$(\rho C_p)_f u \frac{\partial T}{\partial x} = (\lambda(k_{eff} - k_f) + k_f) \frac{\partial^2 T}{\partial y^2} \quad (7.17)$$

Where  $k_f$  and  $k_{eff}$  are the thermal conductivity of the fluid and the effective conductivity of the porous structures. The parameter of  $\lambda$  is defined as:

$$\begin{aligned} \xi H \leq y < H &\Rightarrow \lambda = 0 \\ -H \leq y \leq \xi H &\Rightarrow \lambda = 1 \end{aligned} \quad (7.18)$$

Writing the dimensionless temperature definition and the other dimensionless variables Equation (7.5) onto the Equation (7.17) gives the following form:

$$(\rho C_p)_f u \left[ \frac{\partial T_{w\mu}}{\partial x} + \theta \left( \frac{\partial T_m}{\partial x} - \frac{\partial T_{w\mu}}{\partial x} \right) + (T_m - T_{w\mu}) \frac{\partial \theta}{\partial x} \right] = (\lambda(k_{eff} - k_f) + k_f) (T_m - T_{w\mu}) \frac{\partial^2 \theta}{\partial Y^2} \quad (7.19)$$

If we consider the heat fluxes are constant and the gradient of the wall heat fluxes with respect to x-direction must be zero, the followings can be written:

$$\begin{aligned} \frac{dq''}{dx} = \frac{d[h_1(T_{w1} - T_m)]}{dx} = 0 &\Rightarrow \frac{dT_{w1}}{dx} = \frac{dT_m}{dx} \\ \frac{dq''}{dx} = \frac{d[h_2(T_{w2} - T_m)]}{dx} = 0 &\Rightarrow \frac{dT_{w2}}{dx} = \frac{dT_m}{dx} \\ \frac{dT_{w1}}{dx} + \frac{dT_{w2}}{dx} = \frac{d(T_{w1} + T_{w2})}{dx} = 2 \frac{dT_{w\mu}}{dx} = 2 \frac{dT_m}{dx} &\Rightarrow \frac{dT_{w\mu}}{dx} = \frac{dT_m}{dx} \end{aligned} \quad (7.20)$$

The thermally and hydrodynamically fully developed assumption brings the dimensionless temperature gradient in x-direction be zero. By using this assumption and Equation (7.19), the energy equation becomes:

$$(\rho C_p)_f u \frac{\partial T_m}{\partial x} = (\lambda(k_{eff} - k_f) + k_f)(T_m - T_w) \frac{\partial^2 \theta}{\partial Y^2} \quad (7.21)$$

If we consider a differential volume such as Figure 7.2 the total energy of the fluid is conserved. It should be reminded that there is no heat generation.

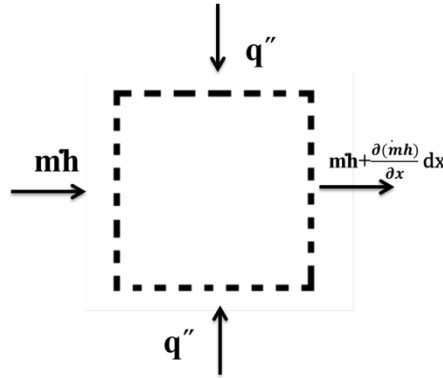


Figure 7.2. Differential volume from the considered duct

The energy entering must be equal to the energy leaving the boundaries so:

$$2H \rho u_m C_p T_m + q'' dx + q'' dx = 2H \rho u_m C_p T_m + \frac{\partial(2H \rho u_m C_p T_m)}{\partial x} dx$$

$$q'' = H \rho u_m C_p \frac{dT_m}{dx} \Rightarrow \frac{dT_m}{dx} = \frac{q''}{H \rho u_m C_p} \quad (7.22)$$

A new variable such as “overall Nu” is considered as Equation (7.23). If it is considered as applied heat fluxes at the walls will be transferred to the fluid, the overall Nu based on fluid thermal conductivity and heat transfer rate to the fluid can be also expressed as equation (7.23):

$$Nu = \frac{h2H}{k_f}$$

$$q'' = h(T_{w\mu} - T_m) \quad (7.23)$$

The overall Nu for the considered problem can be defined as:



$$Nu = \frac{2Hq''}{k_f(T_{w\mu} - T_m)} \quad (7.24)$$

At this point after some mathematical manipulation with Equation (7.21) and (7.22) with using the definition of overall Nu yields two dimensionless temperature distribution equations: a) for clear flow region, b) for porous region. The dimensionless temperature distribution equation for clear region can be found as:

$$\frac{\partial^2 \theta_c}{\partial Y^2} + \frac{1}{2} \hat{u} Nu = 0 \quad (7.25)$$

According to the definition of overall Nu, the dimensionless temperature distribution equation for porous region can be found as:

$$\frac{\partial^2 \theta_p}{\partial Y^2} + \frac{1}{2} \frac{\hat{u}}{K} Nu = 0 \quad (7.26)$$

Two boundary conditions are needed to solve second order ordinary differential equation shown above, so according to considered problem another parameter for specifying boundary temperature can be defined such as:

$$\beta = \frac{T_{w2} - T_{w1}}{2(T_m - T_{w\mu})} \quad (7.27)$$

By considering the definition of  $\beta$ , the related boundary conditions can be given as:

$$\begin{aligned} Y = 1 &\Rightarrow \theta_c = -\beta \\ Y = -1 &\Rightarrow \theta_p = \beta \\ Y = \xi &\Rightarrow \theta_c = \theta_p = \theta_i \end{aligned} \quad (7.28)$$

In the above boundary conditions, the term,  $\theta_i$ , designates the dimensionless interface dimensionless temperature of porous and clear region. When the dimensionless heat transfer equation for clear region, Equation (7.25), solve with related boundary conditions, Equation (7.28), the equation for dimensionless temperature distribution for clear region can be found like:

$$\theta_c(Y) = \frac{(y - \xi)(24B - Nu(y - 1)((\xi - 1)(6C_0 + 2C_1(y + 1 + \xi) + C_2(1 + y + y^2 + \xi + y\xi + \xi^2)))) + 24(y - 1)\theta_i}{24(\xi - 1)} \quad (7.29)$$

The coefficients of  $C_0$ ,  $C_1$ , and  $C_2$  are given by Equation (7.9) before. The dimensionless heat transfer equation for porous region, Equation (7.26), can be solved with related boundary conditions, Equation (7.28). The solution of the equation for dimensionless temperature distribution for porous region can be found as:

$$\begin{aligned} \theta_p(Y) = \frac{1}{4K(1 + \xi)} & (-y - \xi)(4BK + Nu P_0(1 + y)(1 + \xi)) + 2NuS^2(-P_2(1 \\ & + \xi)\text{Sinh}[\frac{1 + y}{S}] + P_1(1 + \xi)\text{Sinh}[\frac{y - \xi}{S}] + (P_2 - P_1y + P_2y \\ & + P_1\xi)\text{Sinh}[\frac{1 + \xi}{S}]) + 4K(1 + y)\theta_i \end{aligned} \quad (7.30)$$

The coefficients of  $P_0$ ,  $P_1$ , and  $P_2$  are given by Equation (7.11) before. If we want to investigate the distribution of dimensionless temperature throughout the channel according to Equation (7.29) and Equation (7.30), we should find more clear definition for  $\beta$ ,  $\theta_i$  and  $Nu$ . Additional definition for  $\beta$  can found as dividing the heat fluxes at the walls with making the fluxes dimensionless as:

$$\begin{aligned} q'' = -k_f \frac{\partial T}{\partial y} \Big|_{y=H} &= -k_f \frac{(T_m - T_{w\mu})}{H} \frac{\partial \theta_c}{\partial Y} \Big|_{Y=1} \\ q'' = -k_{eff} \frac{\partial T}{\partial y} \Big|_{y=-H} &= -k_{eff} \frac{(T_m - T_{w\mu})}{H} \frac{\partial \theta_p}{\partial Y} \Big|_{Y=-1} \end{aligned} \Rightarrow K^* \frac{\partial \theta_p}{\partial Y} \Big|_{Y=-1} = \frac{\partial \theta_c}{\partial Y} \Big|_{Y=1} \quad (7.31)$$

The derivative of dimensionless clear fluid and porous medium temperatures  $\left( \frac{\partial \theta_p}{\partial Y} \text{ and } \frac{\partial \theta_c}{\partial Y} \right)$  can be found from equations of 7.30 and 7.29 for  $Y = -1$  and  $Y = 1$

locations. If the derivatives for  $Y=1$  and  $-1$  are substituted to Equation (7.31), following extra equations can be found. This equation provides an extra relation between,  $\beta$ ,  $Nu$  and  $\theta_i$ .

$$\beta = b_1 Nu + b_2 \theta_i \quad (7.32)$$

The constants  $b_1$  and  $b_2$  are given in Equation (A.1) and Equation (A.2) in Appendix A.

Additional definition for  $\theta_i$  can found as using continuity of the heat flux as an interface boundary condition:

$$\begin{aligned} -k_{eff} \frac{\partial T}{\partial y} \Big|_{y=\xi H} = -k_f \frac{\partial T}{\partial y} \Big|_{y=\xi H} &\Rightarrow -k_{eff} (T_m - T_{w\mu}) \frac{\partial \theta_p}{\partial y} \Big|_{y=\xi} = -k_f (T_m - T_{w\mu}) \frac{\partial \theta_c}{\partial y} \Big|_{y=\xi} \Rightarrow \\ K^* \frac{\partial \theta_p}{\partial y} \Big|_{y=\xi} &= \frac{\partial \theta_c}{\partial y} \Big|_{y=\xi} \end{aligned} \quad (7.33)$$

Dimensionless temperature equations for clear region and porous region are shown in Equations of (7.29) and (7.30). If the derivatives of these equations for  $Y=\xi$  are substituted to Equation (7.33), following extra equations can be found. This equation provides another extra relation between,  $\beta$ ,  $Nu$  and  $\theta_i$ .

$$\theta_i = t_1 Nu + t_2 \beta \quad (7.34)$$

The constants  $t_1$  and  $t_2$  are given in Equation (A.3) and Equation (A.4) in Appendix A.

To obtain an expression for overall  $Nu$  we can use the compatibility condition[32]:

$$\int_{-1}^1 \theta \hat{u} dY = 2 \Rightarrow \int_{-1}^{\xi} \theta_p \hat{u} dY + \int_{\xi}^1 \theta_c \hat{u} dY = 2 \quad (7.35)$$

The dimensionless temperature for clear region and porous region and the normalized velocity were found in Equation (7.29), Equation (7.30) and Equation (7.15). If these expressions are substituted to Equation (7.35) and after taking integral between -1 and  $\xi$  for porous part and  $\xi$  and 1 for clear part, the following relation can be obtained for overall Nu:

$$Nu = n_1 + n_2\beta + n_3\theta_i \quad (7.36)$$

The constants  $n_1$ ,  $n_2$  and  $n_3$  are given in Equation (A.5), Equation (A.6) and Equation (A.7) in Appendix A. For three unknown;  $\beta$ ,  $\theta_i$  and  $Nu$ , we have three equation which are Equation (7.32), Equation (7.34) and Equation (7.36). If we solve three equations simultaneously,  $\beta$ ,  $\theta_i$  and  $Nu$  can be found in terms of known parameters:

$$\begin{aligned} \beta &= -\frac{n_1(b_1 + b_2 t_1)}{B} \\ \theta_i &= -\frac{n_1(t_1 + b_1 t_2)}{B} \\ Nu &= \frac{n_1(-1 + b_2 t_2)}{B} \end{aligned} \quad (7.37)$$

where  $B$  is :

$$B = -1 + n_3 t_1 + b_2 (n_2 t_1 + t_2) + b_1 (n_2 + n_3 t_2)$$

The constants  $b_1$ ,  $b_2$ ,  $t_1$ ,  $t_2$ ,  $n_1$ ,  $n_2$  and  $n_3$  are given in Equations of (A.1), (A.2), (A.3), (A.4), (A.5), (A.6) and (A.7) in Appendix A.

The definition of individual Nu for each wall can be expressed as by using overall Nu expression.

$$\begin{aligned}
Nu_1 &= -\frac{2Hq''}{k_f(T_{w1}-T_m)} & \text{and} & & Nu_1 &= \frac{h2H}{k_f} \\
Nu_2 &= -\frac{2Hq''}{k_{eff}(T_{w2}-T_m)} & & & Nu_2 &= \frac{h2H}{k_{eff}}
\end{aligned} \tag{7.38}$$

We can apply the conservation of energy onto each wall which gives:

$$\begin{aligned}
h_1(T_m - T_{w1}) &= k_f \left. \frac{(T_m - T_{w\mu})}{H} \frac{\partial \theta_c}{\partial Y} \right|_{Y=1} \\
h_2(T_m - T_{w2}) &= k_{eff} \left. \frac{(T_m - T_{w\mu})}{H} \frac{\partial \theta_p}{\partial Y} \right|_{Y=-1}
\end{aligned} \tag{7.39}$$

To determine the individual Nu, Equation (7.38), the following mathematical manipulations are done with using Equation (7.39):

$$\begin{aligned}
\left. \frac{\partial \theta_c}{\partial Y} \right|_{Y=1} &= \frac{hH(T_m - T_{w1})}{k_f(T_m - T_{w\mu})} = \frac{1}{2} Nu_1 \frac{(T_m - T_{w1})}{(T_m - T_{w\mu})} \\
&= \frac{1}{2} Nu_1 \frac{\left( T_m - \frac{T_{w1}}{2} - \frac{T_{w1}}{2} + \frac{T_{w2}}{2} - \frac{T_{w2}}{2} \right)}{(T_m - T_{w\mu})} = \frac{1}{2} Nu_1 \frac{\left( T_m - T_{w\mu} + \frac{T_{w2} - T_{w1}}{2} \right)}{(T_m - T_{w\mu})} \\
&= \frac{1}{2} Nu_1 (1 + \beta)
\end{aligned} \tag{7.40}$$

The same procedure can be applied to the lower wall so:

$$\begin{aligned}
\left. \frac{\partial \theta_p}{\partial Y} \right|_{Y=-1} &= \frac{hH(T_m - T_{w2})}{k_{eff}(T_m - T_{w\mu})} = \frac{1}{2} Nu_2 \frac{(T_m - T_{w2})}{(T_m - T_{w\mu})} \\
&= \frac{1}{2} Nu_2 \frac{\left( T_m - \frac{T_{w2}}{2} - \frac{T_{w2}}{2} + \frac{T_{w1}}{2} - \frac{T_{w1}}{2} \right)}{(T_m - T_{w\mu})} = \frac{1}{2} Nu_2 \frac{\left( T_m - T_{w\mu} + \frac{T_{w1} - T_{w2}}{2} \right)}{(T_m - T_{w\mu})} \\
&= \frac{1}{2} Nu_2 (1 - \beta)
\end{aligned} \tag{7.41}$$

The individual  $Nu$ ,  $Nu_1$  and  $Nu_2$ , can be found by solving Equation (7.40) and Equation (7.41) with using Equation (7.29), Equation (7.30).

$$\begin{aligned}
 Nu_1 &= -\frac{24(\beta + \theta_i) + Nu(\xi - 1)^2(6C_0 + 3C_2 + (\xi + 2)(2C_1 + \xi C_2))}{12(1 + \beta)(\xi - 1)} \\
 Nu_2 &= \frac{4K * (\beta - \theta_i) - Nu \left( (\xi + 1)(P_0 - 2P_2 S + \xi P_0) + 2S \left( -P_1(\xi + 1) \text{Cosh} \left( \frac{\xi + 1}{S} \right) + (P_1 - P_2) S \text{ Sinh} \left( \frac{\xi + 1}{S} \right) \right) \right)}{2K(\beta - 1)(\xi + 1)}
 \end{aligned} \quad (7.42)$$

where  $C_0$ ,  $C_1$  and  $C_2$  are given in Equation (7.9),  $P_0$ ,  $P_1$  and  $P_2$  are given in (7.11), and  $Nu$ ,  $\beta$  and  $\theta_i$  are found in Equation (7.37).

### 7.2.3. Pressure Drop Calculations

The porous media in the channel brings pressure drop increments. The pressure drop can be calculated as previous chapters. Firstly, friction factor “ $f$ ” should be defined. If we consider a channel which has the mean velocity of  $u_{mean}$ , the friction factor for this channel can be written as:

$$f = \frac{\left( -\frac{dP}{dx} \right) 2H}{\frac{1}{2} \rho u_m^2} \quad (7.43)$$

The flow has a constant pressure gradient along the x-axis according to fully developed assumption and this negative gradient is denoted by  $G$ , as given in dimensionless parameters, Equation (7.5), so:

$$f = \frac{4GH}{\rho u_m^2} \quad (7.44)$$

The definition of dimensionless velocity, Equation (7.5), brings more clear equation for friction factor.

$$f = \frac{4}{U_m} \frac{\mu}{\rho u_m H} \quad (7.45)$$

The equation of friction factor can have following form with using the definition of Reynolds number for internal flow:

$$f \text{ Re} = \frac{8}{U_m} \quad (7.46)$$

The mean velocity term in Equation (7.46) was found in Equation (7.14), so by using Equation (7.46) the friction factor for specified Reynolds number can be found.

## CHAPTER 8

# NUMERICAL APPROACH FOR THE SOLUTION OF GOVERNING EQUATIONS

The dimensional governing equations given in Chapter 4 and Chapter 6 are solved numerically. The solutions of dimensional differential equations are found with related boundary conditions by using finite difference method by the help of MATLAB software. In this chapter, the information about numerical procedure and the derivation of nodal equations for each dimensional problem are given.

### 8.1. Numerical Solution Procedure for Completely Filled Problem Discussed in Chapter 4

The momentum and energy equations with boundary conditions for forced convection in a channel filled with porous medium are presented in Chapter 4. The numerical solution approach for these governing equations is finite difference method. For reminding the method; the definition of the derivatives used in finite difference methods are written in Equation 8.1. For a function of  $f(x)$  and with a distance of  $\Delta x$ ;

Forward difference approximation for a point can be defined as:

$$\left. \frac{\partial f}{\partial x} \right|_{x=x_i} = \frac{f(x_i + \Delta x) - f(x_i)}{\Delta x} + O(\Delta x) \quad (8.1a)$$

Backward difference approximation for a point can be defined as:

$$\left. \frac{\partial f}{\partial x} \right|_{x=x_i} = \frac{f(x_i) - f(x_i - \Delta x)}{\Delta x} + O(\Delta x) \quad (8.1b)$$

Central difference approximation for a point can be defined as:



$$\left. \frac{\partial f}{\partial x} \right|_{x=x_i} = \frac{f(x_i + \Delta x) - f(x_i - \Delta x)}{2\Delta x} + O[(\Delta x)]^2 \quad (8.1c)$$

For calculation of second derivative the following equation can be used:

$$\left. \frac{\partial^2 f}{\partial x^2} \right|_{x=x_i} = \frac{f(x_i + \Delta x) - 2f(x_i) + f(x_i - \Delta x)}{(\Delta x)^2} + O[(\Delta x)]^2 \quad (8.1d)$$

### 8.1.1. Solution of the Momentum Equation

The momentum equation for completely filled problem Equation 4.2 and related boundary conditions Equation 4.5 are solved by using finite difference methods with using  $n+1$  node. Solution procedure starts with a given specific flow rate (in the laminar flow region) and an assumed negative pressure gradient value. The mean velocity is calculated by numerical solution of the momentum equations with using the assumed pressure value. The calculation continues until the mean velocity which is found by numerically converges to the given specific flow rate. The flowchart of the solution of the momentum equation can be shown as:

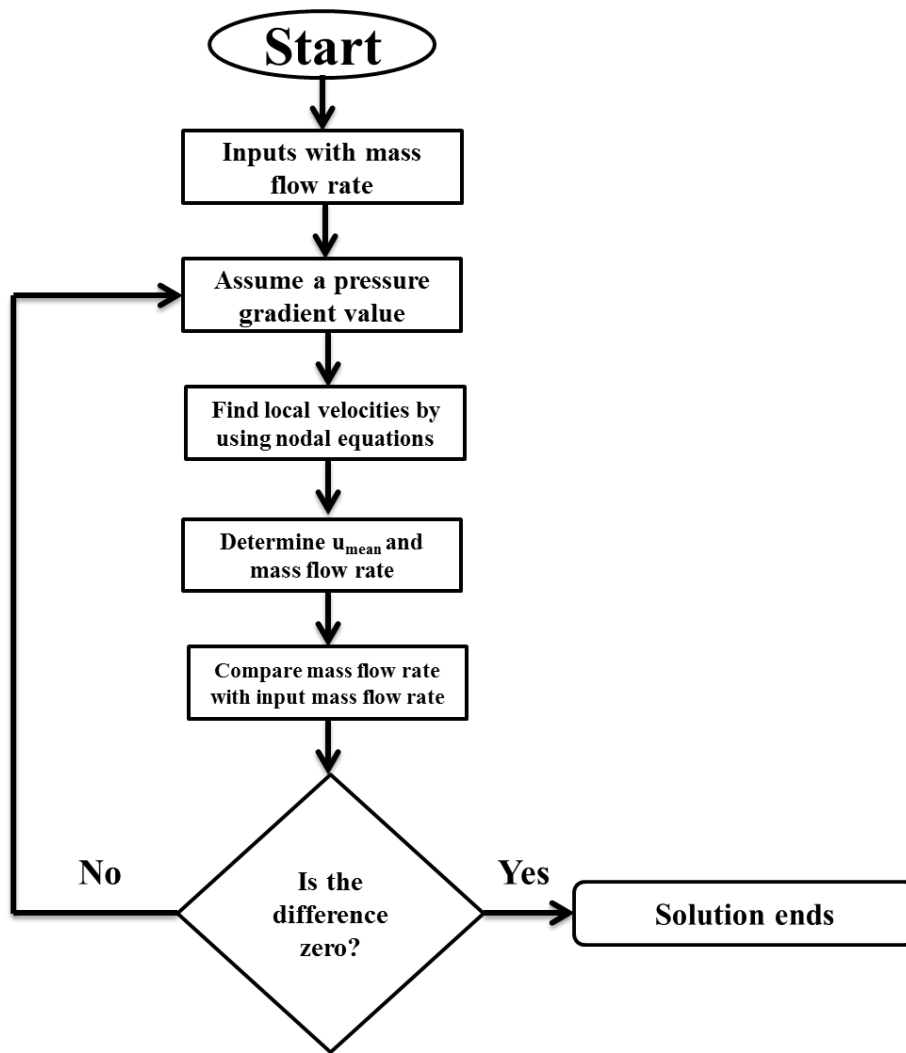


Figure 8.1. The flowchart for the solution of the momentum equation

The domain from  $-H$  to  $+H$  is divided in  $n+1$  nodes. Number of nodes  $n+1$ , taken as 101 for this problem. So:

$$dy = \frac{H - (-H)}{n} \quad (8.2)$$

The direction of  $j$  can be shown as:



Figure 8.2. The node direction used in momentum equation

Nodal equation for internal nodes for the velocity distribution in completely filled channel with porous material can be derived as:

$$\begin{aligned} \frac{1}{\varepsilon} \frac{d^2 u}{dy^2} - \frac{1}{K} u + \frac{G}{\mu} &= 0 \Rightarrow \\ \frac{1}{\varepsilon} \frac{u(j+1) - 2u(j) + u(j-1)}{(dy)^2} - \frac{1}{K} u(j) + \frac{G}{\mu} &= 0 \Rightarrow \\ u(j) &= \frac{K(\varepsilon dy^2 G + \mu(u(j+1) + u(j-1)))}{\mu(\varepsilon dy^2 + 2K)} \end{aligned} \quad (8.3)$$

Nodal equation for no-slip boundary conditions can be written as:

$$u(1) = 0 \quad u(n+1) = 0 \quad (8.4)$$

### 8.1.2. Solution of the Energy Equation

The dimensional heat flow analyzes are made numerically with the help of finite difference method. The energy equation is second order partial difference equation so a 2-dimensional domain is set off to obtain the solution of the Equation 4.7. The velocity distribution values which are obtained from the solution of momentum equation are used. The flowchart of the solution of the energy equation can be shown as:

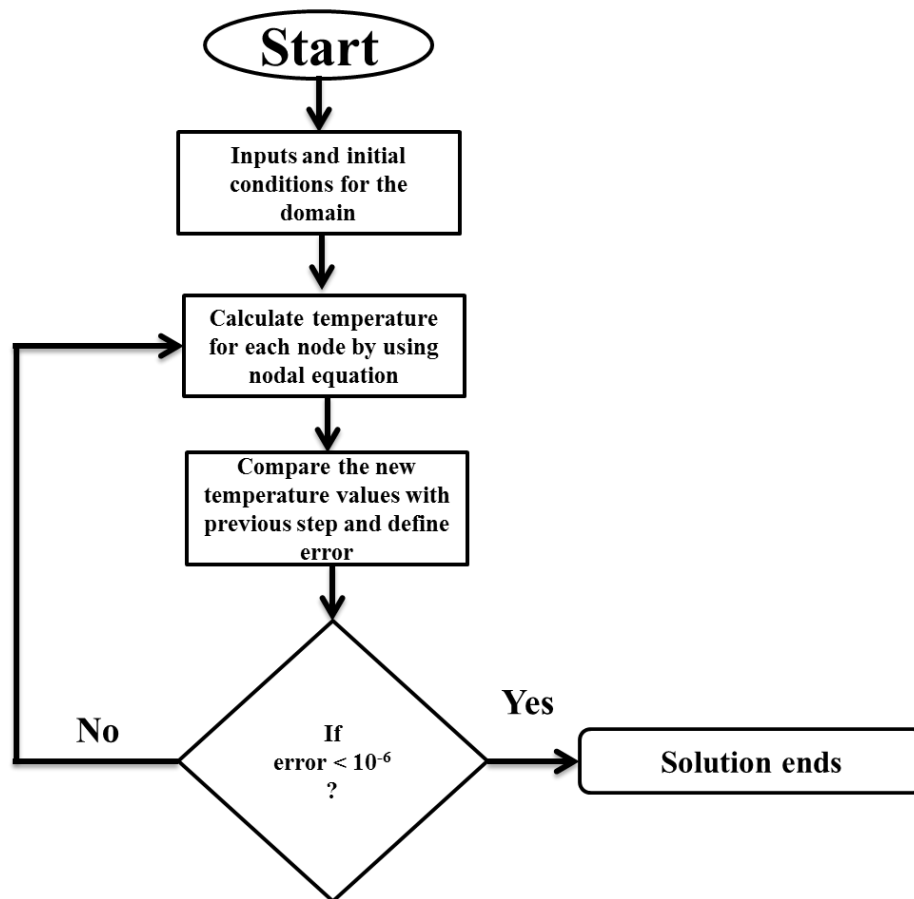


Figure 8.3. The flowchart for the solution of the energy equation

The channel is divided in  $m+1$  node from  $0$  to  $L$  in x-direction. Number of nodes in x- direction  $m+1$  is taken as 301 for this differential equation. So:

$$dx = \frac{L - (0)}{m} \quad (8.5)$$

The domain can be shown as:

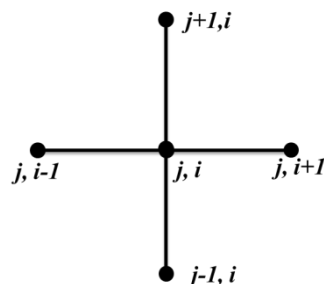


Figure 8.4. The node directions used in energy equation

Nodal equation for internal nodes of the dimensional temperature distribution in completely filled channel with porous material can be derived by applying Equations 8.1 on to the Equation 4.7:

$$\begin{aligned}
 (\rho C_p)_f u \frac{\partial T}{\partial x} &= k_{eff} \frac{\partial^2 T}{\partial y^2} \Rightarrow \\
 (\rho C_p)_f u(j) \left( \frac{T(j,i) - T(j,i-1)}{dx} \right) &= k_{eff} \left( \frac{T(j+1,i) - 2T(j,i) + T(j-1,i)}{dy^2} \right) \Rightarrow \quad (8.6) \\
 T(j,i) &= \frac{C_1 u(j) T(j,i-1) + C_2 (T(j-1,i) + T(j+1,i))}{C_1 u(j) + 2C_2}
 \end{aligned}$$

Where  $C_1$  and  $C_2$  is the constants as:

$$C_1 = \frac{(\rho C_p)_f}{dx}, \quad C_2 = \frac{k_{eff}}{dy^2} \quad (8.7)$$

The nodal equations for asymmetrical constant heat flux boundary conditions Equation 4.9 and the boundary condition for  $x=0$  can be found as:

$$\begin{aligned}
 T(m+1,i) &= T(m,i) + \frac{q''_{w1} dy}{k_{eff}} & T(1,i) &= T(2,i) + \frac{q''_{w2} dy}{k_{eff}} \\
 T(j,1) &= T_i
 \end{aligned} \quad (8.8)$$

where  $T_i$  is the entrance temperature and taken as  $0^\circ\text{C}$ .

The error is taken as  $10^{-6}$  on each iteration step for the convergence of the numerical solution.

## 8.2. Numerical Solution Procedure for Completely Filled Problem Discussed in Chapter 6

The discussed problem in Chapter 6 is a problem about forced convection in a partially filled channel. The momentum and energy equations with boundary conditions

for this channel are presented in Chapter 6. The numerical solution approaches for these governing equations are given in following sections.

### 8.2.1. Solution of the Momentum Equation

The momentum equations for partially filled problem Equation 6.2 and Equation 6.3 and related boundary conditions Equation 6.4 are solved by using finite difference methods with using  $n+1$  nodes. Like Section 8.1, the solution procedure starts with a given specific flow rate (in the laminar flow region) and an assumed negative pressure gradient value. The mean velocity is calculated by numerical solution of the momentum equations with using the assumed pressure value. The calculation continues until the mean velocity which is found by numerically converges to the given specific flow rate. The flowchart of the solution is the same as Figure 8.1.

The domain from  $-H$  to  $+H$  is divided again in  $n+1$  nodes and  $n$  is taken as 100. So Equation 8.1 and Figure 8.2 are also valid in this section.

Like Equation (8.3), nodal equation for internal nodes of the velocity distribution in the clear region which derived with the help of Equation 8.1 is calculated as:

$$u(j) = \frac{dy^2 G + \mu_f (u(i+1) + u(i-1))}{2\mu_f} \quad (8.9)$$

Nodal equation for internal nodes of the velocity distribution in the porous region which derived with the help of Equation 8.1 is calculated as:

$$u(j) = \frac{K(\varepsilon dy^2 G + \mu(u(j+1) + u(j-1)))}{\mu(\varepsilon dy^2 + 2K)} \quad (8.10)$$

Nodal equation at the interface can be written as:

$$\frac{u(\xi_l + 1) - u(\xi_l)}{dy} = \frac{1}{\varepsilon} \frac{u(\xi_l) - u(\xi_l - 1)}{dy} \Rightarrow u(\xi_l) = \frac{\varepsilon(u(\xi_l - 1) + u(\xi_l + 1))}{1 + \varepsilon} \quad (8.11)$$

$\xi_i$  indicates which node is  $\xi$  and it can be found as

$$\xi_i = \frac{H + \xi}{dy} + 1 \quad (8.12)$$

Nodal equation for no-slip boundary conditions can be written as:

$$u(1) = 0 \quad u(n+1) = 0 \quad (8.13)$$

### 8.2.2. Solution of the Energy Equation

The dimensional heat flow analyzes for partial filling problem are made numerically with the help of finite difference method. The energy equation is second order partial difference equation so a 2-dimensional domain is set off to obtain the solution of the Equation 6.7. The velocity distribution values which are obtained from the solution of momentum equation are used. That's why the channel is again divided in  $m+1$  nodes from 0 to  $L$  in x-direction and  $m$  is taken as 300. So equation 8.4 and Figure 8.4 is valid at this section. The flowchart of the energy equation is same as Figure 8.3.

The nodal equation for dimensionless temperature is found separately for clear fluid and porous region. By following the same procedure with Equation (8.6), nodal equation of the dimensional temperature distribution for internal nodes of the clear region in partially filled problem can be derived as:

$$T(j,i) = \frac{C_1 u(j)T(j,i-1) + C_3 (T(j-1,i) + T(j+1,i))}{C_1 u(j) + 2C_3} \quad (8.14)$$

where  $C_1$  and  $C_3$  is the constants as:

$$C_1 = \frac{(\rho C_p)_f}{dx}, \quad C_3 = \frac{k_f}{dy^2} \quad (8.15)$$

Nodal equation of the dimensional temperature distribution for internal nodes of the porous region in partially filled problem is derived as:

$$T(j,i) = \frac{C_1 u(j)T(j,i-1) + C_2 (T(j-1,i) + T(j+1,i))}{C_1 u(j) + 2C_2} \quad (8.16)$$

where  $C_1$  and  $C_2$  is the constants as:

$$C_1 = \frac{(\rho C_p)_f}{dx}, \quad C_2 = \frac{k_{eff}}{dy^2} \quad (8.17)$$

Like Equation 8.11, the nodal equations for the interface region can be found as:

$$k_f \left. \frac{\partial T}{\partial y} \right|_{y=\xi H} = k_{eff} \left. \frac{\partial T}{\partial y} \right|_{y=\xi H} \Rightarrow T(\xi_l, i) = \frac{k_f T(\xi_l + 1, i) + k_{eff} T(\xi_l - 1, i)}{k_f + k_{eff}} \quad (8.18)$$

The nodal equations for symmetrical constant heat flux boundary conditions and the boundary condition for  $x=0$  can be found as:

$$T(m+1, i) = T(m, i) + \frac{q'' dy}{k_f} \quad T(1, i) = T(2, i) + \frac{q'' dy}{k_{eff}} \quad (8.19)$$

$$T(j, 1) = T_i$$

where  $T_i$  is the entrance temperature and taken as  $0^\circ\text{C}$ . The number of nodes in  $y$  direction  $n+1$  is taken as  $101$  and the number of nodes in  $x$  direction  $m+1$  is taken as  $301$  for this case.

The error is taken as  $10^{-6}$  on each iteration step for the convergence of the numerical solution.



## CHAPTER 9

### RESULTS AND DISCUSSION

The dimensional and dimensionless heat and fluid flow equations are given in previous chapters. The results of the heat and fluid flow analysis for considered channels discussed in Chapter 4, Chapter 5, Chapter 6, and Chapter 7 are presented in this chapter respectively. The effects of several parameters are discussed.

The consistency of the dimensional and dimensionless solutions is also investigated in this chapter.

#### 9.1. Results for a Channel with Symmetrical Heated Walls

The first analysis is made for symmetrical heated walls in order to find the effects of parameters such as  $Da$ , porosity, permeability on fluid flow and heat transfer.

##### 9.1.1. Dimensional Analysis

A two-dimensional computational model is developed to analyze fluid and heat flow in a channel completely filled with porous medium. The governing equations are given in Chapter 4.

##### 9.1.1.1. The Analyzed Channels

For the dimensional symmetrical heated problem, the channels of Figure 9.1 are considered. A constant heat flux of 100 W is imposed to the channel walls. The total height of the channel is taken as 0.1 m while length of channel 30 m. Three channels are analyzed to find the effect of permeability on heat and fluid flow named as high permeable, medium permeable and low permeable channels. The channels are filled with square bars and fluid flows to the bars perpendicularly. The height (or width) of

bars are different as 0.2, 1.5 and 3.75 mm. The distances between two bars are 1.8, 2.5 and 1.25 mm. The fluid in the channel is considered as air and it flows to the channel at 273 K. The study is performed for bar materials of glass and Aluminum alloy.

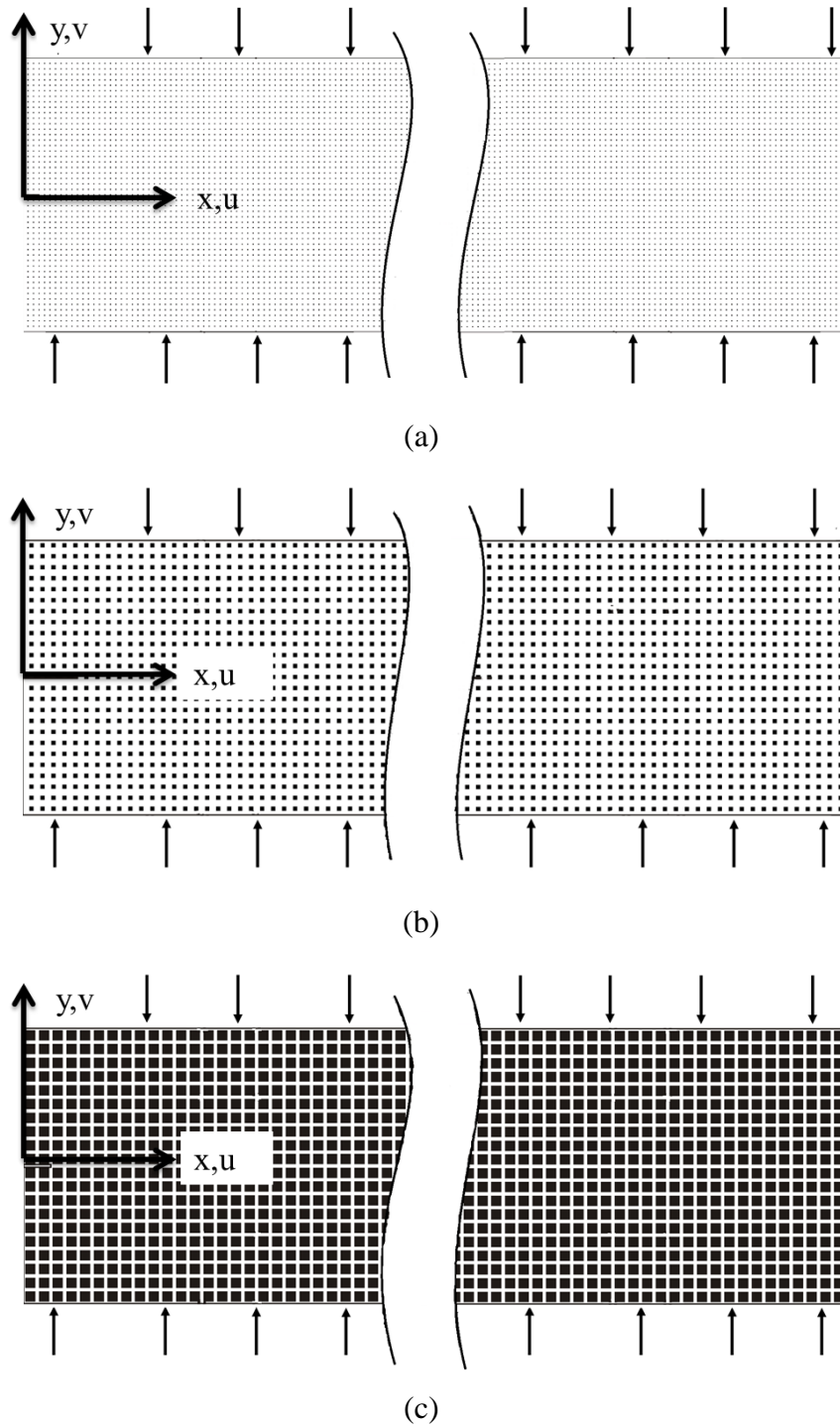


Figure 9.1. Three channels filled with square bars analyzed in this section: (a) High Permeable channel (b) Medium Permeable channel (c) Low Permeable channel

Air flow in the voids between bars and heat is transferred from the channel walls to both bars and fluid. A thermal equilibrium exists between the bars and fluid. Radiation heat transfer among the particles and particles and walls is omitted. The flow is laminar in the channel. The bars are too long that is why the heat and fluid flow can be accepted as two dimensional. The thermophysical properties of fluid and solid are assumed constants and they are taken at  $T = 300$  K. The thermophysical properties of the fluid and solids are given in Table 9.1. The mean velocity of the fluid is taken as 0.38 m/s. The air flow is laminar and a fully developed velocity profile is assumed through the channel. In the other words, the velocity profile is function of  $y$  and it is not changed along the channel in  $x$  direction.

Table 9.1. Thermophysical properties of fluid and solids

Thermophysical Properties of Fluid (Air)		Thermal Conductivities of Solids	
Viscosity ( $\mu$ )	$1.983 \cdot 10^{-5}$ kg/m s	Glass	1.1 W/m K
Density ( $\rho$ )	1161 kg/m <sup>3</sup>	Aluminum Alloy	120 W/m K
Conductivity (k)	0.025 W/m K		
Specific Heat Capacity (Cp)	1.005 kJ/kg K		

The porosity and permeability of the porous media in the channel are given in Table 9.2. Porosity values should be known before doing any calculation. A micro-view of a bar in the channel is shown in Figure 9.2. As seen, the width (or height) of the square bar is shown by  $a$ . The distance between two bars is shown by  $b$ . The values of “ $a$ ” and “ $b$ ” for three high permeable, medium permeable and low permeable channel are given in Table 9.2. Based on the equation derived for this kind of porous medium (Equation 9.1), the porosity values for three channels are calculated and porosity values are given in Table 9.2.

$$\varepsilon = \frac{(a+b)^2 - a^2}{(a+b)^2} \quad (9.1)$$

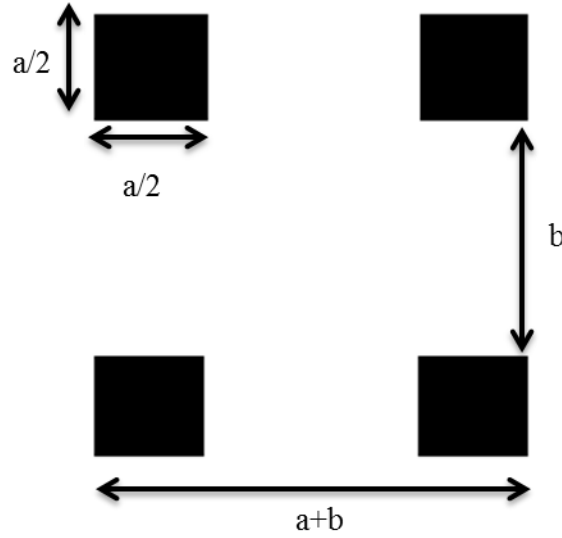


Figure 9.2. A micro-view of a square bar

Permeability value is another parameter which should be known before analyzing heat and fluid flow in the channel. Many correlations have been proposed by researchers for determination of permeability. Peng and Du made a literature survey and presented different correlations of various researchers for determination of permeability. However; one of the common relations for determination of permeability is Carman-Kozeny relation.

$$K = \frac{\varepsilon^3 H^2}{\bar{k}(1-\varepsilon)^2} \quad (9.2)$$

where “H” is the height of the channel which is 0.1 m for the present study . The parameter of  $\bar{k}$  is Kozeny constant and its value for square rods is 120.

Another characteristic parameter of the fluid flow in porous media is the effective viscosity of the fluid and the porous structure shown by  $\mu_{\text{eff}}$  and the dynamic viscosity of the fluid shown by  $\mu_f$ . The ratio of  $\mu_{\text{eff}}$  and  $\mu_f$  is found by using the Equation 4.3.

Table 9.2. The flow parameters for the considered channels.

	a	b	Number of squares in vertical plane	Porosity	Permeability (m <sup>2</sup> )	Darcy	$\mu_{\text{eff}}/\mu_f$
High permeable	0.2	1.80	50	0.99	$3.23 \cdot 10^{-6}$	$1.29 \cdot 10^{-3}$	1.01
Medium permeable	1.5	2.50	25	0.86	$6.02 \cdot 10^{-7}$	$2.41 \cdot 10^{-4}$	1.16
Low permeable	3.75	1.25	20	0.44	$3.10 \cdot 10^{-8}$	$1.24 \cdot 10^{-5}$	2.29

### 9.1.1.2. Results

In chapter 4, the dimensional form of heat and fluid flow equations for a channel completely filled with porous medium are presented. According to the given equations and boundary conditions, heat and fluid flow in the channels described in the previous sections are investigated. Moreover, the heat transfers through the channels are also investigated for two solid materials as Glass and Aluminum alloy. The thermal conductivity for the glass and Aluminum alloy are 1.1 W/mK and 120 W/mK respectively.

Figure 9.3 shows the velocity profiles for the channels with three different permeability coefficients given in Table 9.2. As seen in this figure, the velocity profiles in the channel are not highly changed with the considered three permeability values. The profiles are similar to the profiles of a turbulent flow since square bars causes mixing of fluid in the channel. As expected, the velocity values are zero at the boundaries and a steep velocity gradient is observed at the wall region. The velocity variation is almost uniform at the channel center. Velocity value decreases at the center region decreases with decrease of permeability value. The velocity gradient at the wall region increases with decrease of permeability value.

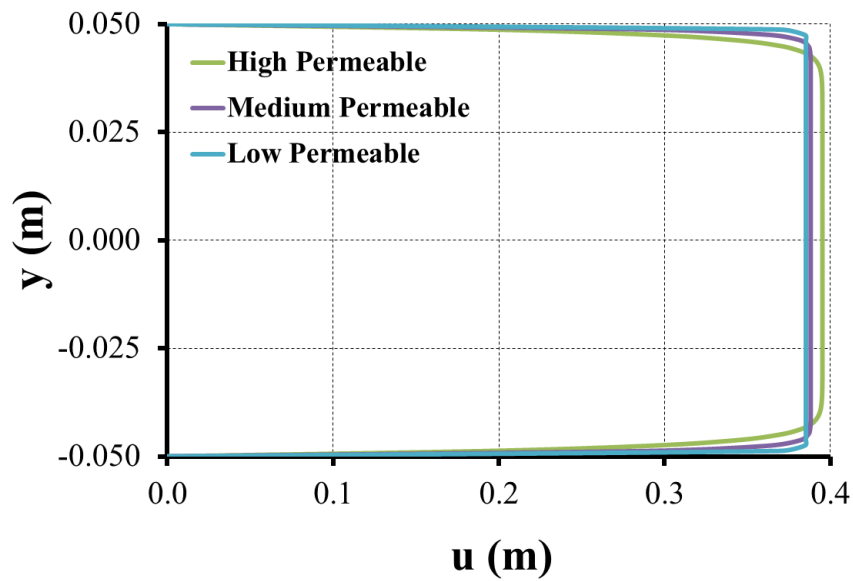


Figure 9.3. Dimensional velocity distributions for the flows with different permeabilities.

Figure 9.4 shows isotherms in the channels with three different permeability coefficients when the material of the solid is glass. Figure 9.4(a) shows the isotherms for the high permeable channel. As seen, the isotherms are symmetrical respect to the centerline since a symmetrical heat flux is imposed to the channel. The maximum air temperature is observed at the walls. The temperature decreases towards the centerline. The minimum temperature for a cross section is at the center of the channel since heat is transferred from the boundaries. Although isotherms are similar with each other, they are not identical and they change along x axis. Figure 9.4(b) indicates isotherms in the medium permeable channel. There are similarities between isotherms of medium and high permeable channels. Maximum temperature is observed at the walls and its value decreases towards the channel center. The isotherms are symmetrical respect to channel center. The permeability of medium permeable ( $k = 6.02 \times 10^{-7} \text{ m}^2$ ) is lower than high permeable channel. It brings higher effective thermal conductivity so it causes the heat transfer is enhanced in y direction and the temperature changes in y direction becomes smaller. Figure 9.4(c) shows isotherms in a low permeable channel. As seen, the temperature change in y direction becomes smaller due to the increase of thermal conductivity for a low permeable channel and almost a flatten isotherms are seen.

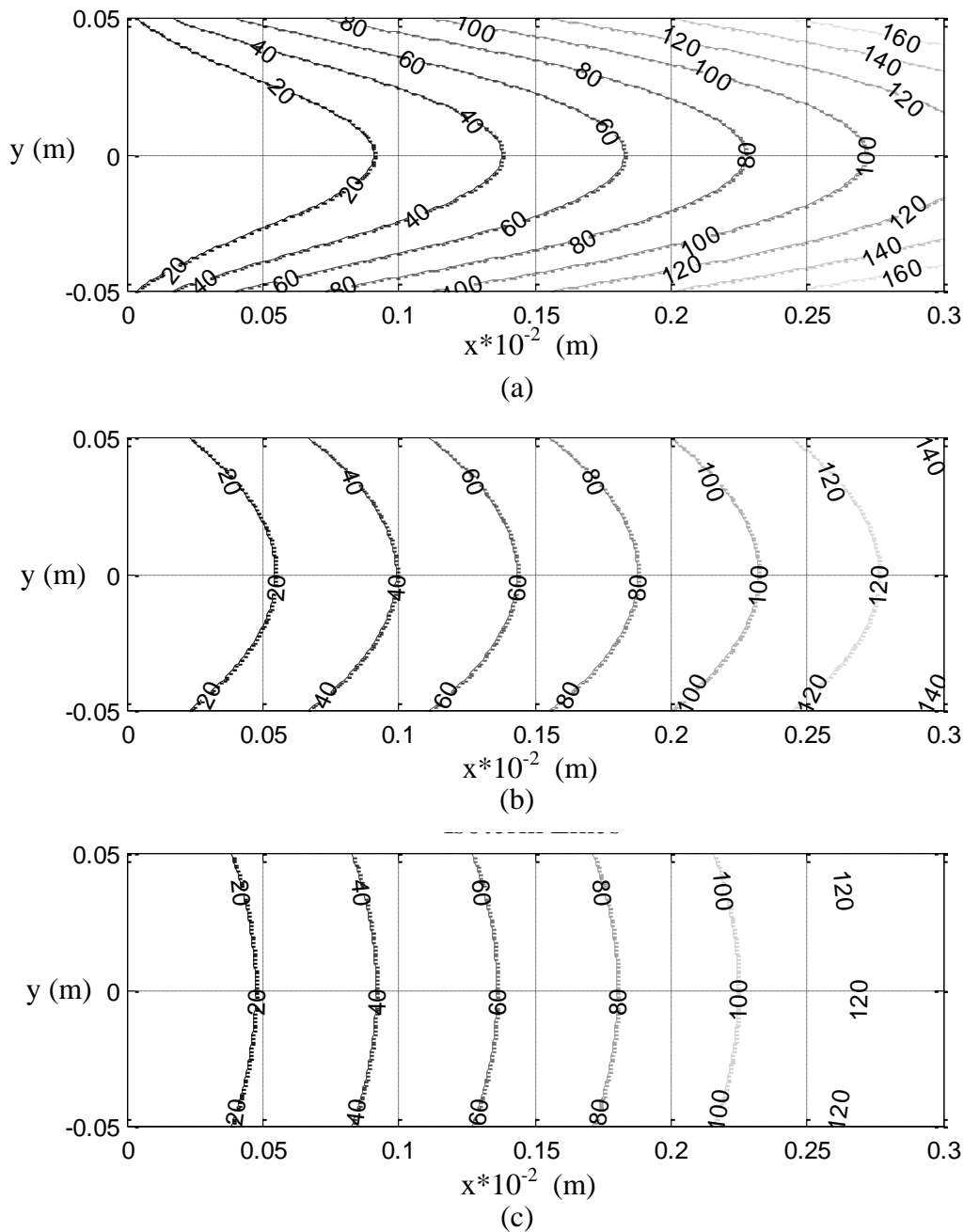


Figure 9.4. Isotherm lines through the low conductive solid used channel: (a) High Permeable channel (b) Medium Permeable channel (c) Low Permeable channel

The isotherms of the channels with three different permeability coefficients when the material of the solid is aluminum alloy are seen in Figure 9.5. Due to the symmetrical heat flux is imposed to the channel; the isotherms are symmetrical respect to the centerline. The isotherms seem similar with each other and they are not change along the x direction because of the high conductivity of solid. Figure 9.5(a) shows the isotherms in the high permeable channel. In high permeable channel, the maximum air temperature is observed at the walls. The high temperatures drop through the center of

the channel. The minimum temperature for a cross section is at the center of the channel since heat is transferred from the boundaries. Figure 9.5(b) indicates isotherms in the medium permeable channel. The isotherms are almost flat due to the decreased permeability and high conductivity of aluminum alloy. Figure 9.5(c) shows isotherms in a low permeable channel. There is very small difference between Figure 9.5(b) and Figure 9.5(c). The isotherms are symmetrical respect to channel center and they are almost flat. The low permeability of the channel and high conductivity of the solid cause the enhancement of heat transfer in y direction and the temperature changes in y direction is almost zero.



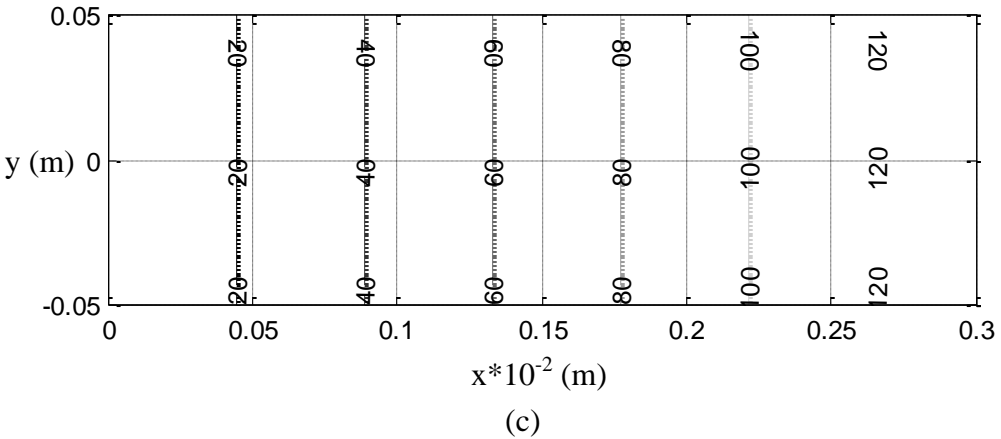
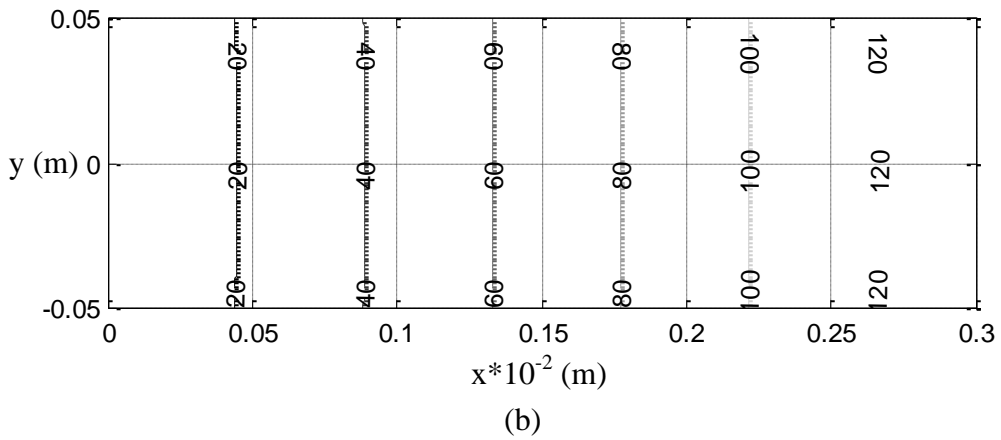
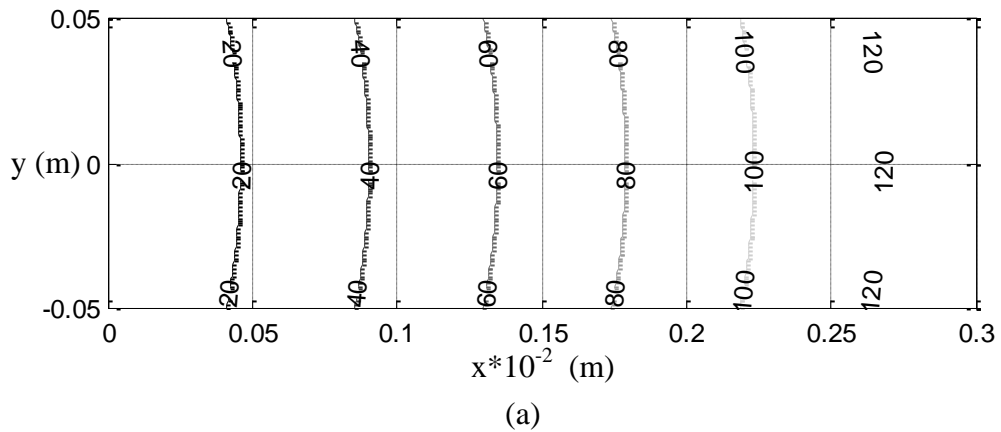


Figure 9.5. Isotherm lines through the high conductive solid used channel:(a) High Permeable channel (b) Medium Permeable channel (c) Low Permeable channel

Figure 9.6 shows mean temperature values for low permeable channel and wall temperature values through the considered channels with three different permeability coefficients when the material of the solid is glass ( $k_s=1.1$  W/mK). The mean temperature and wall temperature values for the aluminum alloy filled channel are

almosts identical for all permeability values. These temperatures are also the same with mean temperature of the glass filled channel. However, when the material of the solid is glass, the wall temperature values are different than mean temperature. The wall temperature value of the glass-used channel is grater than the mean temperature value. In this channel, the difference between wall temperature and mean temperature values is increasing in x direction at the entrance region but the difference become constant at a certain point, the flow can be assumed as fully developed flow after this point when the material of the solid is glass. As permeability decreases or conductivity of solid increaeses, the difference between the wall temperatures and mean temperatures become smaller.

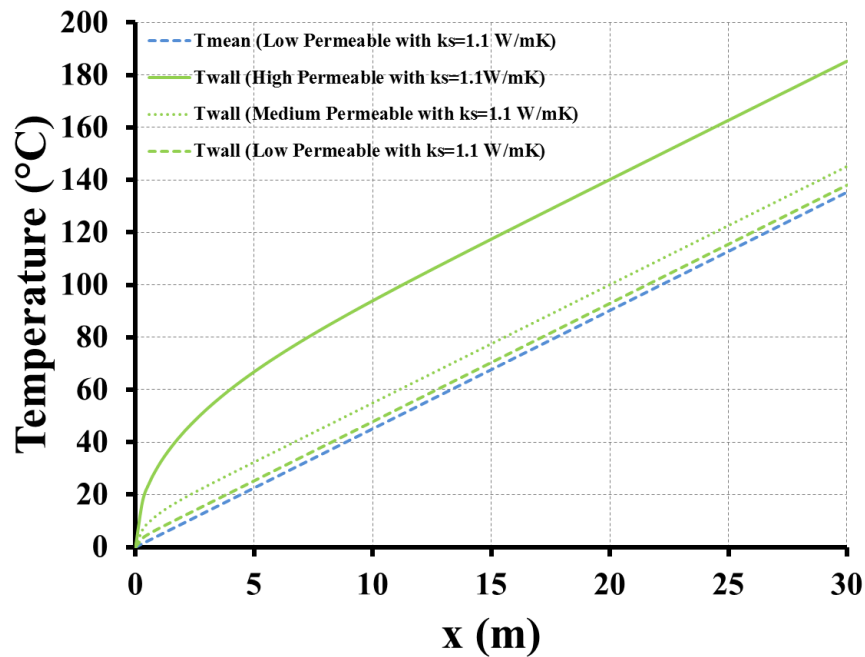


Figure 9.6. Mean Temperature and wall temperature values through the channels.

Another analyzed parameter is Nu. Figure 9.7 shows Nu variation through the channels. The Nu is given by Equation 5.32 to define heat transfer at a boundary within a fluid. The heat flux term in Equation 5.32 can be solved by using Equation 4.9. In this figure, the blue lines indicate the channel which the material of the solid is glass ( $k_s = 1.1$  W/mK) while black lines indicate the channel which the material of solid is aluminum alloy ( $k_s = 120$ W/mK). As seen in this figure, the Nu decrease until the flow become fully developed. If the conduction of material increases, the flow become fully

developed more quickly. If the permeability of flow decreases, the flow also become fully developed earlier due to the mixing affect of the porosity. According to the figure, Nu only depends on the permeability of the flow. Conduction of the solid does not affect the Nu of fully developed region.

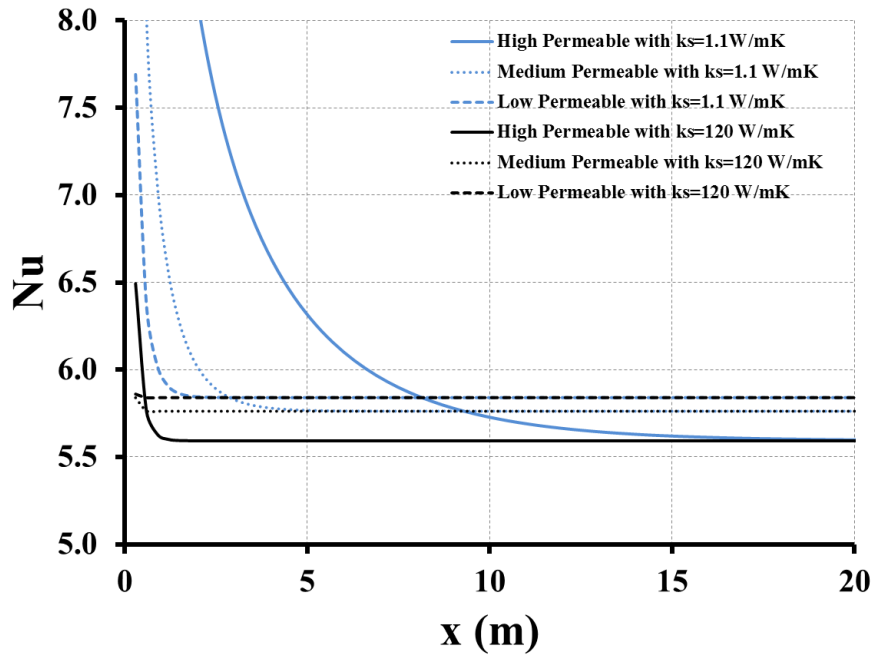


Figure 9.7. Nu values through the channels: Blue lines indicate glass used channel while black lines indicate aluminum alloy used channel

The solution procedure for pressure drop are given at the end of the Chapter 4. According to the numerical results, the negative gradient values of the pressure along the x axes for the high permeable, medium permeable and low permeable channels are calculated as 2.4230, 12.79, 246.308 respectively.

### 9.1.2. Dimensionless Analysis

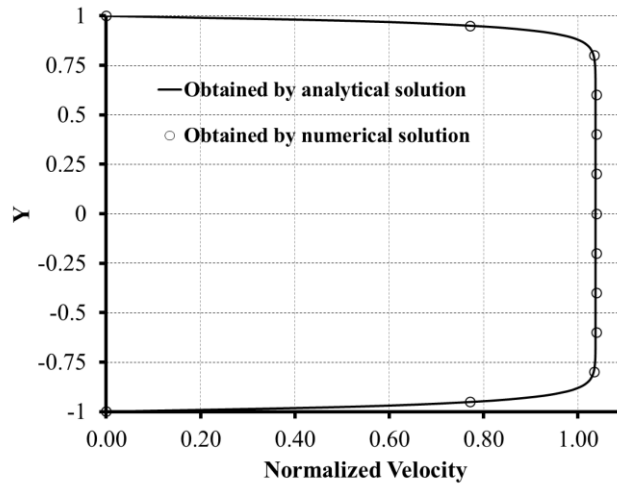
In Chapter 5, the heat and fluid flow in a channel which is completely filled with porous medium with constant heat flux boundary conditions is investigated analytically. In this section, firstly, the numerical results which are given in Section 9.1.1 are compared with the analytical results, after checking compatibility, the effects of Da on

the normalized velocity profile; dimensionless temperature profile, Nu and pressure drop are analyzed.

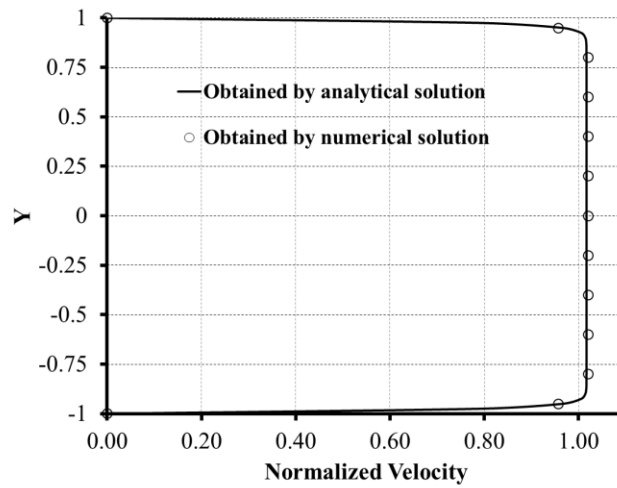
The numerical results which are given in Section 9.1 are converted to the dimensionless results with using defined dimensionless parameters as Equation 5.5. The converted results are compared with the results from the solutions of the analytical equations presented in Chapter 5.

### **9.1.2.1. Comparison of the Numerical with Analytical Results**

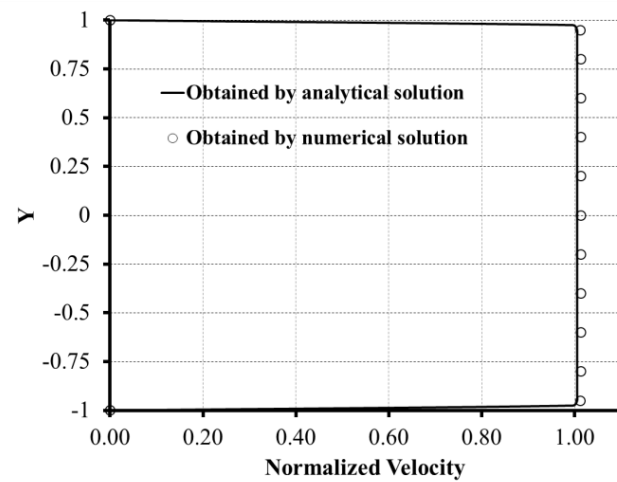
The comparison of the numerical solution with the analytical solution is done with the calculation of dimensionless parameters of the analytical equations such as Da, M, Y, S, U, H, K,  $\theta$  by using the dimensional parameters of analyzed channels in Section 9.1.1.1. The normalized velocity profiles from the converted forms of numerical solutions to the dimensionless results and the normalized velocity profiles from analytical solutions which are given in Chapter 5 are shown in Figure 9.8. As it can be seen in Figure 9.8, the analytical results are consistent with the numerical results.



(a)



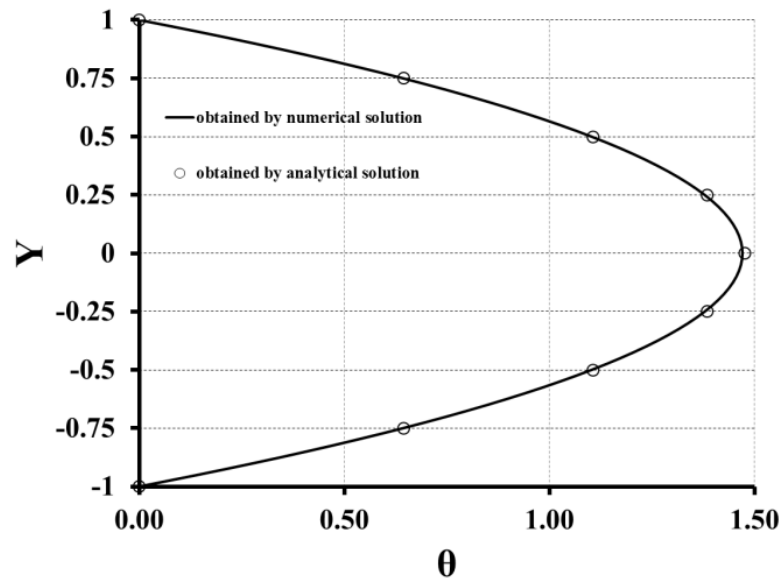
(b)



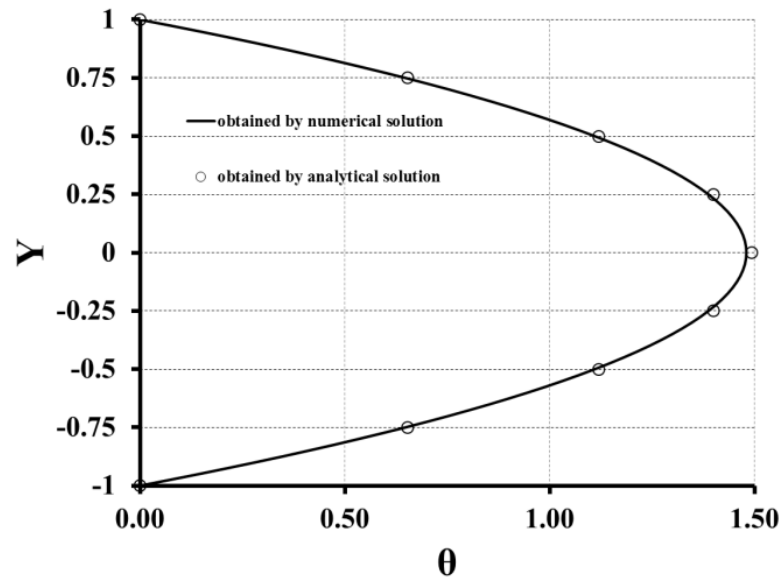
(c)

Figure 9.8. Comparison of the converted normalized velocity profiles, which are obtained by numerical results, with the analytical results: (a) High Permeable channel (b) Medium Permeable channel (c) Low Permeable channel

Figure 9.9 shows the comparison of dimensionless temperature profiles from the converted forms of numerical solutions and the dimensionless temperature profiles from analytical solutions. Figure 9.9(a) belongs to the dimensionless temperature profile of the medium permeable channel when the material of the solid is glass and Figure 9.9(b) belongs to the low permeable channel when the material of solid is aluminum alloy. According to the Figure 9.9, the results obtained by numerical solutions are consistent with the results obtained by analytical solutions. Only two of the figures are shown because of the all of the dimensionless temperature profiles of the numerical solution for high permeable, medium permeable and low permeable channels are consistent with the dimensionless temperature profiles of the analytical solution.



(a)



(b)

Figure 9.9. Comparison of the converted dimensional temperature profiles which are obtained by numerical results with the analytical results: (a) The medium permeable channel when the material of the solid is glass (b) The low permeable channel when the material of solid is aluminum alloy

Table 9.3 shows the Nu calculated both numerically and analytically for all considered channels. As seen, there is not a big difference between results. This table shows accuracy of our solutions for numerical and analytical.

Table 9.3. Comparison of the analytical and numerical results for the Nu

	Conductivity of Solid=1.1 W/mK		Conductivity of Solid=120 W/mK	
	Nu From Numerical Solution	Nu From Analytical Solution	Nu From Numerical Solution	Nu From Analytical Solution
High Permeable	5.5934	5.6161	5.5925	5.6161
Medium Permeable	5.7624	5.8104	5.7623	5.8104
Low Permeable	5.86	5.9373	5.86	5.9373

### 9.1.2.2. Effect of Da

The effects of Da on the normalized velocity profile, dimensionless temperature profile, Nu and pressure drop are analyzed according to the equations given in Chapter 5. Da is changed between 10 and  $10^{-5}$  to obtain the effect of it. The relation between  $\mu_{\text{eff}}/\mu$  is taken as 1.3 for the porosity value as 0.75. The ratio of fluxes is 1 for the symmetrical heat flux boundary condition.

The analyzing of velocity profile for the low Da is hard to observe so the normalized velocity profiles are investigated in Figure 9.10. The velocity profiles are similar to the profiles of a turbulent flow since the obstacles in the channel causes mixing of fluid in the channel. The velocity values are zero at the boundaries because of the no-slip boundary condition and a sharp velocity gradient is observed at the wall region. The velocity gradient at the wall region increases with decrease of Da. The velocity variation is almost uniform at the channel center. If Da decreases, the effect of porous media increases in the channel so velocity value decreases at the center region by reducing Da.



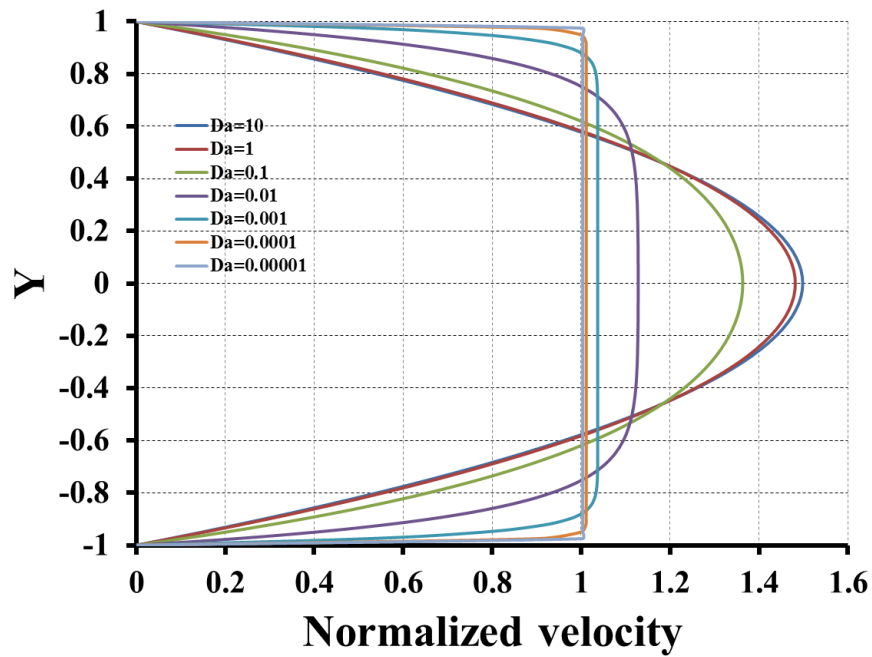


Figure 9.10. Normalized velocity distributions for the flows with different Da.

Figure 9.11 indicates the dimensionless temperature profiles for the flows with different Da. The dimensionless temperature values are zero at the boundaries because of the symmetrical heating. The gradient of the dimensionless temperatures at the surface for flows with low Da is larger than high Da because the mixing effects of Da increase the conduction between surface and fluid. The gradients of the dimensionless temperatures are zero and the dimensionless temperatures take the largest value at the center of the channel.

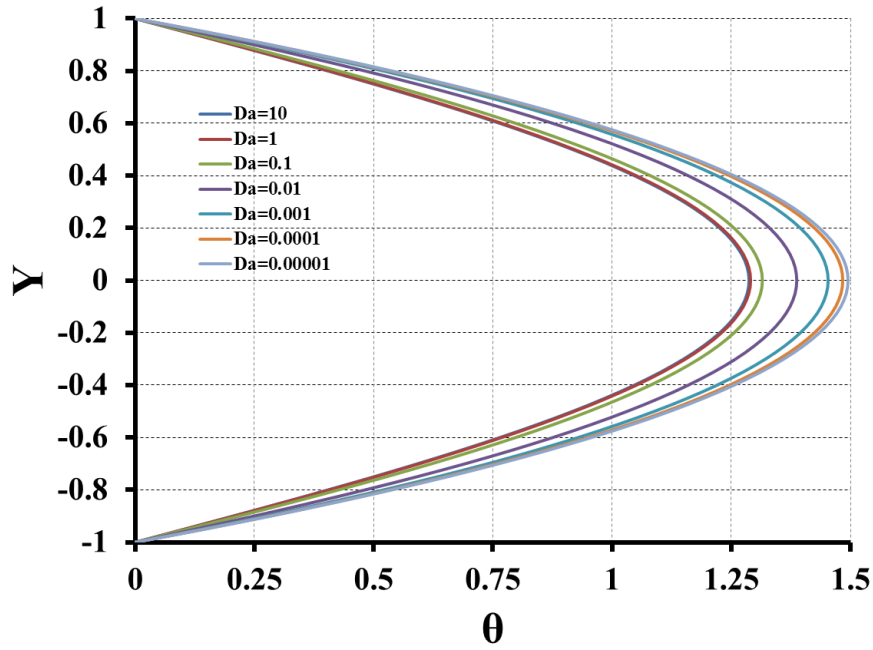


Figure 9.11. Dimensionless temperature distributions for the flows with different Da.

The variation of Nu with increasing Da can be seen in Figure 9.12. Da is plotted using a logarithmic scale to observe the variation of Nu more clearly. When Da increases, the Nu decreases. For flows with low Da, the Nu increases and consequently we have enhancement of heat transfer. When Da increases, the effect of porous media become smaller and Nu becomes closer to 4.1176, which indicates the flow through a clear channel.

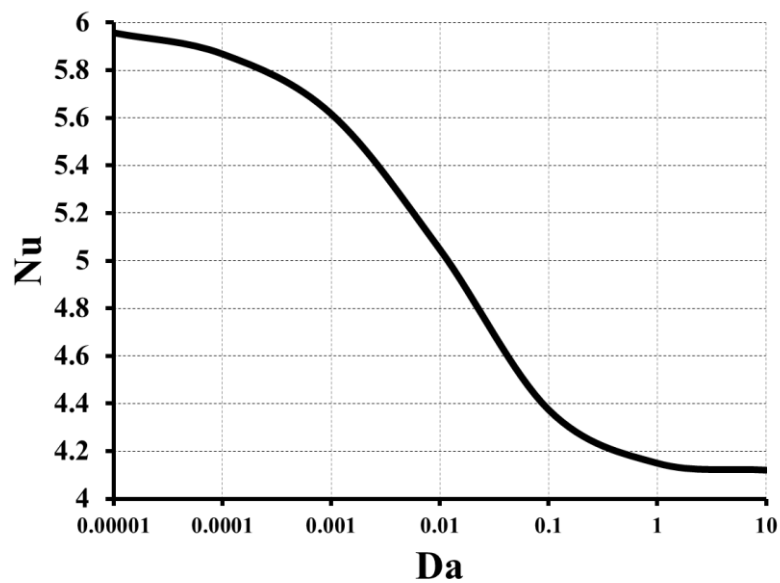


Figure 9.12. Logarithmic plot of Da vs. Nu

The Nu for clear fluid fully developed channel with constant heat flux is given as 4.1176. The heat transfer enhancement in porous media can be observed with the help of Nu for clear fluid channel and Nu based on fluid thermal conductivity as:

$$Nu_{pc} = Nu K^* \quad (9.2)$$

Where  $Nu_{pc}$  is the Nu based on fluid thermal conductivity,  $Nu$  is Nu of channel and  $K^*$  is the ratio of effective thermal conductivity to the fluid thermal conductivity. Heat transfer improvement ratio,  $\epsilon_{th}$ , can be calculated by dividing Nu based on fluid thermal conductivity to the Nu for clear fluid channel which is 4.1176. Figure 9.13 shows the heat transfer improvement ratio by using porous media for three different effective thermal conductivity ratios. The figure is plotted using a logarithmic scale to observe the variation of the heat transfer increment ratio more clearly. As seen in the figure, decreasing Da increases the heat transfer.

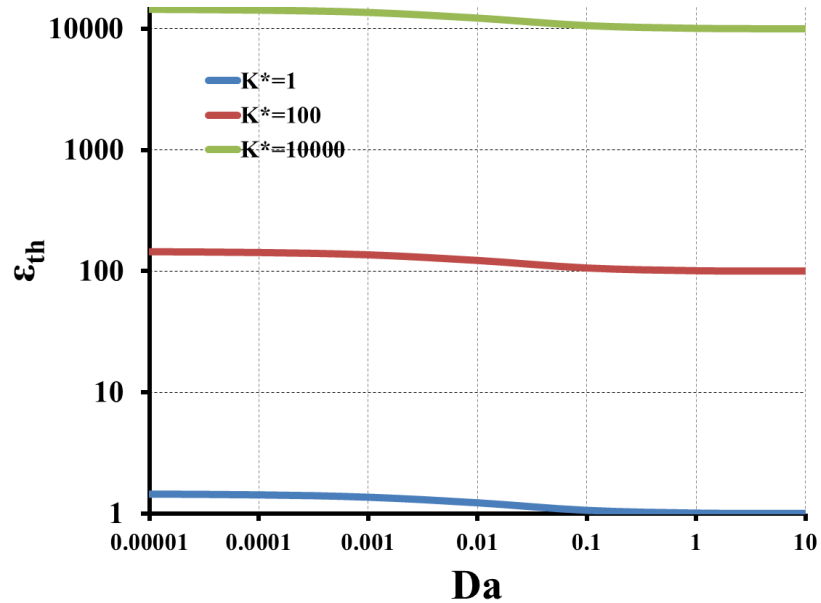


Figure 9.13. Logarithmic plot of Heat transfer increment ratio vs. the Da

The porous media in the channel brings pressure drop defined as friction coefficient in Chapter 5.1.3. The friction coefficient can be found by using Equation (5.40) which its variation can be seen in Figure 9.14. The figure is plotted using a logarithmic scale to observe the variation of friction coefficient more clearly. When Da

increases, the friction coefficient decreases. While there is not a very large friction coefficient in  $Da$  greater than  $10^{-2}$ . For the  $Da$  less than  $Da = 10^{-2}$ , the friction coefficient takes extremely large values.

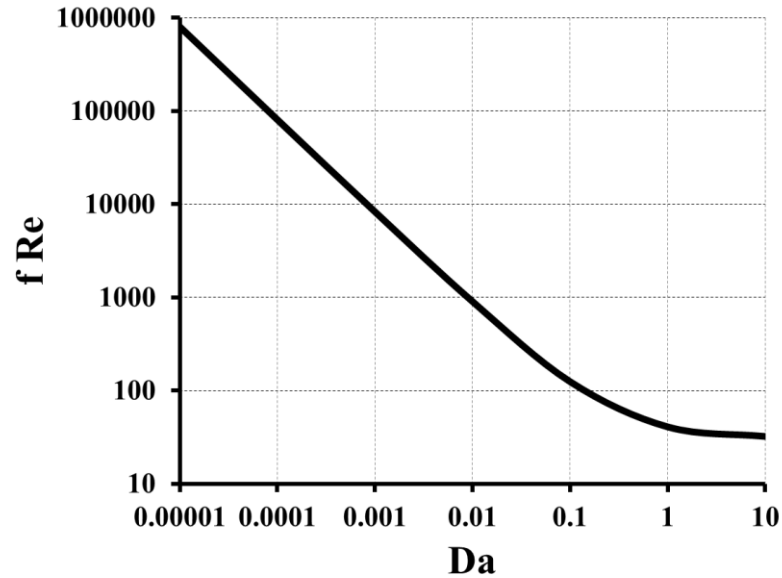


Figure 9.14. Logarithmic plot of friction coefficient vs.  $Da$

Pressure drop increment ratio,  $\epsilon_p$ , can be found by using the same procedure with finding heat transfer increment ratio. The pressure drop increment ratio for clear fluid fully developed channel with constant heat flux is given as 24. The increment of pressure drop by using porous media can be observed with the help of pressure drop increment ratio for clear fluid channel. Pressure drop increment ratio,  $\epsilon_p$ , can be calculated as dividing friction coefficient of the porous channel in to the friction coefficient of a flow in a clear channel which is 24. Figure 9.15 shows the pressure drop increment ratio by using porous media.  $Da$  is plotted using a logarithmic scale to observe the variation of the pressure increment ratio more clearly. As seen in the figure, decreasing  $Da$  increases pressure increment ratio. Like Figure 9.14, there is a huge increment for smaller than  $10^{-2}$   $Da$ .

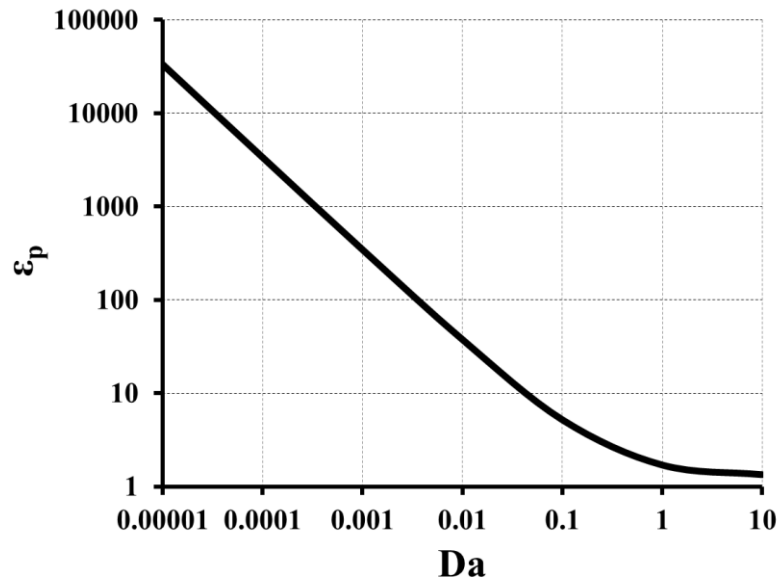


Figure 9.15. Logarithmic plot of pressure drop increment ratio vs. Da

The ratio of  $\varepsilon_{th}$  and  $\varepsilon_p$  is called as overall performance,  $\varepsilon$ . For the values of  $\varepsilon$  greater than 1 means the heat transfer enhancement is greater than the increase of pressure drop while for the values of  $\varepsilon$  less than 1 means the increase of pressure drop is greater than the heat transfer enhancement in the channel. Figure 9.16 shows the variation of overall performance of the channels with Da. The overall performance is rising with increased Da and increased the ratio of effective thermal conductivity the fluid thermal conductivity ( $K^*$ ). For Da greater than 1 which means almost clear channel there is a constant overall performance. The increased overall performance is coming from only  $K^*$  ratio for Da greater than 1. The figure shows channels completely filled with the solids which have  $K^* = 1$  is not useful for heat transfer enhancement if the pressure drop is considered. The Da number should be chosen at least between 0.001 and 0.01 for the  $K^* = 100$ . Almost all Da number gives a reasonable overall performance value for the ratio of  $K^*$  is 10000.

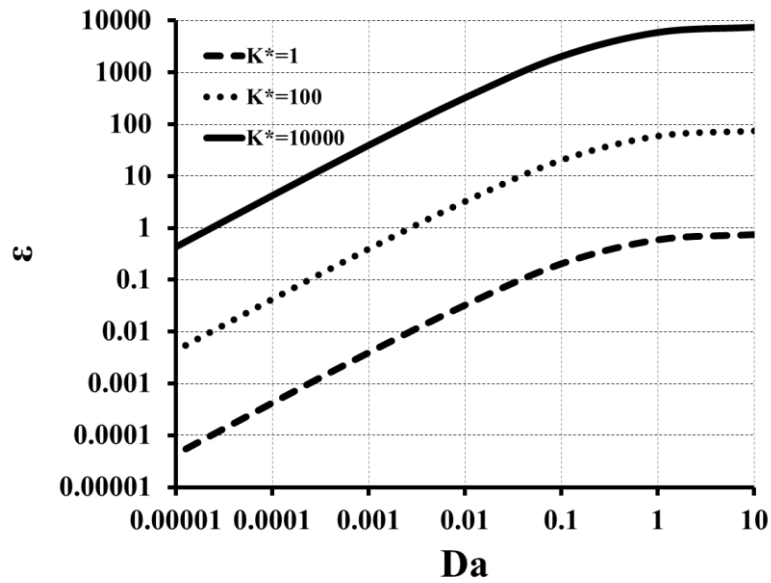


Figure 9.16. Logarithmic plot of overall performance vs. the Da

Thermal conductivities for several fluids and solids are given in Table 9.4. The table helps comprehension of the ratio between effective conductivity over conductivity of fluid,  $K^*$ .

Table 9.4. Thermal Conductivities of several solids and fluids [33]-[34]-[35]-[36]

Fluid	Fluid Conductivity ( $k_f$ ) (w/mK)	Solid	Solid Conductivity ( $k_s$ )(w/mK)	Porosity $\epsilon$	$k_{eff}$	$K^*$ ( $k_{eff}/k_f$ )
Air	0.025	Wood	0.21	0.99	0.03	1.07
Air	0.025	Glass	1.1	0.99	0.04	1.43
Air	0.025	Cast Iron	55	0.99	0.57	22.99
Air	0.025	Aluminum alloy	120	0.99	1.22	48.99
Air	0.025	Gold	315	0.99	3.17	126.99
Hydrogen	0.172	Wood	0.21	0.99	0.17	1.00
Hydrogen	0.172	Glass	1.1	0.99	0.18	1.05
Hydrogen	0.172	Cast Iron	55	0.99	0.72	4.19
Hydrogen	0.172	Aluminum alloy	120	0.99	1.37	7.97
Hydrogen	0.172	Gold	315	0.99	3.32	19.30
Air	0.025	Wood	0.21	0.86	0.05	2.04
Air	0.025	Glass	1.1	0.86	0.18	7.05
Air	0.025	Cast Iron	55	0.86	7.76	310.23
Air	0.025	Aluminum alloy	120	0.86	16.90	675.86
Air	0.025	Gold	315	0.86	44.32	1772.73
Hydrogen	0.172	Wood	0.21	0.86	0.18	1.03

(cont. on next page)

Table 9.4. (cont.)

Hydrogen	0.172	Glass	1.1	0.86	0.30	1.76
Hydrogen	0.172	Cast Iron	55	0.86	7.88	45.83
Hydrogen	0.172	Aluminum alloy	120	0.86	17.02	98.97
Hydrogen	0.172	Gold	315	0.86	44.44	258.40
Air	0.025	Wood	0.21	0.44	0.13	5.14
Air	0.025	Glass	1.1	0.44	0.63	25.08
Air	0.025	Cast Iron	55	0.44	30.81	1232.44
Air	0.025	Aluminum alloy	120	0.44	67.21	2688.44
Air	0.025	Gold	315	0.44	176.41	7056.44
Hydrogen	0.172	Wood	0.21	0.44	0.19	1.12
Hydrogen	0.172	Glass	1.1	0.44	0.69	4.02
Hydrogen	0.172	Cast Iron	55	0.44	30.88	179.51
Hydrogen	0.172	Aluminum alloy	120	0.44	67.28	391.14
Hydrogen	0.172	Gold	315	0.44	176.48	1026.02

## 9.2. Results for a Channel with Asymmetrical Heated Walls

The second analysis is made with same channels which used in Chapter 9.1 but asymmetrical heated walls is used in order to find the effects of heat flux ratio on to the heat transfer and Nu.

### 9.2.1. Dimensional Analysis for Completely Filled Channels

A two-dimensional computational model is developed to analyze heat flow in a channel completely filled with porous medium with imposing different heat fluxes on to the walls. The governing equations are given in Chapter 4.

#### 9.2.1.1. The Analyzed Channels

For the dimensional asymmetrical heated problem, the channels of Figure 9.1 are considered again. All of the properties of considered channels are the same with the analyzed channels which is mentioned in Chapter 9.1 except heat fluxes on the walls. Different amount of heat fluxes are imposed into the channel walls. A constant 100 W

heat flux is imposed to the upper wall while a constant 50 W heat flux is imposed lower wall as seen in Figure 9.17.

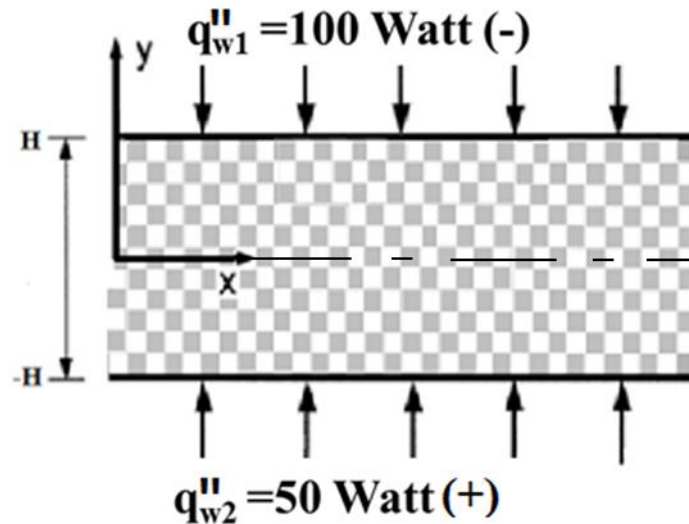


Figure 9.17. The considered channel with exposed heat fluxes on to the walls

The thermophysical properties of the fluid and solids are the same with Chapter 9.1. Tables 9.1 and 9.2 can be used to remind the thermophysical properties of the fluid, solids and the flow parameters of considered channels. The mean velocity of the fluid is the same with Chapter 9.1 which is 0.38 m/s. The same assumptions for the flow are also valid in this chapter and the velocity profile is not analyzed because the velocity profile is not a function of heat fluxes. The comments on the velocity profiles in Chapter 9.1 are valid for this chapter.

### 9.2.1.2. Results

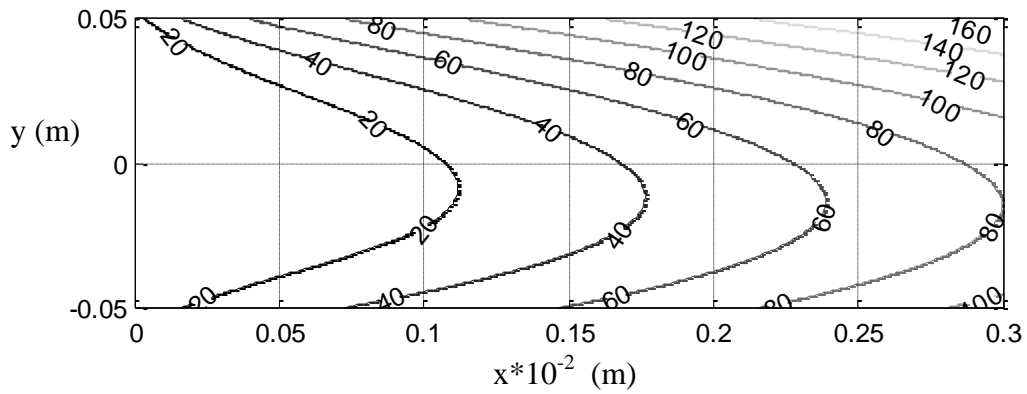
Heat flow in the channels described in the previous sections is investigated for symmetrical boundary conditions. In chapter 4, the dimensional form of heat and fluid flow equations for a channel completely filled with porous medium are presented. In this section, a constant 100 W heat flux is imposed to the upper wall while a constant 50 W heat flux is imposed lower wall. According to the given equations and boundary conditions, the heat transfer through the channels is investigated for the same two solid



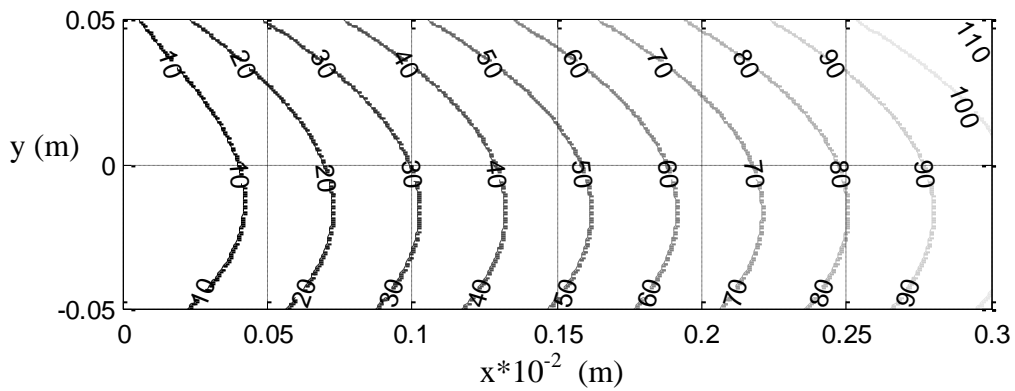
materials as Glass and Aluminum alloy. The thermal conductivity for the glass and Aluminum alloy are 1.1 W/mK and 120 W/mK respectively.

The velocity profiles for the channels are not examined in this section because the velocity profile is not a function of heat fluxes. The velocity profiles in Figure 9.3 can be seen to remind the velocity profiles and their properties according to the different permeabilities.

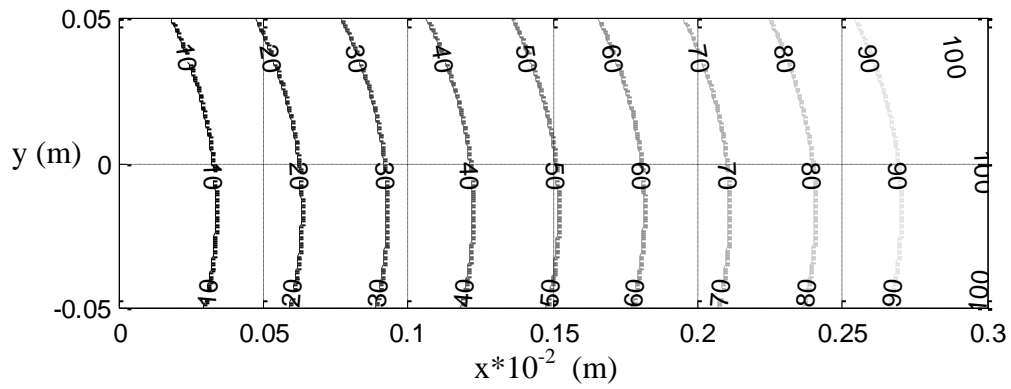
Figure 9.18 shows the isotherms in the asymmetrical heated channels with three different permeability coefficients when the material of the solid is glass. Figure 9.18(a) shows the isotherms for the high permeable channel. The effect of convection can be seen clearly towards the center of the channel. However, the isotherms are not symmetrical respect to the centerline since asymmetrical heat fluxes are imposed to the channel walls which are 100 and 50 W for upper and lower wall, respectively. The maximum air temperature is observed at the upper wall. The temperature decreases towards the centerline but the minimum temperature for a cross section is closer to the lower wall since the lower wall is imposed lower heat flux ( $q''_{w1}=100$  Watt and  $q''_{w2}=50$  Watt). Although isotherms are similar with each other, they are not identical and there are small changes along x axis. Figure 9.18(b) indicates the isotherms in the medium permeable channel. There are similarities between isotherms of medium and high permeable channels but the effect of convection for medium permeable channel decreases. Maximum temperature is observed at the upper wall and its value decreases towards the channel center. The minimum temperature point is closer to the lower wall because of the asymmetrical heating. The permeability of medium permeable ( $k=6.02*10^{-7}$  m<sup>2</sup>) is lower than high permeable channel. It brings higher effective thermal conductivity so it causes the enhancement of heat transfer in y direction and consequently the temperature changes in y direction become smaller. Figure 9.18(c) shows isotherms in a low permeable channel. As seen, the temperature change in y direction becomes smaller due to the increase of thermal conductivity for a low permeable channel and more flatten isotherms are seen.



(a)



(b)



(c)

Figure 9.18. Isotherm lines through the low conductive solid used channel with asymmetrical heating:(a) High Permeable channel (b) Medium Permeable channel (c) Low Permeable channel

The isotherms of the channels with three different permeability coefficients when the material of the solid is aluminum alloy are seen in Figure 9.19. Due to the asymmetrical imposed heat fluxes onto the channel wall; ( $q''_{w1}=100$  Watt and  $q''_{w2}=50$  Watt) the isotherms should not be symmetrical with respect to the centerline. The isotherms seem similar with each other and they are not change along the x direction

because of the high conductivity of solid. Figure 9.19(a) shows isotherms in the high permeable channel. In high permeable channel, the maximum air temperature is observed at the upper wall because of the higher flux. The high temperatures at the upper wall drop through the center of the channel. However, the isotherms become almost flatten in the region between center and lower wall of the channel. Figure 9.19(b) indicates isotherms in the medium permeable channel. The isotherms are almost flat due to the decreased permeability and high conductivity of aluminum alloy. Figure 9.19(c) shows isotherms in a low permeable channel. There is very small difference between Figure 9.19(b) and Figure 9.19(c). The isotherms are almost symmetrical respect to channel center and they are almost flat because of the increasing effect of low permeability and the conductivity of aluminum alloy on the effective conductivity of the flow. The low permeability of the channel and high conductivity of the solid cause the heat transfer is enhanced in y direction and the temperature changes in y direction is almost zero.

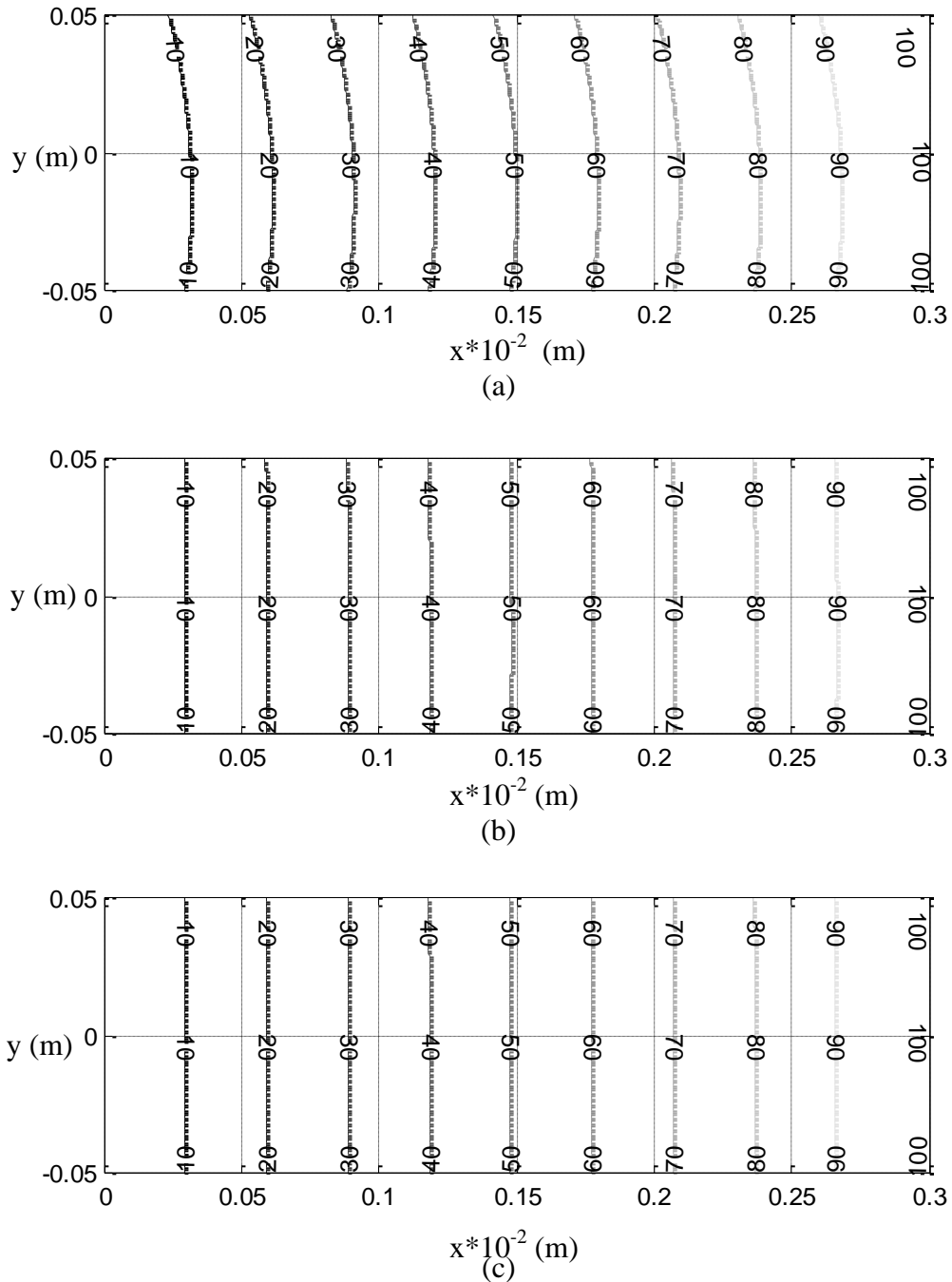
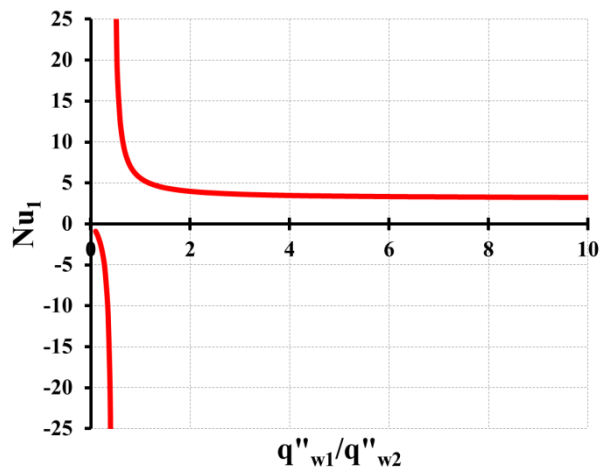


Figure 9.19. Isotherm lines through the high conductive solid used channel with asymmetrical heating: (a) High Permeable channel (b) Medium Permeable channel (c) Low Permeable channel

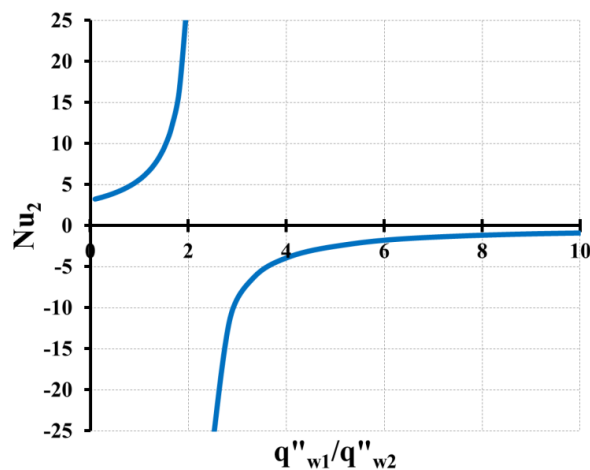
The variation of the individual Nu for upper and lower wall are analyzed to understand heat transfer relation with heat flux ratio more clearly. The results belong only the high permable channel when the material of solid is glass because the Nu variation is similar for all permeability and effeteive conduction values. The upper wall is hold fixed 100 Watt of heat flux while the lower heat flux is changed between 5 Watt

and 1000 Watt. Figure 9.20(a) shows the upper wall Nu ( $Nu_1$ ) variation according to the changing heat flux ratio. As seen, Nu takes negative values when the lower wall heat flux is increased between 5 Watt and 45 Watt. However, the Nu goes infinity at heat flux ratio at about 0.45, after this point Nu changes direction. The cause of the change of the direction of the Nu is the value of  $T_{mean}$  become smaller than the value of  $T_{wall}$  after this point. Figure 9.20(b) shows the lower wall Nu ( $Nu_2$ ) variation according to the changing the heat flux ratio. Nu has positive value until the heat flux ratio become 2, the Nu goes infinity at the ratio about 2, and the Nu has negative values after the heat flux ratio ( $q''_{w1}/q''_{w2}$ ) is greater than 2.2.

The values of individual Nu for upper and lower wall and the overall Nu for the specific heat flux ratios given in Table 9.5.



(a)



(b)

Figure 9.20.  $Nu_1$  (upper wall) and  $Nu_2$  (lower wall) variations vs.  $q''_{w1}/q''_{w2}$  for high permeable channel when the material of solid is glass.

Table 9.5. The values of upper wall Nu ( $Nu_1$ ), lower wall Nu ( $Nu_2$ ) and overall Nu

$q''_{w1}$	$q''_{w2}$	$q''_{w1}/q''_{w2}$	$Nu_1$	$Nu_2$	Nu (Overall)
100	5	20	3.17	-0.39	5.6
100	50	2	3.99	29	5.6
100	100	1	5.6	5.6	5.6
100	150	0.67	9.39	4.41	5.6
100	250	0.4	-26.52	3.77	5.6
100	500	0.2	-2.51	3.4	5.6
100	1000	0.1	-0.89	3.24	5.6

While the individual Nu have negative and positive values, the overall Nu does not depend on the heat flux ratio because it varies only depend on to the permeability of the channel. The dimensional calculation of the overall Nu gives the value of 5.6, 5.77, and 5.86 for the high permeable, medium permeable and low permeable channel respectively.

Figure 9.21 shows the outlet temperature for high permeable channel when the material of solid is glass. The heat flux of upper wall is held constant as 100 Watt and the heat flux of lower wall is imposed as 35 Watt, 45 Watt and 55 Watt to see the effects of the change of the direction of the Nu on the temperature distribution and outlet temperature. The temperature distribution and outlet temperature are not affected with the direction of Nu as seen Figure 9.21. The change of the direction of the Nu is caused the relation between  $T_{mean}$  and  $T_{wall}$ . The sign of Nu is changed without changing of heat flux direction at the lower wall, as it can be seen from Figure 9.21.

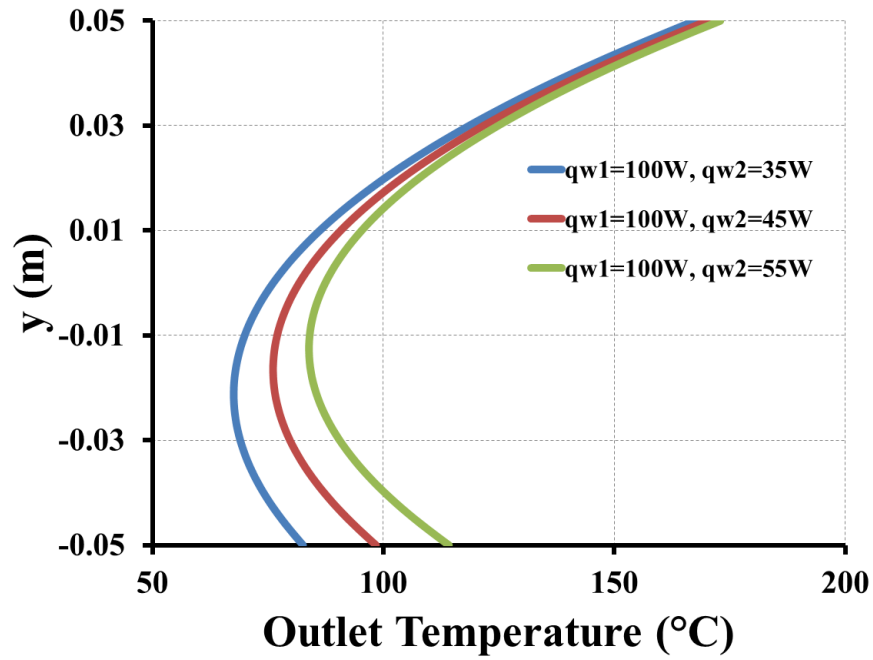


Figure 9.21. The outlet temperatures of the considered channel while  $Nu_2$  changes its direction.

The variations of upper, lower and mean temperature at the exit of channel with the ratio of imposed heat flux are shown in Figure 9.22. The differences between the mean temperature, and temperature of lower and upper walls vary with the change of  $q''_{w1}/q''_{w2}$ . The diagram can be divided into three regions. In the first region ( $q''_{w1}/q''_{w2} < 0.48$ ), the mean temperature is greater than the temperature of upper wall  $T_{w1}$  and smaller than the temperature of lower wall  $T_{w2}$ , hence  $(T_{w1} - T_{mean}) < 0$  while  $(T_{w2} - T_{mean}) > 0$ . In the second region ( $0.48 < q''_{w1}/q''_{w2} < 2.2$ ), the mean temperature is smaller than both the temperature of upper and lower walls and consequently  $(T_{w1} - T_{mean}) > 0$  and  $(T_{w2} - T_{mean}) > 0$ . In third region ( $q''_{w1}/q''_{w2} > 2.2$ ), the mean temperature is smaller than the temperature of upper wall  $T_{w1}$  and greater than the temperature of lower wall  $T_{w2}$ , therefore  $(T_{w1} - T_{mean}) > 0$  while  $(T_{w2} - T_{mean}) < 0$ .

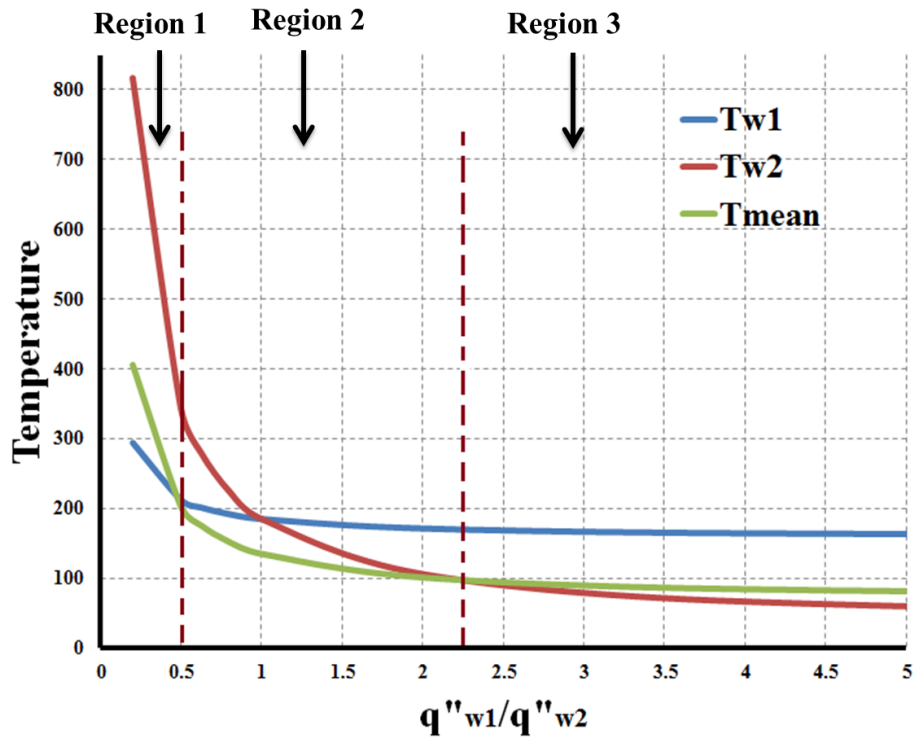


Figure 9.22. The variation of mean, upper and lower walls temperatures at the outlet of the channel with heat flux ratio

## 9.2.2. Dimensionless Analysis for Completely Filled Channels

The equations of the heat and fluid flow in a channel completely filled with porous medium with asymmetric constant heat flux boundary conditions are given in Chapter 5. In this section, firstly, the numerical results which are given in Section 9.2.1 are compared with the analytical results. After checking compatibility, the effects of  $Da$  on the dimensionless temperature profile,  $Nu$  and pressure drop are analyzed. The velocity profiles of the channels are not investigated because the velocity profiles are not function of heat flux ratio.

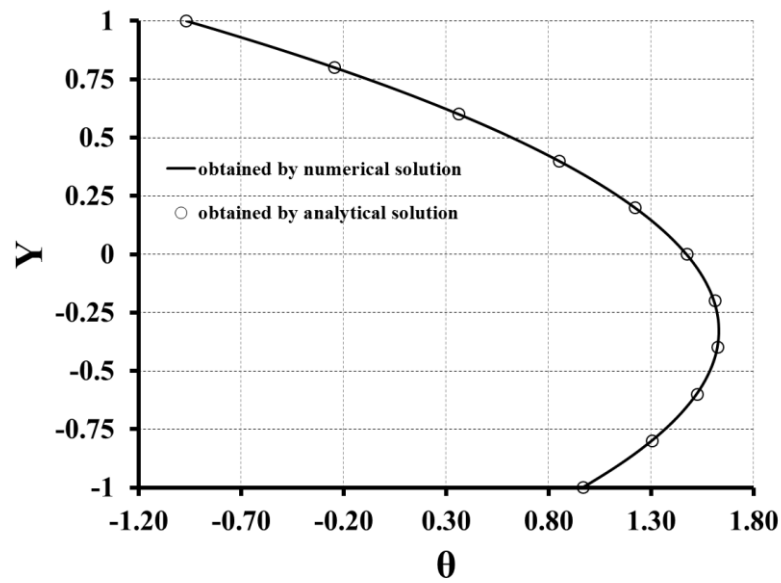
### 9.2.2.1. Comparison of the Numerical with Analytical Results

The numerical results which are given in Section 9.2.1 are converted to the dimensionless results with using defined dimensionless parameters as Equation 5.5. The converted results are compared with the results from the solutions of the analytical equations in Chapter 5.

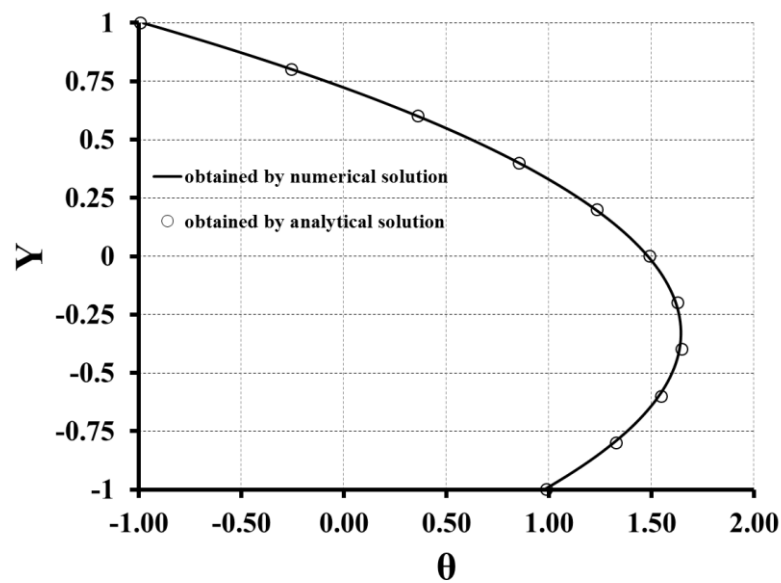


Comparison of the numerical solution with the analytical solution is done with the calculation of dimensionless parameters of the analytical equations such as  $Da$ ,  $M$ ,  $Y$ ,  $S$ ,  $U$ ,  $H$ ,  $K$ ,  $\theta$  by using the dimensional parameters of analyzed channels in Section 9.2.1.1. The comparison of the normalized velocity profiles are not investigated because the normalized velocity profiles do not depend on the heat flux ratio.

Figure 9.23 shows the dimensionless temperature profiles from the converted forms of numerical solutions to the dimensionless results and the dimensionless temperature profiles from analytical solutions. Figure 9.23(a) belongs to the dimensionless temperature profile of the medium permeable channel when the material of the solid is aluminum alloy and Figure 9.23(b) belongs to the low permeable channel when the material of solid is glass. According to the Figure 9.23, the results obtained by numerical solutions are consistent with the results obtained by analytical solutions. Only two of the figures are shown since all dimensionless temperature profiles of the numerical solution for high permeable, medium permeable and low permeable channels are consistent with the dimensionless temperature profiles of the analytical solution.



(a)



(b)

Figure 9.23. Comparison of the dimensionless temperature profiles which are obtained by numerical results with the analytical results: (a) The medium permeable channel when the material of the solid is aluminum alloy (b) The low permeable channel when the material of solid is glass

Table 9.6 shows the Nu calculated both numerically and analytically for different channels with different heat flux ratios. The results of three cases are only shown and as seen from this table a good agreement exists between the numerical and analytical results.

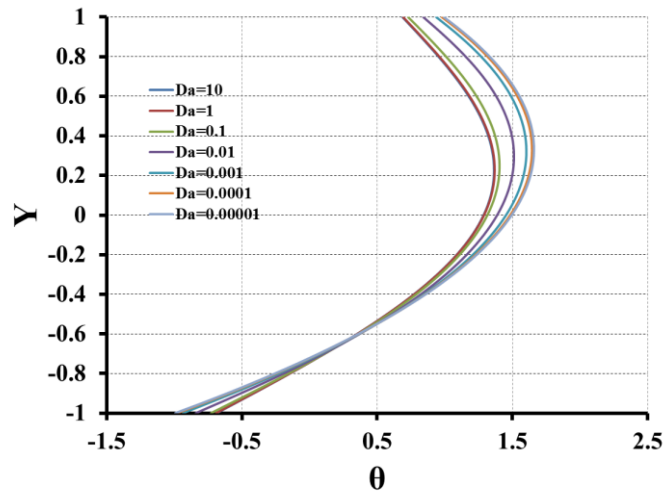
Table 9.6. Comparison of the analytical and numerical results for the Nu

Permeability	Material of Solid	Upper Wall	Lower Wall	Analytical Solution			Numerical solution		
				Nu <sub>1</sub>	Nu <sub>2</sub>	Nu (overall)	Nu <sub>1</sub>	Nu <sub>2</sub>	Nu (overall)
High Permeable	Glass (ks=1.1 W/mK)	100 Watt	90 Watt	5.1505	6.2432	5.6161	5.1825	6.153	5.6
Medium Permeable	Aluminum Alloy (ks=120 W/mK)	100 Watt	50 Watt	3.9358	122.589	5.7906	3.9224	121.583	5.8104
Low Permeable	Glass (ks=1.1 W/mK)	100 Watt	10 Watt	3.1483	-0.7555	5.9373	3.1371	-0.7613	5.8668

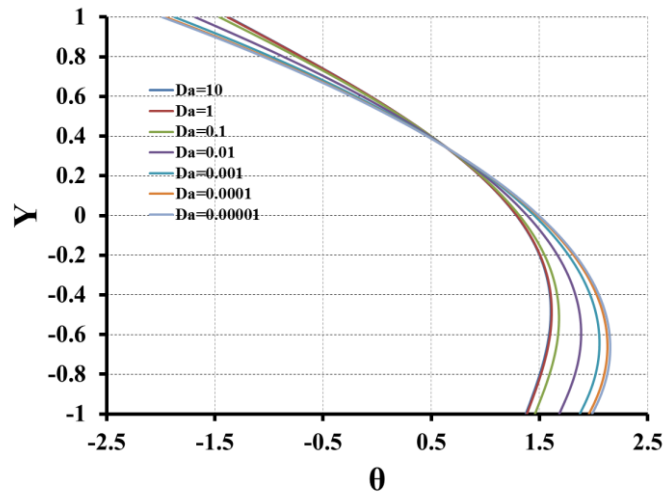
### 9.2.2.2. Effect of Da

The effects of Da on dimensionless temperature profile, Nu and pressure drop are analyzed when asymmetric heat fluxes are imposed to the channel walls. The equations given in Chapter 5 are used to analyze the channels. Da is changed between 10 and  $10^{-5}$  to obtain its effect. The relation between  $\mu_{\text{eff}}/\mu$  is taken as 1.3 for the porosity value as 0.75.

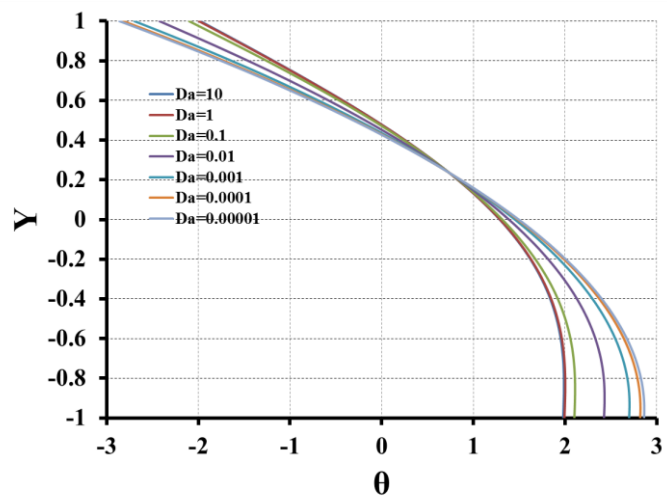
The velocity profiles of the channels are not investigated because the velocity profiles are not affected by different heat flux ratios. Figure 9.24 indicates the dimensionless temperature profiles for the flows with different Da. Figure 9.24(a), 9.24(b) and 9.24(c) show the dimensionless heat profiles when the heat flux ratio is 0.5, 5 and 50, respectively. The maximum value of dimensionless temperatures changes according to the heat flux ratio and maximum point is closer to the more heated wall for all Da. The maximum value of dimensionless temperature is increased when Da is decreased. The dimensionless temperature values are different at the boundaries because of the asymmetrical heating. The gradient of dimensionless temperature at the upper and lower walls has opposite sign of the same value for all Da.



(a)



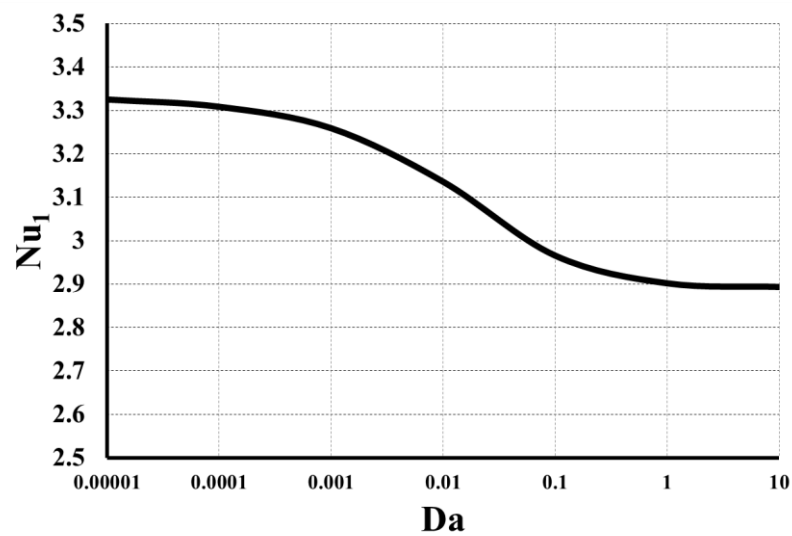
(b)



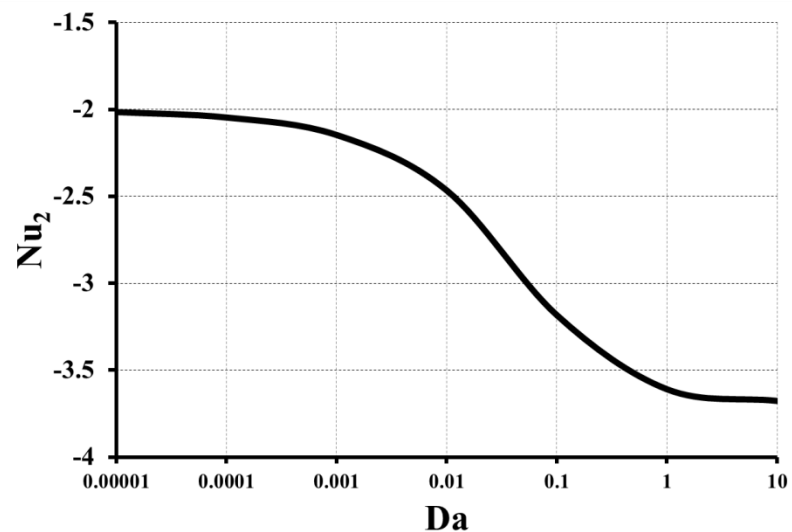
(c)

Figure 9.24. Dimensionless temperature distributions for the flows with different  $Da$  when (a)  $q_r=0.5$ , (b)  $q_r=5$ , (c)  $q_r=50$ .

The variation of individual Nu for upper and lower walls with increasing Da can be seen in Figure 9.25 when  $q_r$  equals 0.5. Da is plotted using a logarithmic scale to observe the variation of individual Nu more clearly. The individual Nu for upper wall ( $Nu_1$ ) have positive values while the individual Nu for lower wall ( $Nu_2$ ) have negative values for all Da. The individual Nu of upper and lower walls decrease, when Da increases. For flows with low Da, the individual Nu increases due to enhancement of heat transfer. The variation of overall Nu with respect to Da can be seen in Figure 9.12 because the overall Nu does not depend on heat flux ratios.



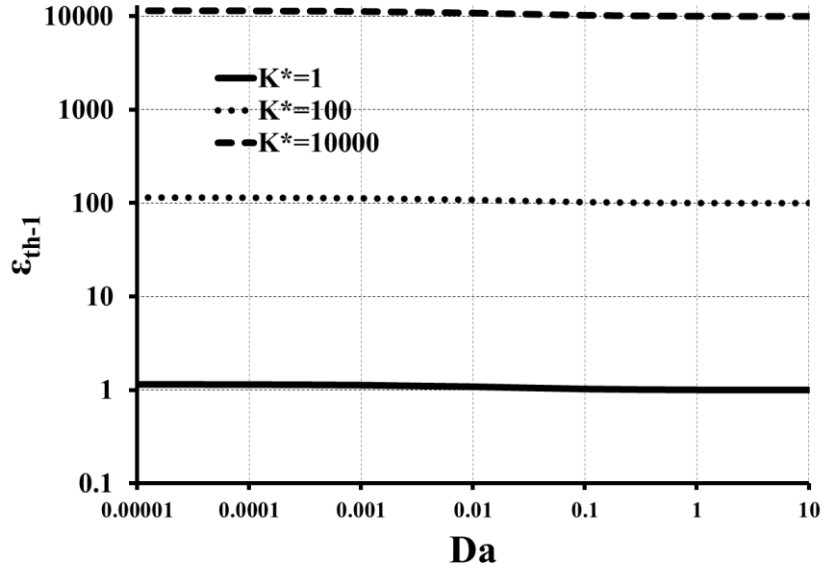
(a)



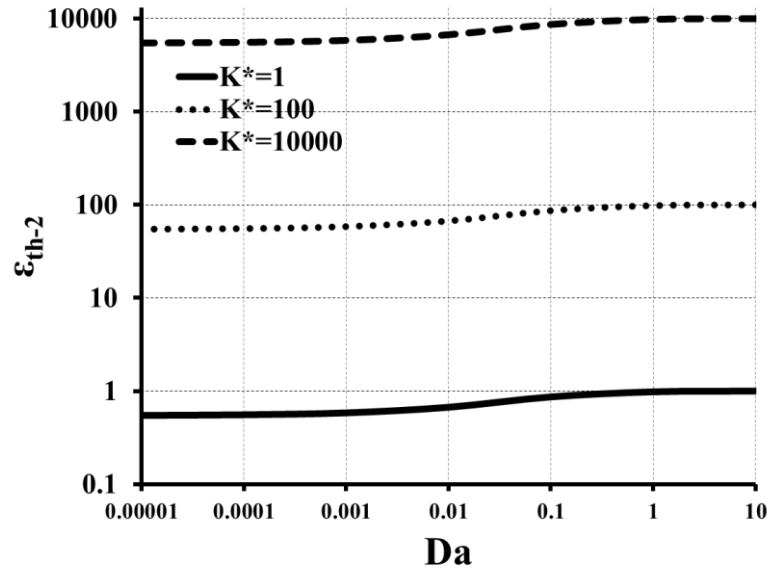
(b)

Figure 9.25. Logarithmic plot of Da vs. Nu for upper wall ( $Nu_1$ ) and Nu for lower wall ( $Nu_2$ ) for  $q_r = 0.5$ .

The upper and the lower wall Nu for clear fluid fully developed channel when asymmetrical heat flux used (when  $q_r$  is 0.5) is found as 2.8936 and -3.6763 respectively. The heat transfer enhancement in porous media can be observed with the help of individual Nu for clear fluid channel and Nu based on fluid thermal conductivity by using Equation 9.2. Heat transfer improvement ratio for each wall,  $\epsilon_{th-1}$  and  $\epsilon_{th-2}$ , can be calculated by dividing individual Nu based on fluid thermal conductivity to the individual Nu for clear fluid channel which are 2.8936 and -3.6763. Figure 9.26 shows the heat transfer improvement ratios of upper wall and lower wall by using porous media for three different effective thermal conductivity ratios. The figure is plotted using a logarithmic scale to observe the variation of the heat transfer increment ratio more clearly. As seen in the Figure 9.26(a), Da does not affect the heat transfer increment of upper wall significantly; the effective thermal conductivity ratio has more importance. Figure 9.26(b) indicates the heat transfer increment ratio for lower wall. When Da increases, the heat transfer also increases for the lower wall. It should be reminded that the heat flux ratio between walls is  $q_r=0.5$ .



(a)



(b)

Figure 9.26. Logarithmic plot of heat transfer increment ratio vs. the  $Da$  (a) The upper wall heat transfer increment (b) The lower wall heat transfer increment

The porous media in the channel brings pressure drop defined as friction coefficient. However, the friction coefficient is not a function of heat flux ratio. Therefore, the friction coefficient, and pressure drop increment ratio,  $\epsilon_p$ , can be known by checking Figure 9.14 and Figure 9.15.

The overall performance for each wall,  $\epsilon_1$  and  $\epsilon_2$ , can be found by calculating the ratio of  $\epsilon_{th}$  and  $\epsilon_p$  for upper and lower wall. For the values of  $\epsilon$  greater than 1 means; the heat transfer enhancement is greater than the increase of pressure drop along the

channel, while for the values of  $\varepsilon$  less than 1 means; the increase of pressure drop is greater than the heat transfer enhancement in the channel. Figure 9.27 shows the variation of overall performance for upper and lower wall of the channels with  $Da$  when heat flux ratio is 0.5. Overall performance is rising with increased  $Da$  and increased the ratio of effective thermal conductivity to the fluid thermal conductivity ( $K^*$ ). For  $Da$  greater than 1 which means almost clear channel so there is a constant overall performance. The increased overall performance is coming from only  $K^*$  ratio for  $Da$  greater than 1. The figure shows completely filling of channels with the solids which have  $K^*=1$  is not useful for heat transfer enhancement compared with the pressure drop in the channel. The  $Da$  number should be chosen at least between 0.001 and 0.01 for the  $K^*=100$ . Almost all  $Da$  number give a reasonable overall performance value for the ratio of  $K^*$  is 10000 when the heat flux ratio is 0.5. There is not a big difference between upper and lower wall overall performance of the channel.

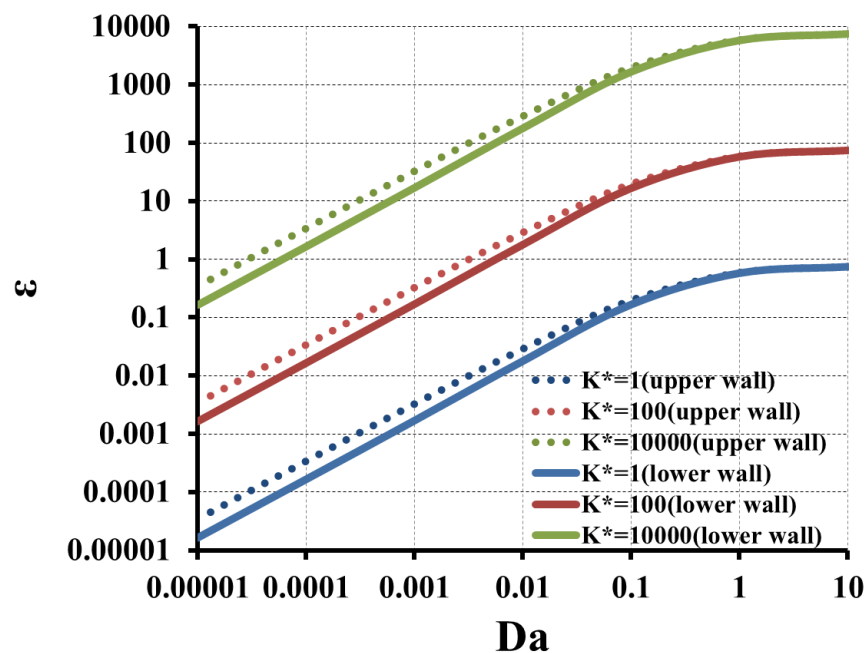


Figure 9.27. Logarithmic plot of overall performance for upper and lower wall vs. the  $Da$

The overall  $Nu$  should be considered due to the meaningless of the negative  $Nu$  (Figure 9.25). The results based on the individual  $Nu$  have also arguable validity (Figure 9.26 and Figure 9.27). That's why, the channel should be considered as a whole system. The average of the upper wall heat flux and lower wall heat flux should be calculated and the overall performance should be obtained as the channel with symmetrical heat



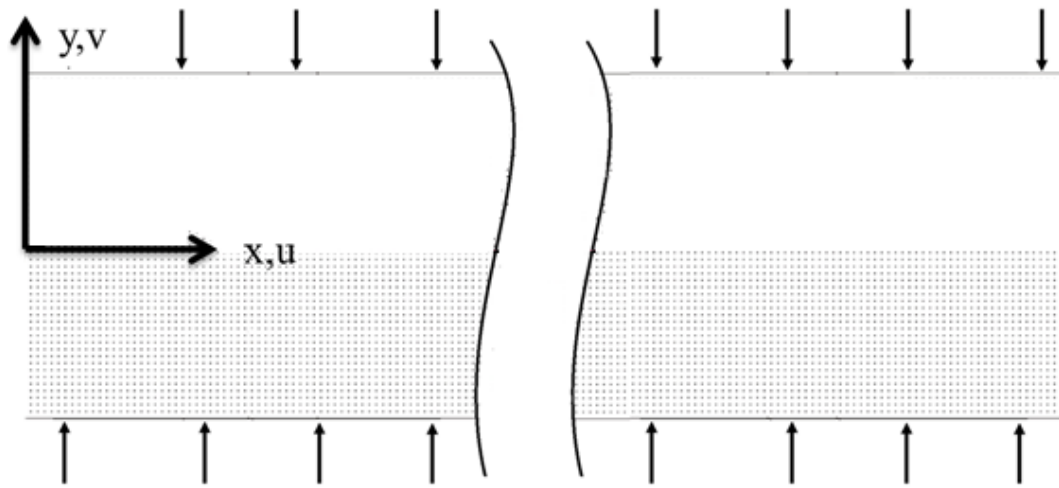
flux boundary condition. Therefore, the overall system performance becomes same with Figure 9.16. Besides, the  $K^*$  values for several materials can be seen from Table 9.4.

### **9.3.1. Dimensional Analysis for Partially Filled Channels**

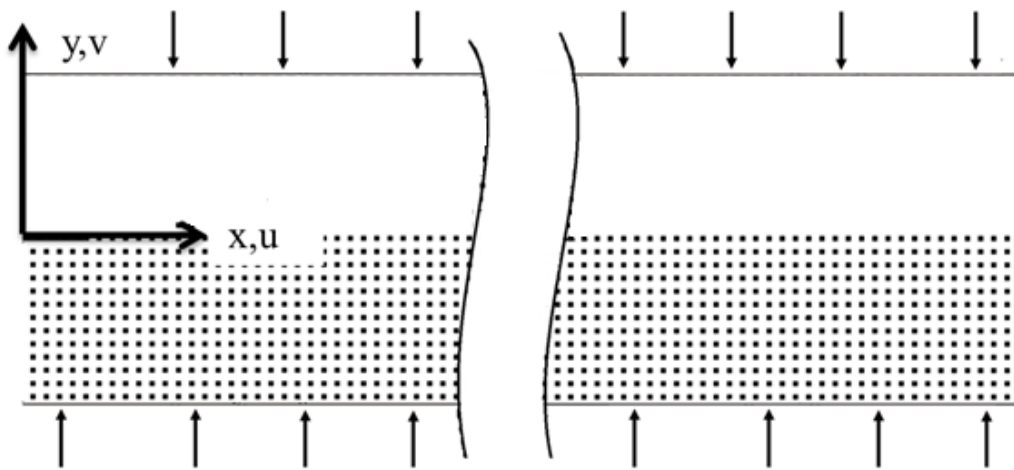
The following section is about analysing fluid and heat flow in a partially filled channel according to the governing equations given in Chapter 6.

#### **9.3.1.1. The Analysed Channels**

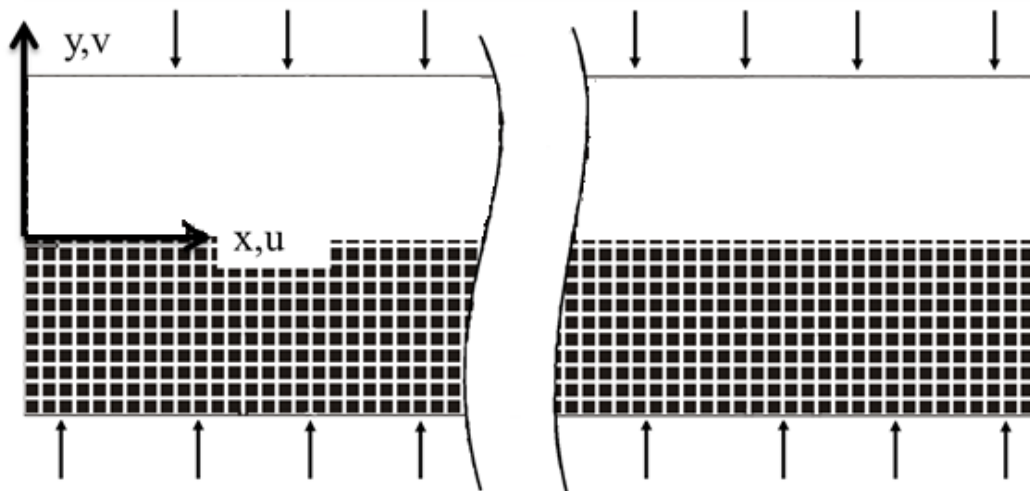
A two dimensional computational model developed according to the channels shown in Figure 9.28. For the dimensional symmetrical heated problem, a constant heat flux of 100 W is imposed to the channel walls. The total height of the channel is taken as 0.1 m while the length of channel 30 m. Three channels are analysed to find the effect of the thickness and permeability of the filled region on heat and fluid flow. The channels are named as high permeable, medium permeable and low permeable channels with respect to their permeability value. The channels are partially filled with square bars from bottom wall up to half of the channel. The fluid flows in the clear region in the upper half of the channel while in the lower half of the channel it flows perpendicular to the bars. The height (or width) of bars are different as 0.2, 1.5 and 3.75 mm. The distances between two bars are 1.8, 2.5 and 1.25 mm. The fluid in the channel is considered as air and it flows to the channel at 273 K. The study is performed for bar materials of glass and aluminium alloy.



(a)



(b)



(c)

Figure 9.28. Three channels filled with square bars analysed in this section: (a) High Permeable channel (b) Medium Permeable channel (c) Low Permeable channel

The assumptions for the heat and fluid flow in section 9.1.1 are also valid in this section. The thermophysical properties of the fluid and the thermophysical properties of solids, which are used in lower part of the channel, are the same with section 9.1.1. Table 9.1 and Table 9.2 can be used to remind the thermophysical properties of the fluid, solids and the flow parameters of considered channels. The mean velocity of the fluid is the same with section 9.1.1 which is 0.38 m/s. The fully developed velocity profile of air is assumed through the channel so velocity profile is function of  $y$  and it is not changed along the channel in  $x$  direction.

### **9.3.1.2. Results**

The dimensional form of heat and fluid flow equations for a channel partially filled with porous medium are presented in Chapter 6. According to the given equations and boundary conditions, heat and fluid flow in the channels described in the previous sections are investigated. Moreover, the heat transfers through the channels are also investigated for two solid materials as glass and aluminium alloy. The thermal conductivity for the glass and aluminium alloy are 1.1 W/mK and 120 W/mK respectively.

The permeability values of the lower parts of the channels are given in Table 9.2. Figure 9.29 shows the velocity profiles for the channels with three different permeability coefficients. As seen in this figure, the velocity values are zero at the channel walls because of the no-slip boundary condition and there are not great differences between velocity profiles. The maximum velocity values are in the upper part of the channel because of the clear fluid flow. The maximum velocity increases when the permeability of the lower part of the channel decreases. There is almost a uniform velocity distribution in the lower part of the channel and the velocity increases with the increased permeability. The difference is so small that the increment of velocity cannot be seen clearly.

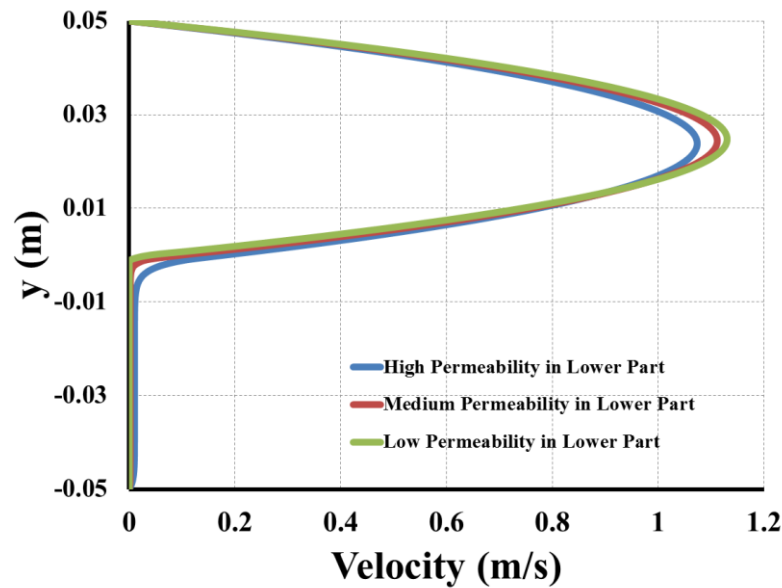
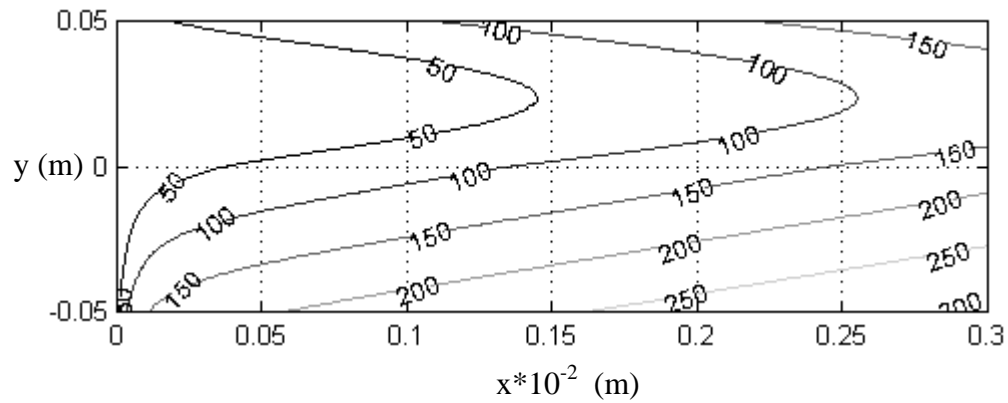


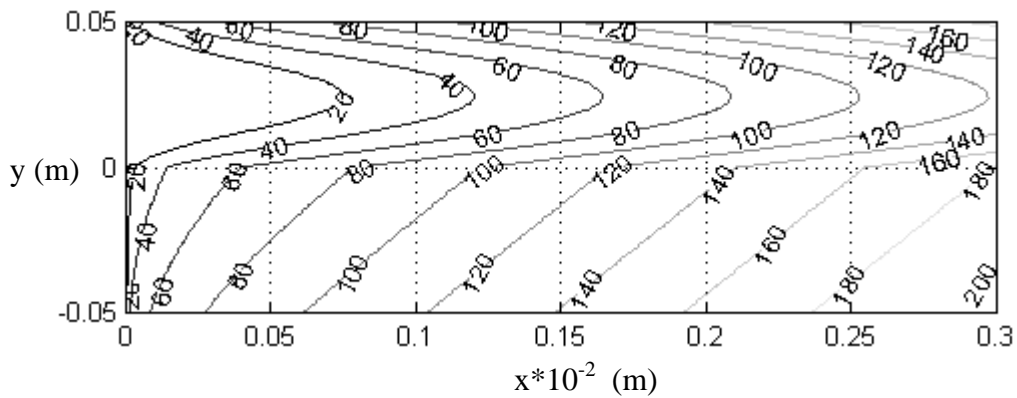
Figure 9.29. The dimensional velocity distributions for the flows with different permeability values for partially filled channel.

Figure 9.30 shows the isotherms in the channels with three different permeability coefficients when the material of the solid is glass. Figure 9.30(a) shows the isotherms for the channel partially filled with high permeable material. As seen, although a symmetrical heat flux is imposed to the channel the isotherms are not symmetrical respect to the centreline because of the partial filling. The maximum air temperature is observed at the lower wall. The temperature decreases until the centre of the upper part of the channel, the temperature starts to increase from this point. The minimum temperature for a cross section is at the centre of the upper part of the channel. Although isotherms are similar with each other, they are not identical and they change along  $x$  axis. Figure 9.30(b) indicates the isotherms for the channel when lower part of the channel filled with medium permeable material. Maximum temperature is again observed at the lower wall and its value decreases towards the centre of the upper part channel. The isotherms almost have same slope at the lower part of the channel. The permeability of medium permeable channel is lower than high permeable channel. It provides higher effective thermal conductivity so it causes heat transfer enhancement in  $y$  direction. That's why the temperature changes in  $y$  direction become smaller in the lower part of the channel. Therefore, the temperature value of the lower wall of the medium permeable channel is smaller than the temperature value of the lower wall of the high permeable channel. Figure 9.30(c) shows the isotherms for the channel bottom half filled with low permeable material. As seen, the temperature change in  $y$  direction

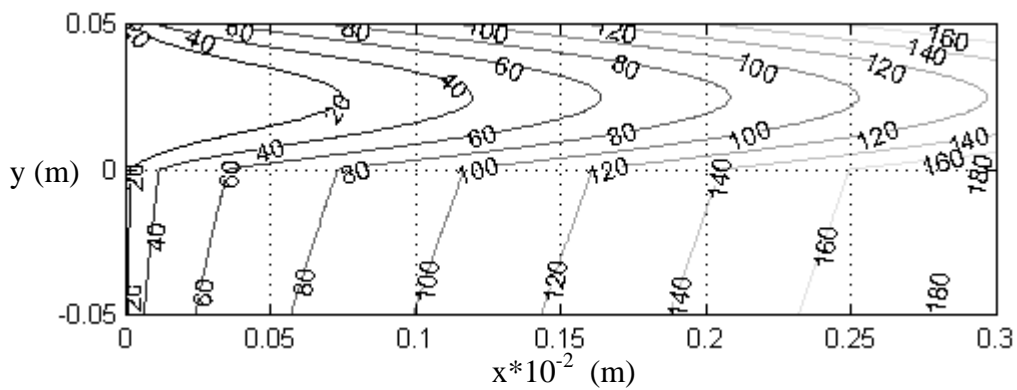
in the lower part of the channel becomes smaller due to the increase of thermal conductivity and flatter isotherms are seen. The upper parts of the high permeable, medium permeable and low permeable channels have almost same isotherms due to the fact that they are in the clear region.



(a)



(b)



(c)

Figure 9.30. Isotherm lines through the low conductive solid (glass) used channel: (a) Partially filled with high permeable material (b) Partially filled with medium permeable material (c) Partially filled with low permeable material

The isotherms of the partially filled channels with three different permeability coefficients when the material of the solid is aluminium alloy are seen in Figure 9.31. A symmetrical heat flux is imposed to the channel walls however the isotherms are not symmetrical respect to the centreline because of the partial filling. The isotherms for the channel partially filled with high permeable material when the solid is aluminium alloy is shown in Figure 9.31(a). The maximum air temperature is observed at the upper wall because of the effective conductivity in the lower part of the channel. The temperature decreases until the centre of the upper part of the channel, the temperature starts to increase at this point. The minimum temperature for a cross section is at the centre of the upper part of the channel because of the increased convection and decreased conduction effect of the heat transfer in the upper part of the channel. The isotherms are similar with each other but they are not identical and they change along x axis. Figure 9.31(b) indicates the isotherms for the channel partially filled with medium permeable material when the solid is aluminium alloy. Maximum temperature is observed at the upper wall and its value decreases towards the centre of the upper part channel and then it again increases. The isotherms are almost perpendicular to the y axis in the lower part of the channel and the temperature value of the lower wall of the channel is smaller than the temperature of the lower wall of the high permeable channel. The decreased permeability provides higher effective thermal conductivity so it causes the heat transfer enhancement in y direction and the temperature changes in y direction becomes smaller in the lower part of the channel. Figure 9.31(c) shows the isotherms for the channel partially filled with low permeable material. There is a similarity between the isotherms of medium permeable channel and low permeable partially filled channel because the dominant cause of the increment of effective thermal conductivity is the usage of high conductive material (aluminium alloy). The difference between isotherms of medium permeable channel and low permeable channel is the temperature decrease for a cross section in the lower part of the channel. The upper parts of the channels have almost same isotherms because there is not any porous material in the upper parts of the channels.

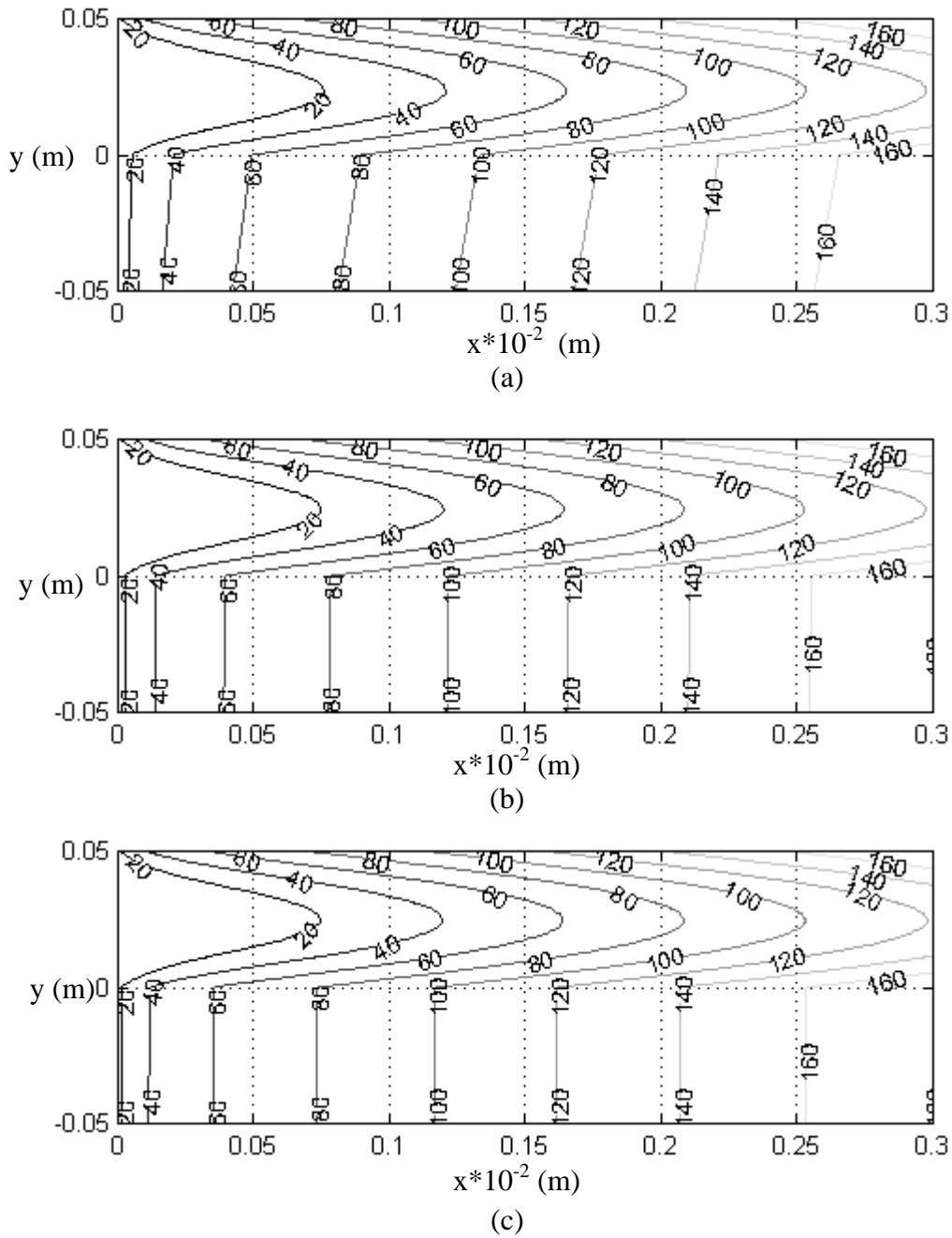
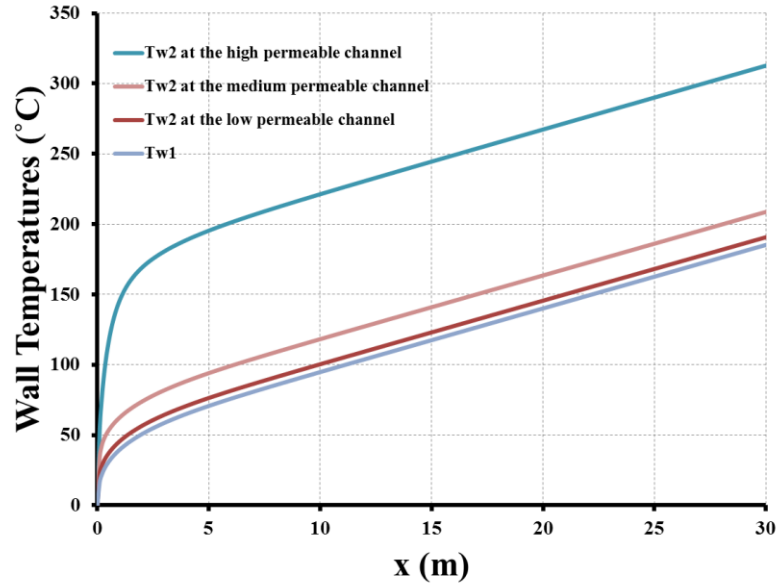


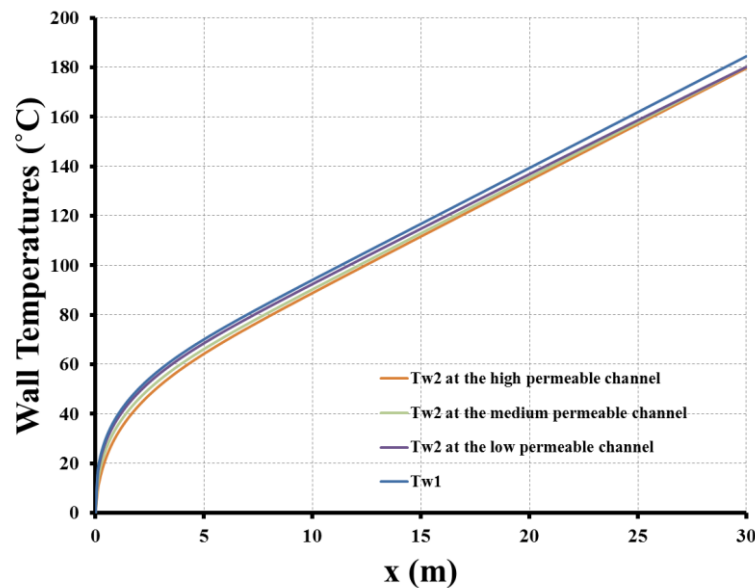
Figure 9.31. Isotherm lines through the high conductive solid (aluminium) used channel: (a) Partially filled with high permeable material (b) Partially filled with medium permeable material (c) Partially filled with low permeable material

Figure 9.32 shows the wall temperature values for the channels which are partially filled with glass particles(a) and aluminium alloy(b) particles. The temperature distribution of the upper walls are same for all cases because the lower part of the channels filled with glass or aluminium alloy particles. As it can be seen in Figure 9.32(a) and 9.32(b), when the permeability decrease, the wall temperature values

decrease for a cross section for both glass and aluminium alloy used channels. Figure 9.32(a) and 9.32(b) also show that the permeability is more effective when the porous material is glass (less conductive material).



(a)



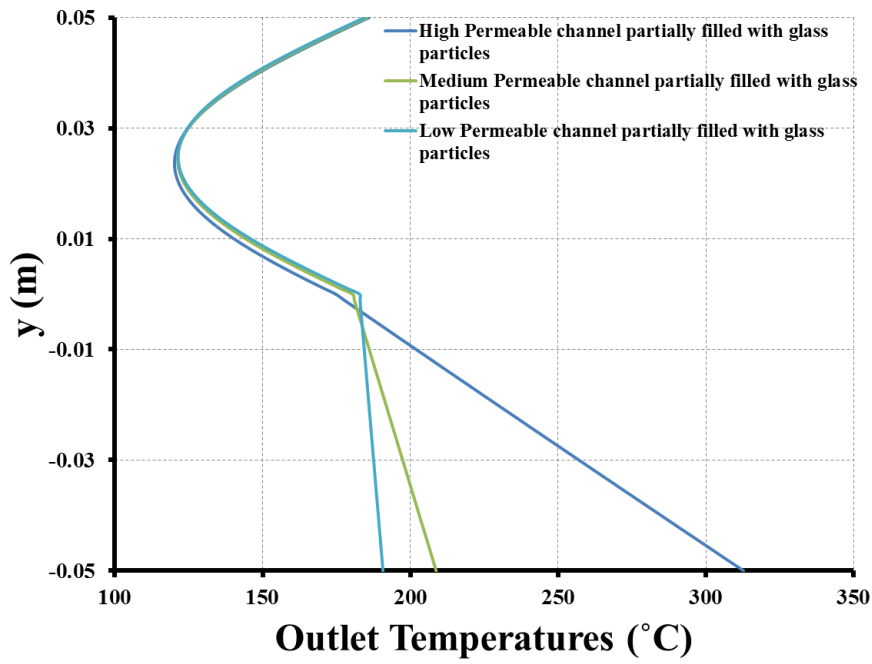
(b)

Figure 9.32. Wall temperature values through the channels (a) The channel partially filled with glass particles (b) The channel partially filled with aluminium particles.

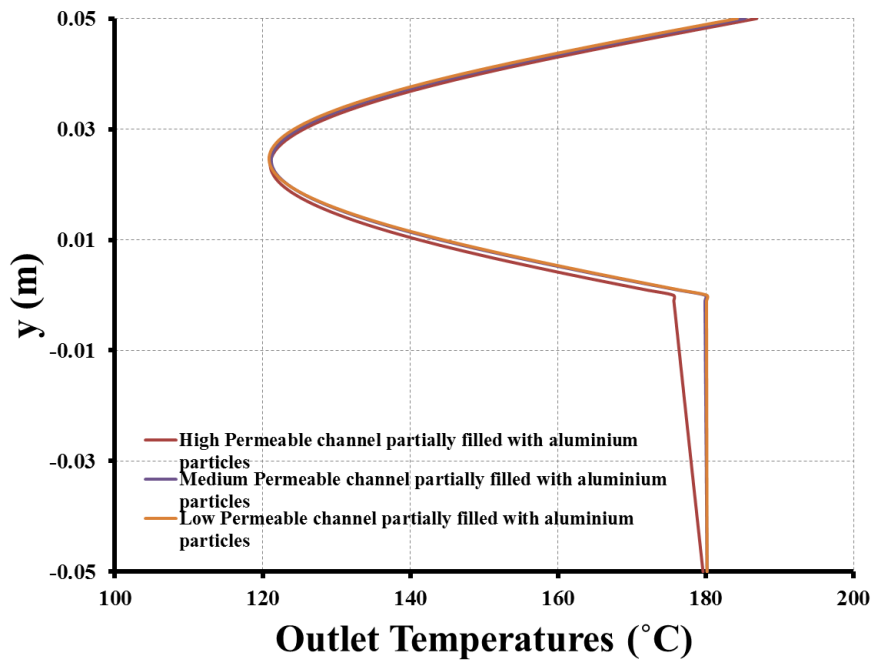
The outlet temperatures of the partially filled channel are also investigated according to the permeability and effective conductivity of the filled region. Figure



9.33(a) indicates the distribution of the outlet temperatures of the partially filled channels when glass particles are used in the bottom half of the channel. As seen, the temperature distributions are not affected significantly with permeability in the upper part of the channel but the heat transfer increases in  $y$  direction with decreasing permeability in the bottom part of the partially filled channel. This enhanced heat transfer brings temperature decrease at the lower wall temperature. The outlet temperature distribution can be seen in Figure 9.33(b) when aluminium alloy particles are used in the lower half of the partially filled channel. The usage of aluminium alloy particles brings higher effective conductivity. The temperature values of lower wall are almost equal for all permeability values. The high permeable channel shows a little difference in the centre region of the channel but the temperature distribution for medium permeable and low permeable channel is almost same that's why their distribution lines are coincides with each other.



(a)



(b)

Figure 9.33. Outlet temperature values through the channels (a) the channel partially filled with glass particles (b) the channel partially filled with aluminium particles.

Table 9.7. The fully developed Nu for upper and lower wall according to the particle types used in the lower part of the channel.

Permeability	Solid	Nu <sub>1</sub>	Nu <sub>2</sub>
High	Glass	8.00458	1.58322
	Alum	7.87197	0.18752
Medium	Glass	8.06362	0.77674
	Alum	8.03994	0.01325
Low	Glass	8.16297	0.28731
	Alum	8.0794	0.00326

Table 9.7 indicates the upper and lower wall Nu for glass filled and aluminium alloy filled channel. The Nu for lower wall (Nu<sub>2</sub>) have different values according to the permeability value and solid particle because of partially filling while the Nu for upper wall (Nu<sub>1</sub>) do not show much variation. The Nu for lower wall is smaller in the channel partially filled with aluminium alloy for all permeability values than the channel partially filled with glass.

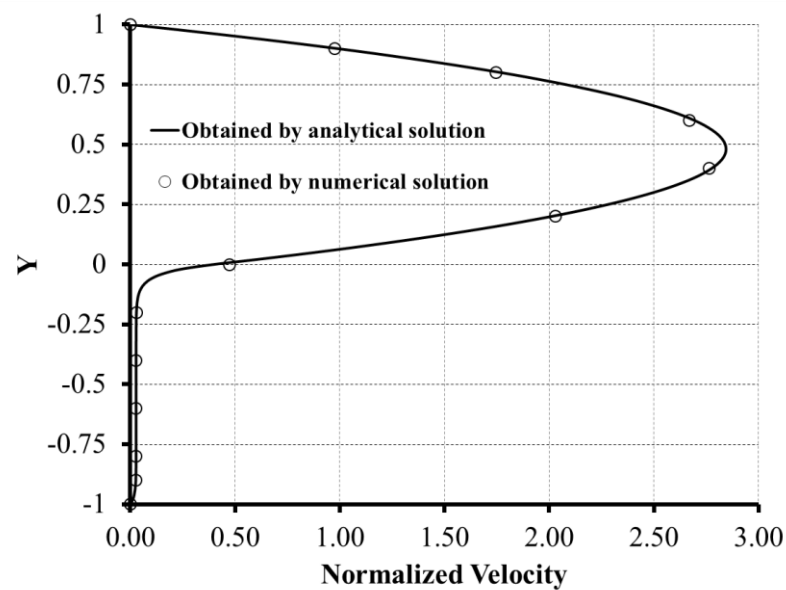
### 9.3.2. Dimensionless Analysis for Partially Filled Channels

Heat and fluid flow in a channel which is partially filled with porous medium with constant heat flux boundary conditions is investigated analytically in Chapter 7. In this section, firstly, the numerical results which are given in Section 9.3.1 are compared with the analytical results. After checking compatibility, the effects of Da and the thickness of porous region on the normalized velocity profile; dimensionless temperature profile, Nu and pressure drop are analyzed.

#### 9.3.2.1. Comparison of the Numerical with Analytical Results

The channels which are shown in Figure 9.28 are used to analyze the consistency between numerical and analytical results. Numerical results which are given in Section 9.3 are converted to the dimensionless results with using defined dimensionless parameters as Equation 7.5. The converted results are compared with the results from the solutions of the analytical equations in Chapter 7.

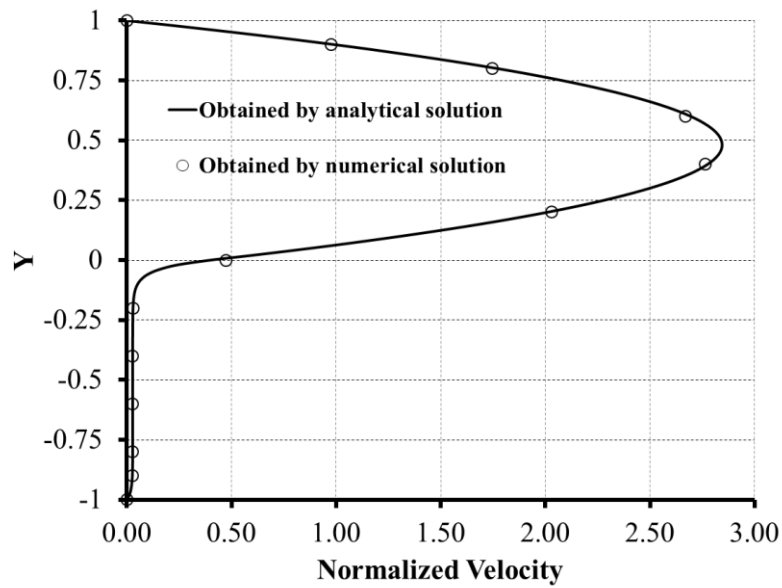
Dimensionless parameters of the analytical equations such as  $Da$ ,  $M$ ,  $Y$ ,  $S$ ,  $U$ ,  $H$ ,  $K$ ,  $\theta$  are calculated according to the definition of these parameters which are given in Equation 7.5 with using the results of numerical solutions found in Section 9.3.1.2. The dimensionless results which are converted form of the numerical results and the dimensionless results from analytical solutions are compared with each other. The obtained dimensionless normalized velocity profiles from the converted forms of numerical solutions and the dimensionless normalized velocity profiles obtained from analytical solutions which are given in Chapter 7 are shown in Figure 9.34. As it can be seen in Figure 9.34, the analytical results are consistent with the numerical results.



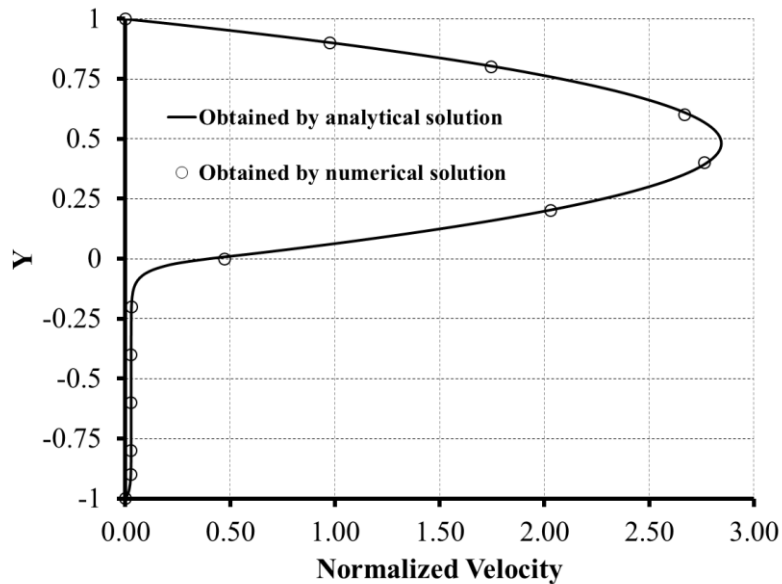
(a)

Figure 9.34. Comparison of the normalized velocity profiles which are obtained by converted form of numerical results and the analytical results: (a) The channel partially filled with high permeable material (b) The channel partially filled with medium permeable material (c) The channel partially filled with low permeable material

(cont. on next page)



(b)

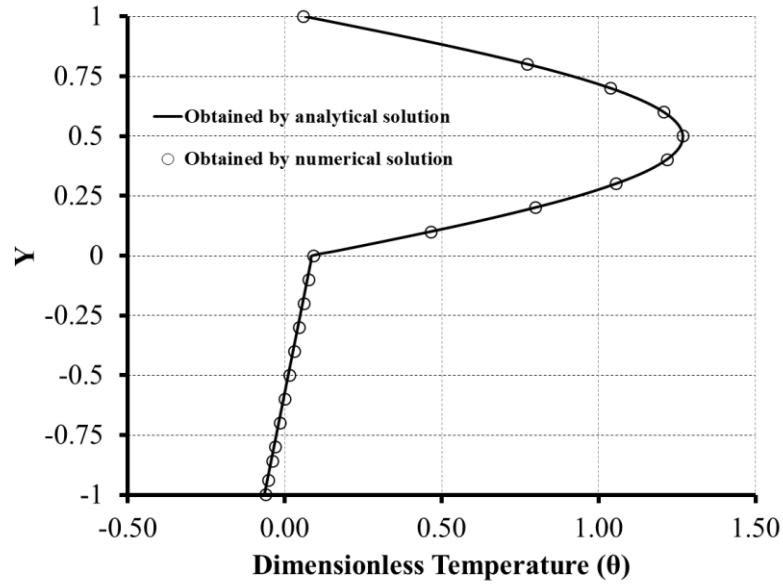


(c)

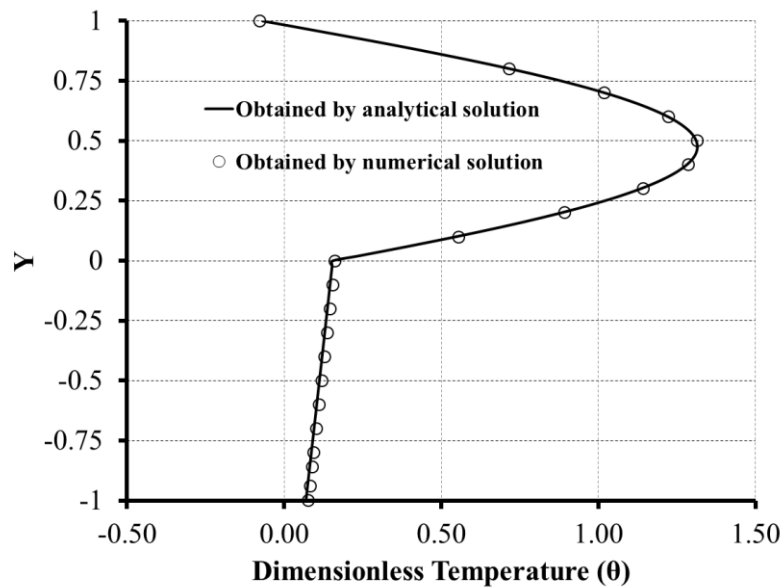
Figure 9.34. (cont.)

The dimensionless temperature profiles from the converted forms of numerical solutions and the dimensionless temperature profiles from analytical solutions are shown in Figure 9.35. Figure 9.35(a) indicates the dimensionless temperature profile of the high permeable channel when the material of the solid is aluminum alloy and Figure 9.35(b) indicates the low permeable channel when the material of solid is glass. According to the Figure 9.35, the results obtained by numerical solutions are consistent with the results obtained by analytical solutions. All of the dimensionless temperature

profiles of the numerical solution for high permeable, medium permeable and low permeable channels are consistent with the dimensionless temperature profiles of the analytical solution, that's why only two of figures are shown.



(a)



(b)

Figure 9.35. Comparison of the dimensionless temperature profiles which are obtained by converted form of numerical results and the analytical results: (a) The high permeable channel partially filled with aluminum alloy particles (b) The low permeable channel partially filled with glass particles

Table 9.8 shows the individual Nu calculated both numerically and analytically for different channels. As seen from this table, there is a good agreement exists between the numerical and analytical results.

Table 9.8. Comparison of the analytical and numerical results for the individual Nu

Permeability	Solid	From Numerical Solution		From Analytical Solution	
		Nu <sub>1</sub>	Nu <sub>2</sub>	Nu <sub>1</sub>	Nu <sub>2</sub>
High	Glass	8.0046	1.5832	8.0493	1.579
	Alum	7.8720	0.1875	7.9092	0.1854
Medium	Glass	8.0636	0.7767	8.1004	0.771
	Alum	8.0399	0.0133	8.0943	0.013
Low	Glass	8.1630	0.2873	8.1916	0.2853
	Alum	8.0794	0.0033	8.1915	0.0031

### 9.3.2.2. Effect of Da

The temperature profiles of considered channels are investigated by equations given in Chapter 7. Da is changed between 10 and  $10^{-5}$  to obtain the effect of it. The ratio of effective conductivity over conductivity of fluid ( $K^*$ ) is taken as 0.01, 1 and 100 respectively. The dimensionless temperature profile distribution and Nu are analyzed when symmetric heat fluxes are imposed to the channel walls.

The analyzing of velocity profile for the low Da is hard to observe so the normalized velocity profiles are investigated in Figure 9.36. The velocity profiles for upper region are different than lower region because of the partial filling. The maximum velocity occurs at the center of the upper region because of clear fluid flow. If Da decreases, the effect of porous media increases in the lower part of the channel so velocity value increases at the center region of upper part of the channel by reducing Da. The velocity values are zero at the boundaries because of the no-slip boundary condition and a sharp velocity gradient is observed at the lower wall region.

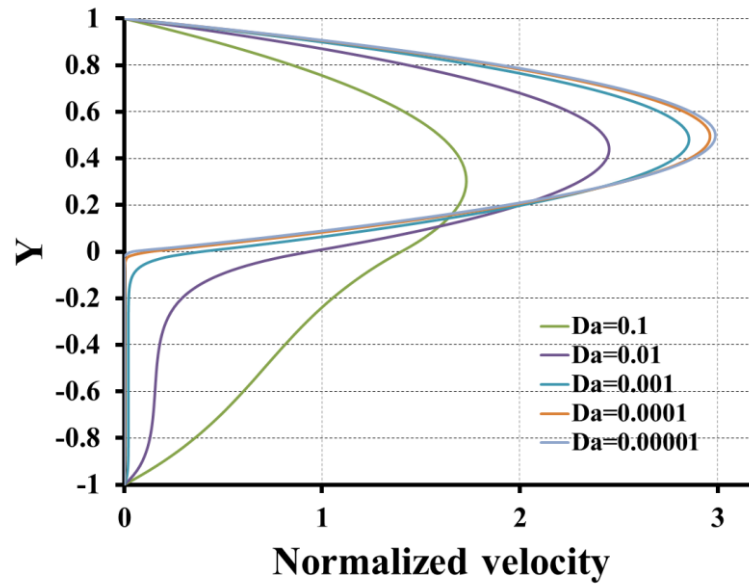
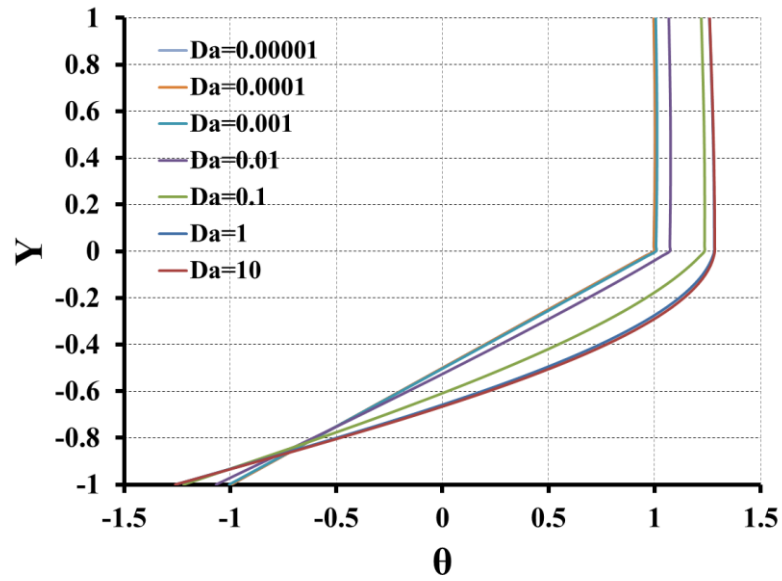


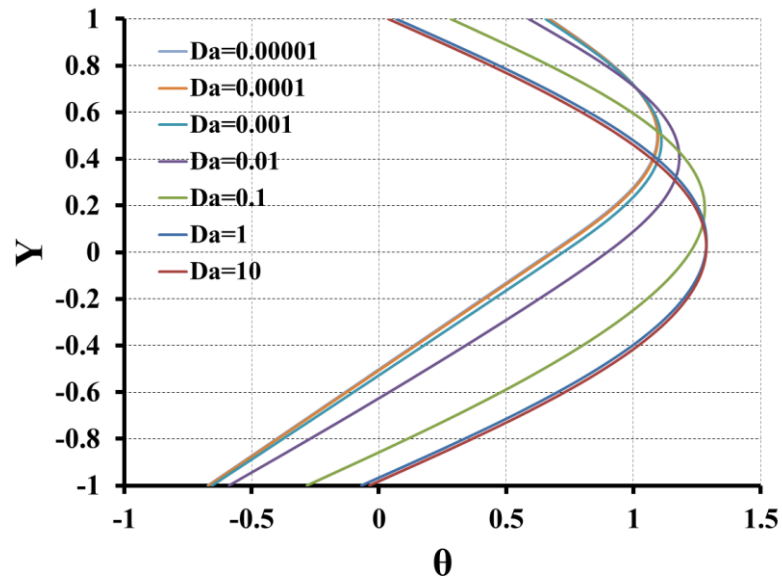
Figure 9.36. Dimensionless velocity distributions for the flows with different Da

Figure 9.37 indicates the dimensionless temperature profiles for the flows with different Da. Figure 9.37(a), 9.37(b) and 9.37(c) show the dimensionless temperature profiles when the ratio of effective conductivity over conductivity of fluid ( $K^*$ ) is 0.01, 1 and 100 respectively. In Figure 9.37(a), the effective conductivity of the upper side is higher than the lower side. The dimensionless temperature values increase when the Da number increases because maximum Da number means the presence of solid phase in the channel is at minimum. The dimensionless temperature values have almost constant value because of the higher effective conductivity in the upper side of channel. The maximum dimensionless temperature value is at the center of channel when Da equals 10. In Figure 9.37(b), the effective conductivity and the conductivity of fluid are same. That's why; a symmetrical behavior is observed when Da is 1 or 10. It is seen that, the dimensionless temperature values of the channel are increasing when Da number increase. Figure 9.37(c) shows the dimensionless temperature values when  $K^*$  equals 100. This means a solid which have higher conductivity then the fluid is present at the lower part of the channel. There is almost a linear temperature distribution at lower part because of the increased effective conductivity.





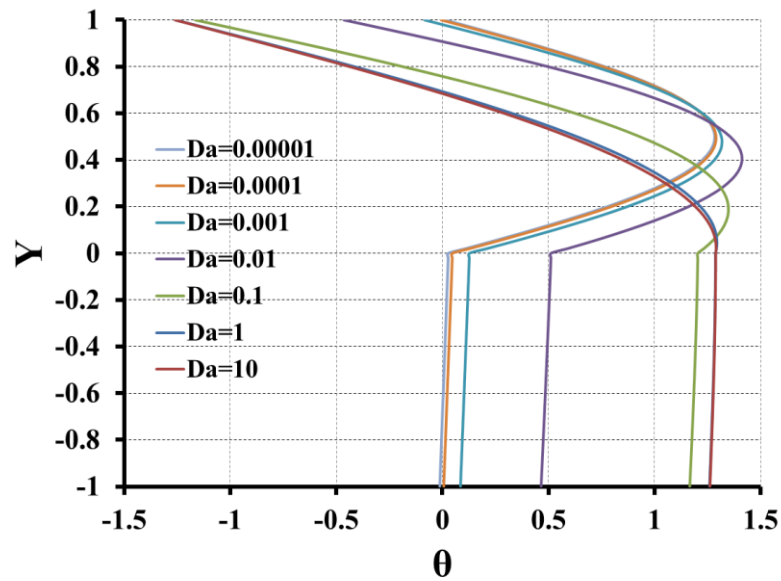
(a)



(b)

Figure 9.37. Dimensionless temperature distributions for the flows with different  $Da$  when (a)  $K^*=0.01$ , (b)  $K^*=1$ , (c)  $K^*=100$ .

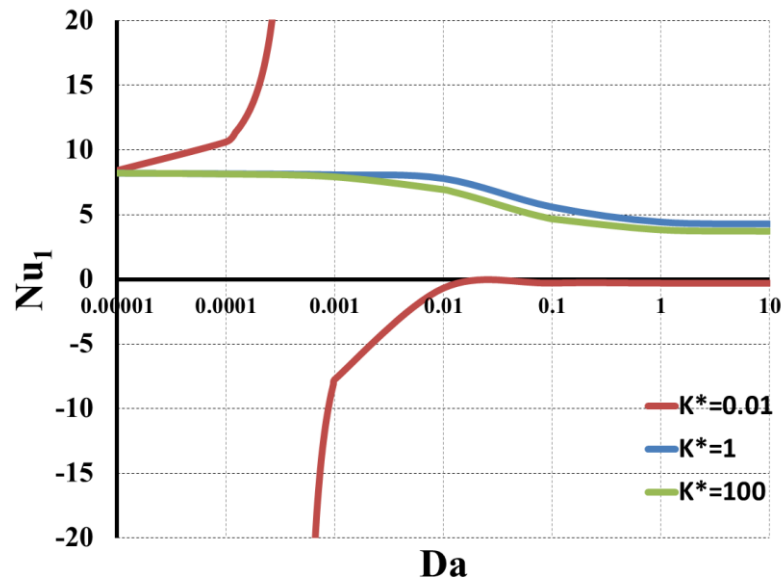
(cont. on next page)



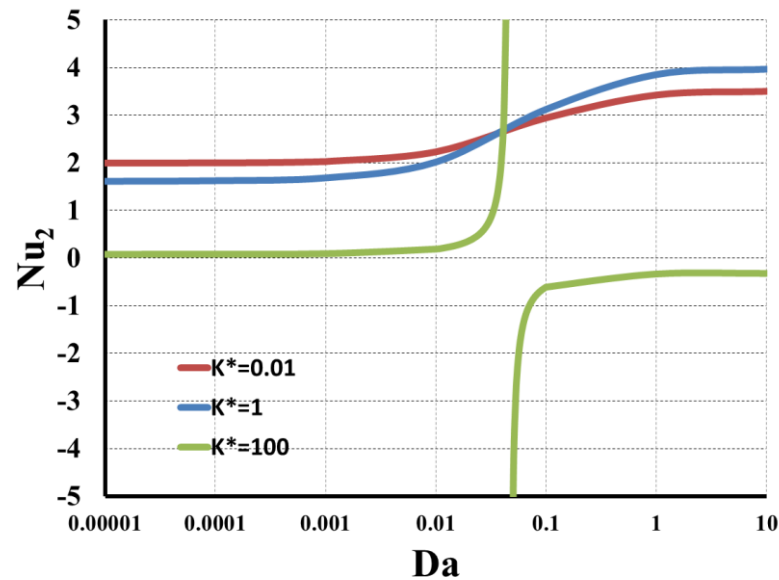
(c)

Figure 9.37. (cont)

The variation of individual  $Nu$  for upper and lower wall with increasing  $Da$  can be seen in Figure 9.38.  $Da$  is plotted using a logarithmic scale to observe the variation of individual  $Nu$  more clearly. The individual  $Nu$  for upper wall ( $Nu_1$ ) have almost same value for  $K^*$  equals 1 and 100.  $Nu_1$  decreases when  $Da$  increases for  $K^*=1$  and  $K^*=100$ . But  $Nu_1$  has a discontinuity for  $K^*$  equals 0.01. The individual  $Nu$  for lower wall ( $Nu_2$ ) has increasing positive values with increasing  $Da$  number for  $K^*$  equals 0.01 and 1. The value of  $Nu_2$  has also discontinuity when  $K^*=100$ .



(a)



(b)

Figure 9.38. Logarithmic plot of  $Da$  vs.  $Nu$  for upper wall ( $Nu_1$ ) and  $Nu$  for lower wall ( $Nu_2$ ).

The variation of  $Nu$  do not give an idea about the heat transfer in the upper and lower wall due to discontinues of values for certain  $Da$  numbers. Rather than individual  $Nu$ , the overall  $Nu$  can be investigated to make comments on the heat transfer mechanism in the partially filled channel. Figure 9.39 shows the variation of the overall  $Nu$  of the partially filled channel according to the  $Da$  number.  $Da$  is shown by using logarithmic scale to observe the overall  $Nu$  variation effectively. Figure 9.39 shows that

the channel is not able to benefit if  $K^*$  is equal 0.01. The figure also indicates that; the overall Nu increases with the increment of Da number. The overall Nu reaches the value of 4.11 which is Nu of clear fluid channel when  $K^*$  equals 1. However, there is more than two-fold increase in the overall Nu when  $K^*$  equals 100. And also there is an optimum point for this increment. It can be said that the overall Nu has largest value when the Da is between 0.01 and 0.1 with using  $K^*$  as 100.

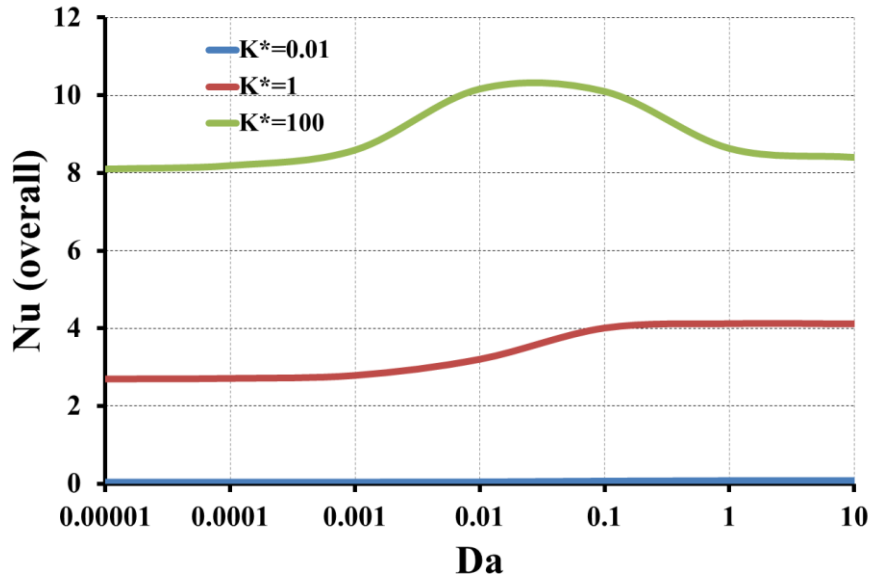


Figure 9.39. Logarithmic plot of Da vs. overall Nu

The Nu for clear fluid fully developed channel when symmetrical heat flux used is found as 4.1176. The heat transfer enhancement by using partially porous media can be observed with the help of Nu for clear fluid channel and Nu based on fluid thermal conductivity by using Equation 9.2. Heat transfer improvement ratio,  $\epsilon_{th}$  can be calculated by dividing overall Nu based on fluid thermal conductivity to the Nu for clear fluid channel. Figure 9.40 shows the heat transfer improvement ratios of overall system by using porous media for three different effective thermal conductivity ratios. The figure is plotted using a logarithmic scale to observe the variation of the heat transfer increment ratio more clearly. As seen in the Figure 9.40, Da does not affect the heat transfer increment of the channel significantly; the ratio of effective thermal conductivity over fluid thermal conductivity,  $K^*$ , has more importance.

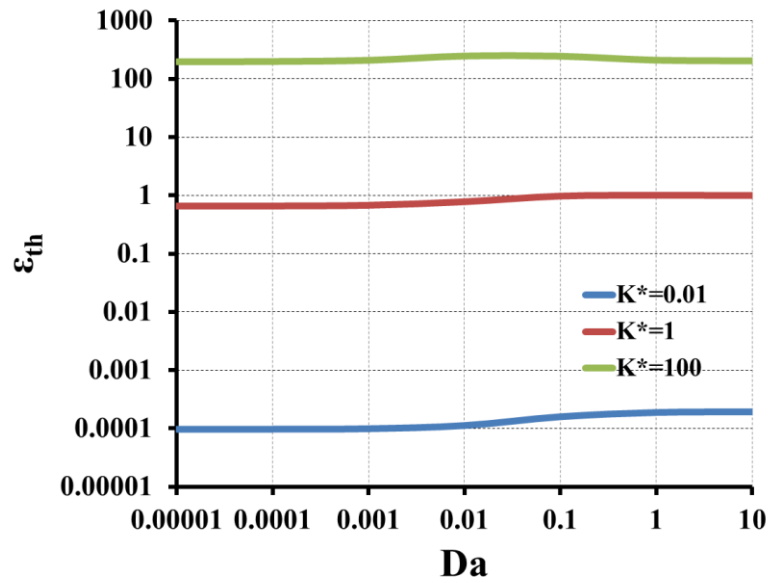


Figure 9.40. Logarithmic plot of heat transfer increment ratio vs. the  $Da$  for partially filled channel

The partially porous media in the channel brings pressure drop defined as friction coefficient expressed in the Equation 7.46. The variation of friction coefficient is found by using mean velocity and it can be seen in Figure 9.41. The  $Da$  number is plotted using a logarithmic scale to observe the variation of friction coefficient more clearly. When  $Da$  increases, the friction coefficient decreases. While there is not a very large friction coefficient in  $Da$  greater than  $10^{-2}$ , for numbers less than  $10^{-2}$  Darcy, the friction coefficient reaches extremely big values.

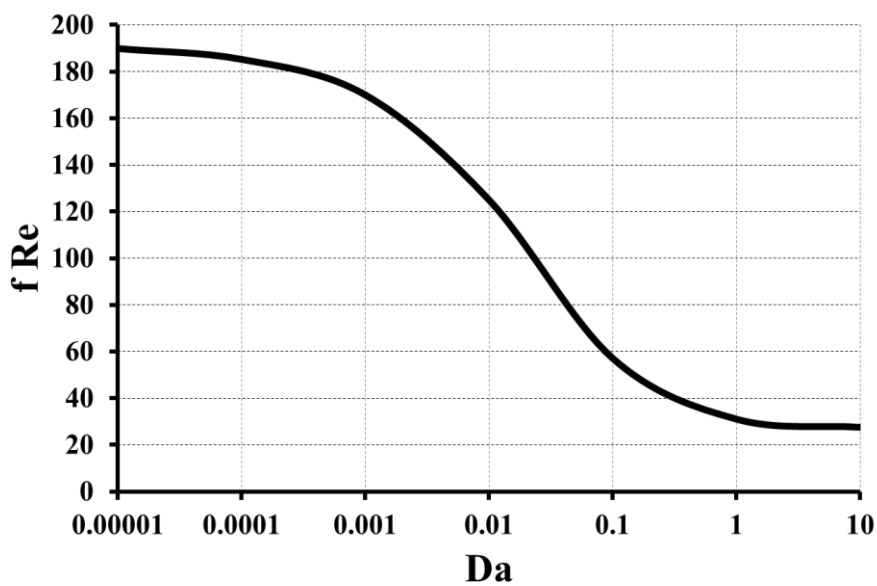


Figure 9.41. Friction coefficient vs. logarithmic plot of  $Da$  for partially filled channel

The pressure drop increment ratio for clear fluid fully developed channel with constant heat flux is given as 24. The increment of pressure drop by using partially porous media can be observed with the help of pressure drop increment ratio for clear fluid channel. Pressure drop increment ratio,  $\varepsilon_p$ , can be calculated as dividing friction coefficient of the porous channel in to the friction coefficient of a flow in a clear channel which is 24. Figure 9.42 shows the pressure drop increment ratio by using porous media in the partially filled channel.  $Da$  is plotted using a logarithmic scale to observe the variation of the pressure increment ratio more clearly. As seen in the figure, decreasing  $Da$  increases pressure increment ratio. And there is a huge increment for smaller than  $10^{-2}$   $Da$ .

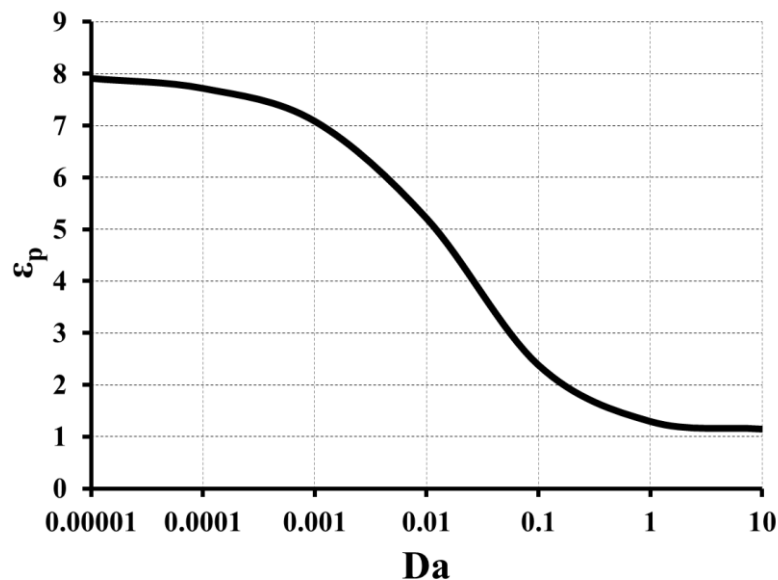


Figure 9.42. Friction coefficient vs. logarithmic plot of  $Da$  for partially filled channel

The overall performance for the channel,  $\varepsilon$ , can be found by calculating the ratio of  $\varepsilon_{th}$  and  $\varepsilon_p$  for the channel. For the values of  $\varepsilon$  greater than 1 means the heat transfer enhancement is greater than the increase of pressure drop while for the values of  $\varepsilon$  less than 1 means the increase of pressure drop is greater than the heat transfer enhancement in the channel. Figure 9.42 shows the variation of overall performance of partially filled channel with  $Da$  for different  $K^*$ . Overall performance is rising with increased  $Da$  and it is also increased with the ratio of effective thermal conductivity to the fluid thermal conductivity ( $K^*$ ). For  $Da$  greater than 1 which means almost clear channel there is a constant overall performance. The increased overall performance is coming from only  $K^*$  ratio for  $Da$  greater than 1. The figure shows partial filling of channels with the

solids which have  $K^*$  as 0.01 or 1 is not useful for heat transfer enhancement compared with the pressure drop in the channel. The important factor of partial filling with porous media is  $K^*$ . It is seen that, for any Da number value the channel overall performance is greater than 1 when  $K^*$  is 100.

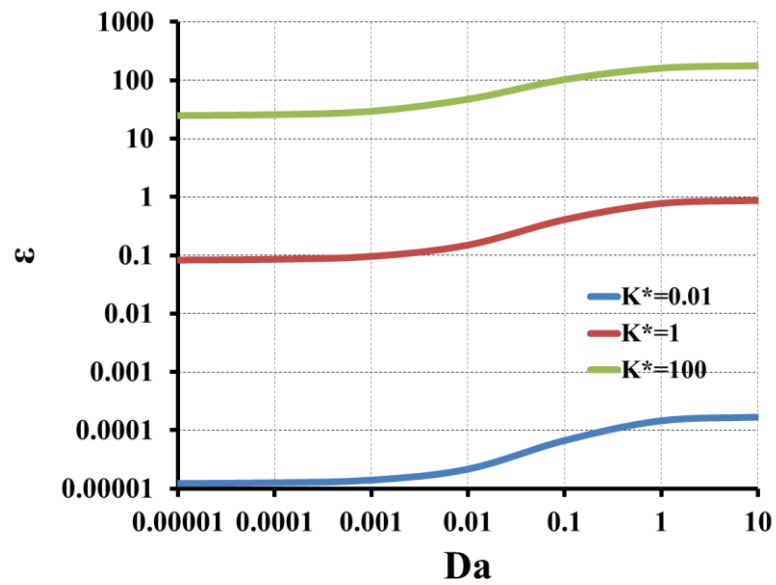


Figure 9.43. Logarithmic plot of overall performance vs. Da for partially filled channel

## CHAPTER 10

### CONCLUSION

The main focus on this thesis is investigating forced convection mechanism in a parallel plate channel with using porous media theoretically. Generally the effects of porous media on the fluid flow and the heat transfer in forced convection are examined. The numerical results of dimensional analysis and the analytical results of dimensionless analysis are given.

The examination starts with a dimensional study about forced convection in a channel which is completely filled by porous media. In the guidance of given equations, two cases are analyzed; symmetrical and asymmetrical heated walls. Three different permeabilities and two different solids are used to analyze the effect of porous media. In the symmetrical heated case, the isotherms in the porous channels are obtained for each channel. It is found that, the decrease of permeability and the usage of more conductive solid (aluminum alloy) increase the conductivity in the channel. So the isotherms become straight lines in a cross section of the channel as effective conductivity increase. Also the mean and wall temperatures are obtained. It is seen that the wall temperature is very high for high permeable glass filled channel. The Nu is also studied for this case. For low conductive materials, the Nu approaches the fully developed case more slowly. The permeability of the channel also affects the fully developed location; if the permeability of the flow decreases, the flow also becomes fully developed earlier. According to the results, it is found that Nu is only a function of permeability of the flow. After making the dimensional study for symmetric case, a dimensionless study is done for it, as well. Before starting to the dimensionless analytical study, the consistency between analytical and numerical results is checked. Later, the analytical study is done with dimensionless parameters for symmetrical heated channel. It is resulted that the normalized velocity, the dimensionless temperature and Nu are influenced by Da. When Da increases, the Nu decreases. The heat transfer improvement, the friction drop and overall performance of the channel is studied. So, for specific ratios of effective conductivity over fluid conductivity, the overall performances of the channels are shown by figures.



Another dimensional study is done for asymmetrical heat flux boundary condition in a forced convection completely filled parallel plate channel. Three different permeability values and two different solids are used again in this channel. The isotherms through the channels are obtained. The isotherms are not symmetrical due to the asymmetrical heating. The variation of Nu for upper and lower wall vs. heat flux ratio is shown. Although an asymmetrical heating is imposed to the walls, the isotherms become almost identical for low permeable aluminum alloy filled channel because of high effective conductivity. It is found that, there are infinite and negative values in the Nu variations. The temperature distribution at the outlet of the channel for specific heat fluxes are examined to find the cause of the negative and infinite Nu. The reason of these infinite and negative values is found as the relation between mean temperature and wall temperatures and shown with a figure. Before making the dimensionless analyses, the consistency of the dimensional and dimensionless analysis is checked. The distributions of normalized velocity, dimensionless temperatures and Nu are obtained by analytically. Like asymmetrical dimensional problem, the dimensionless results of the asymmetrical heated channels contain negative and infinite individual Nu. This behavior of Nu is not rational because there is no change in the direction of heat transfer. The heat flux is imposed from wall to the channel for all cases. For specific heat flux ratio, the overall performance is shown according to the obtained heat transfer increment ratio.

The bottom half of the channel is filled with a porous medium to obtain the effects of permeability on heat and fluid flow in forced convection for parallel plate channel which partially filled with porous media. This analysis is made dimensionally for three channels which have different permeabilities and two different solids. The velocity profiles and the isotherms in the partially filled channel are shown. The isotherms of channels show that; the clear fluid part of channel do not highly effected by permeability, while the lower part is highly effected due to the porous media. The Nu, the distribution of the wall temperatures and the outlet temperatures are given for all type of channels. After checking the consistency between numerical and analytical results, an analytical investigation is done to the symmetrical heated partially filled channel. The normalized velocity, dimensionless temperature and individual Nu variations are observed with different ratio of effective conductivity over fluid conductivity. It is observed that, Da number highly affects the normalized velocity and the dimensionless temperature of the channel. There are infinite and negative values of

individual Nu for this case, too. The negative Nu do not give an idea about the enhancement of heat transfer, for this reason, the overall Nu is observed for this case. An optimum interval is found for overall Nu according to the Da. It can be said that the overall Nu has largest value when the Da is between 0.01 and 0.1 with using  $K^*$  as 100. The friction coefficient is also shown for partial filling case. According to the required heat transfer enhancement and the pressure drop which can be tolerated, the channel can be completely filled or partially filled by checking the overall efficiency of the channel.

## REFERENCES

- [1] A. E. Bergles, "Techniques to Enhance Heat Transfer," in *Handbook of Heat Transfer*, W. M. Rohsenow, J. P. Hartnett, and Y. I. Cho, Eds., 3 ed. New York: McGraw-Hill, 1998.
- [2] K. Vafai, *Handbook of Porous Media*, 1 ed. New York, 2000.
- [3] D. A. Nield and A. Bejan, *Convection in Porous Media*, 3 ed. New York: Springer, 2006.
- [4] D. Poulikakos and M. Kazmierczak, "Forced Convection in a Duct Partially Filled with a Porous Material," *Journal of Heat Transfer*, vol. 109, pp. 653-662, 1987.
- [5] M. A. Al-Nimr and M. K. Alkam, "A Modified Tubeless Solar Collector Partially Filled With Porous Substrate," *Renewable Energy*, vol. 13, pp. 165-173, 1997.
- [6] Z. Guo, S. Y. Kim, and H. J. Sung, "Pulsating Flow and Heat Transfer in a Pipe Partially Filled with a Porous Medium," *International Journal of Heat and Mass Transfer*, vol. 40, pp. 4209-4218, 1997.
- [7] A. V. Kuznetsov, "Analytical Investigation of Couette Flow in a Composite Channel Partially Filled with a Porous Medium and Partially with a Clear Fluid," *International Journal of Heat and Mass Transfer*, vol. 41, pp. 2556-2560, 1998.
- [8] A. V. Kuznetsov, "Fluid Flow and Heat Transfer Analysis of Couette Flow in a Composite Duct," *Acta Mechanica*, vol. 140, pp. 163-170, 1999.
- [9] A. A. Mohamad, "Heat Transfer Enhancements in Heat Exchangers Fitted with Porous Media Part I: Constant Wall Temperature," *International Journal of Thermal Sciences*, vol. 42, pp. 385-395, 2003.
- [10] T.-C. Jen and T. Z. Yan, "Developing fluid flow and heat transfer in a channel partially filled with porous medium," *International Journal of Heat and Mass Transfer*, vol. 48, pp. 3995-4009, 2005.
- [11] T. V. Morosuk, "Entropy Generation in Conduits Filled with Porous Medium Totally and Partially," *International Journal of Heat and Mass Transfer*, vol. 48, pp. 2548-2560, 2005.
- [12] H. Sayehvand and H. Shokouhmand, "Study of Forced Convection in a Pipe Partially Filled With a Porous Medium," 2006.

- [13] C. Yang, W. Liu, and A. Nakayama, "Forced Convective Heat Transfer Enhancement in a Tube with its Core Partially Filled with a Porous Medium," *The Open Transport Phenomena Journal*, vol. 1, pp. 1-6, 2009.
- [14] P. Forooghi, M. Abkar, and M. Saffar-Avval, "Steady and Unsteady Heat Transfer in a Channel Partially Filled with Porous Media Under Thermal Non-Equilibrium Condition," *Transport in Porous Media*, vol. 86, pp. 177-198, 2010.
- [15] A. V. Kuznetsov and D. A. Nield, "Forced Convection in a Channel Partly Occupied by a Bidisperse Porous Medium: Asymmetric Case," *International Journal of Heat and Mass Transfer*, vol. 53, pp. 5167-5175, 2010.
- [16] V. V. Satyamurty and D. Bhargavi, "Forced Convection in Thermally Developing Region of a Channel Partially Filled with a Porous Material and Optimal Porous Fraction," *International Journal of Thermal Sciences*, vol. 49, pp. 319-332, 2010.
- [17] D. A. Nield and A. V. Kuznetsov, "Forced Convection in a Channel Partly Occupied by a Bidisperse Porous Medium: Symmetric Case," *Journal of Heat Transfer*, vol. 133, p. 072601, 2011.
- [18] H. Shokouhmand, F. Jam, and M. R. Salimpour, "The Effect of Porous Insert Position on the Enhanced Heat Transfer in Partially Filled Channels," *International Communications in Heat and Mass Transfer*, vol. 38, pp. 1162-1167, 2011.
- [19] M. A. Teamah, W. M. El-Maghlany, and M. M. Khairat Dawood, "Numerical Simulation of Laminar Forced Convection in Horizontal Pipe Partially or Completely Filled with Porous Material," *International Journal of Thermal Sciences*, vol. 50, pp. 1512-1522, 2011.
- [20] G. S. Beavers and D. D. Joseph, "Boundary Conditions at a Naturally Wall," *Journal of Fluid Mechanics*, vol. 30, pp. 197-207, 1967.
- [21] A. V. Kuznetsov, "Influence of the Stress Jump Condition at the Porous-Medium/Clear Fluid Interface on a Flow at a Porous Wall," *International Communications in Heat and Mass Transfer*, vol. 24, pp. 401-410, 1997.
- [22] A. V. Kuznetsov, "Forced Convective Heat Transfer in a Parallel-Plate Channel with a Porous Core," *Journal of Applied Mechanics and Engineering*, vol. 4, pp. 271-290, 1999.
- [23] B. Alazmi and K. Vafai, "Analysis of Fluid Flow and Heat Transfer Interfacial Conditions Between a Porous Medium and a Fluid Layer," *International Journal of Heat and Mass Transfer*, vol. 44, pp. 1735-1749, 2001.

- [24] B. Goyeau, D. Lhuillier, D. Gobin, and M. G. Velarde, "Momentum transport at a fluid-porous interface," *International Journal of Heat and Mass Transfer*, vol. 46, pp. 4071-4081, 2003.
- [25] J.-L. Auriault, "About the Beavers and Joseph Boundary Condition," *Transport in Porous Media*, vol. 83, pp. 257-266, 2009.
- [26] M. K. Alkam and M. A. Al-Nimr, "Transient Non-Darcian Forced Convection Flow in a Pipe Partially Filled with a Porous Material," *International Journal of Heat and Mass Transfer*, vol. 41, pp. 347-356, 1997.
- [27] M. A. Al-Nimr and M. K. Alkam, "Unsteady Non-Darcian Fluid Flow in Parallel-Plates Channels Partially Filled with Porous Materials," *Heat and Mass Transfer*, vol. 33, pp. 315-318, 1998.
- [28] M. K. Alkam and M. A. Al-Nimr, "Transient Flow Hydrodynamics in Circular Channels Partially Filled with a Porous Material," *Heat and Mass Transfer*, vol. 37, pp. 133-137, 2001.
- [29] M. K. Alkam, M. A. Al-Nimr, and M. O. Hamdan, "Enhancing Heat Transfer in Parallel-Plate Channels by Using Porous Inserts," *International Journal of Heat and Mass Transfer*, vol. 44, pp. 931-938, 2001.
- [30] M. K. Alkam, M. A. Al-Nimr, and M. O. Hamdan, "On Forced Convection in Channels Partially Filled with Porous Substrates," *Heat and Mass Transfer*, vol. 38, pp. 337-342, 2002.
- [31] M. Kaviany, *Principles of Heat Transfer in Porous Media*, Second ed.: Springer, 1995.
- [32] Ö. Çekmer, "A Theoretical Study on Enhancement of Heat Transfer in a Solar Air Heater Collector by Using Porous Media," Master of Science, Energy Engineering, İzmir Institute of Technology, İzmir, 2011.
- [33] (2011,04.02) *Air Properties* Available: [http://www.engineeringtoolbox.com/air-properties-d\\_156.html](http://www.engineeringtoolbox.com/air-properties-d_156.html)
- [34] (2011,04.02) *Thermal Conductivity*. Available: [http:// hyperphysics.phy-astr.gsu.edu / hbase/tables/thrcn.html](http://hyperphysics.phy-astr.gsu.edu/hbase/tables/thrcn.html)
- [35] (2011,04.02) *List of Thermal Conductivities*. Available: [http://en.wikipedia.org/wiki/List\\_of\\_thermal\\_conductivities](http://en.wikipedia.org/wiki/List_of_thermal_conductivities)
- [36] W. Simpson and A. TenWolde, "Physical Properties and Moisture Relations of Wood," vol. 190, pp. 1-20, 1999.

# **APPENDIX A**

## **CONSTANTS**

The constants in the Equation 7.32 are as following:

$$b1 = \frac{(-1 + \xi^2)(-4c1 - 3(c2 - 2p0 - 4\text{cosh}p1 + 4p2S + 4(p1 - p2)S\text{sinh}) + 6c0(-1 + \xi) + \xi(c2 + 6(p0 + 2\text{cosh}p1) + (1 + \xi)(2c1 + c2\xi))}{24K(-1 + \xi) - 24(1 + \xi)} \quad (\text{A.1})$$

$$b2 = -\frac{1 + K(-1 + \xi) + \xi}{1 + K + \xi - K\xi} \quad (\text{A.2})$$

The constants in the Equation 7.34 are as following:

$$t1 = \frac{-(-1 + \xi^2)(-2c1 - c2 - 6p0 + 12p1S + 6c0(-1 + \xi) + \xi(-c2 - 6p0 + c2\xi(-1 + 3\xi) + c1(-2 + 4\xi)) - 12p2S\text{Cosh}[\frac{1+\xi}{S}]) + 12(p1 - p2)S^2(-1 + \xi)\text{Sinh}[\frac{1+\xi}{S}]}{24K(-1 + \xi) - 24(1 + \xi)} \quad (\text{A.3})$$

$$t2 = -\frac{1 + K(-1 + \xi) + \xi}{1 + K + \xi - K\xi} \quad (\text{A.4})$$

The constants in the Equation 7.36 are as following:

$$\begin{aligned}
n1 = & - (20160K(1 + \xi)) / (420c0^2K(-1 + \xi)^3(1 + \xi) + 140c1c2K(-1 + \xi)^3(1 + \xi)^2(1 + \xi + \xi^2) \\
& + 28c1^2K(-1 + \xi)^3(1 + \xi)(4 + \xi(7 + 4\xi)) + 84c0K(-1 + \xi)^3(1 + \xi) (5c1(1 + \xi) + c2(3 + \xi(4 + 3\xi))) \\
& + 5 \left( 84 \left( -24p0(p1 + p2)S^3(1 + \xi) - p0^2(1 + \xi)^4 \right. \right. \\
& \left. \left. - 6S^2(-2p1p2S^2 + p1^2(S^2 + (1 + \xi)^2) + p2^2(S^2 + (1 + \xi)^2)) \right) \right. \\
& \left. + c2^2K(-1 + \xi)^3(1 + \xi) \left( 9 + \xi \left( 20 + \xi(26 + \xi(20 + 9\xi)) \right) \right) \right) + 1260S^2(4(1 + \xi)(2p0p2S + p1(p2 + 2p0S \\
& + p2\xi)) \text{Cosh}\left[\frac{1 + \xi}{S}\right] + 2(p1 - p2)^2S^2 \text{Cosh}\left[\frac{2(1 + \xi)}{S}\right] - 4(1 + \xi)(-p1p2S + p0(p1 + p2)(1 + \xi)) \text{Sinh}\left[\frac{1 + \xi}{S}\right] \\
& - (p1^2 + p2^2)S(1 + \xi) \text{Sinh}\left[\frac{2(1 + \xi)}{S}\right])
\end{aligned} \tag{A.5}$$



$$\begin{aligned}
n_2 = & (840K((1 + \xi)(-4c_1 - 3(c_2 - 2p_0 + 4p_2S) + 6c_0(-1 + \xi) + \xi(c_2 + 6p_0 + (1 + \xi)(2c_1 + c_2\xi)) + 12p_1S\text{Cosh}[\frac{1 + \xi}{S}])) \\
& + 12(-p_1 + p_2)S^2\text{Sinh}[\frac{1 + \xi}{S}]))/(420c_0^2K(-1 + \xi)^3(1 + \xi) + 140c_1c_2K(-1 + \xi)^3(1 + \xi)^2(1 + \xi + \xi^2) \\
& + 28c_1^2K(-1 + \xi)^3(1 + \xi)(4 + \xi(7 + 4\xi)) + 84c_0K(-1 + \xi)^3(1 + \xi)(5c_1(1 + \xi) + c_2(3 + \xi(4 + 3\xi))) \\
& + 5(84(-24p_0(p_1 + p_2)S^3(1 + \xi) - 6S^2(-2p_1p_2S^2 + p_1^2(S^2 + (1 + \xi)^2) + p_2^2(S^2 + (1 + \xi)^2)) - p_0^2(1 + \pi^4 \\
& + 2\xi(2 + \xi(3 + 2\xi)))) + c_2^2K(-1 + \xi)^3(1 + \xi)(9 + \xi(20 + \xi(26 + \xi(20 + 9\xi)))) + 1260S^2(4(1 + \xi)(2p_0p_2S \\
& + p_1(p_2 + 2p_0S + p_2\xi))\text{Cosh}[\frac{1 + \xi}{S}] + 2(p_1 - p_2)^2S^2\text{Cosh}[\frac{2(1 + \xi)}{S}] - 4(1 + \xi)(-p_1p_2S + p_0(p_1 + p_2)(1 \\
& + \xi))\text{Sinh}[\frac{1 + \xi}{S}] - (p_1^2 + p_2^2)S(1 + \xi)\text{Sinh}[\frac{2(1 + \xi)}{S}]))
\end{aligned} \tag{A.6}$$

$$\begin{aligned}
n_3 = & -(840K((1 + \xi)(-c_2 - 6p_0 + 12p_1S + 6c_0(-1 + \xi) + 2c_1(-1 + \xi)(1 + 2\xi) + \xi(-6p_0 + c_2(-1 + \xi(-1 + \\
& 3\xi)))) + 12S(-p_2(1 + \xi)\text{Cosh}[\frac{1 + \xi}{S}] - p_1S\text{Sinh}[\frac{1 + \xi}{S}] + p_2S\text{Sinh}[\frac{1 + \xi}{S}]))/(420c_0^2K(-1 + \xi)^3(1 + \xi) + 140c_1c_2K(-1 + \xi)^3(1 + \\
& \xi)^2(1 + \xi + \xi^2) + 28c_1^2K(-1 + \xi)^3(1 + \xi)(4 + \xi(7 + 4\xi)) + 84c_0K(-1 + \xi)^3(1 + \xi)(5c_1(1 + \xi) + c_2(3 + \xi(4 + 3\xi))) + \\
& 5(84(-24p_0(p_1 + p_2)S^3(1 + \xi) - p_0^2(1 + \xi)^4 - 6S^2(-2p_1p_2S^2 + p_1^2(S^2 + (1 + \xi)^2) + p_2^2(S^2 + (1 + \xi)^2))) + c_2^2K(-1 + \\
& \xi)^3(1 + \xi)(9 + \xi(20 + \xi(26 + \xi(20 + 9\xi)))) + 1260S^2(4(1 + \xi)(2p_0p_2S + p_1(p_2 + 2p_0S + p_2\xi))\text{Cosh}[\frac{1 + \xi}{S}] + 2(p_1 - \\
& p_2)^2S^2\text{Cosh}[\frac{2(1 + \xi)}{S}] - 4(1 + \xi)(-p_1p_2S + p_0(p_1 + p_2)(1 + \xi))\text{Sinh}[\frac{1 + \xi}{S}] - (p_1^2 + p_2^2)S(1 + \xi)\text{Sinh}[\frac{2(1 + \xi)}{S}]))
\end{aligned} \tag{A.7}$$